# Directional Channel Characterization for Industrial Robots at mmWave Frequencies

Project Report

Group Number : 924

Aalborg University
Electronics and IT

Here you can write something about which tools and software you have used for typesetting the document, running simulations and creating figures. If you do not know what to write, either leave this page blank or have a look at the colophon in some of your books.

AALBORG UNIVERSITY

STUDENT REPORT

**Electronics and IT**
Aalborg University
http://www.aau.dk

**Title:**
Directional Channel Characterization for Industrial Robots at mmWave Frequencies.

**Theme:**
Scientific Theme

**Project Period:**
September 2021 - May 2022

**Project Group:**
924

**Participant(s):**
Author : Arun Yadav

**Supervisor(s):**
Supervisor 1 : Troels.B Sørensen, Aalborg University

Supervisor 2 : Poul Olesen, Nokia Bell Labs

**Copies:** 1

**Page Numbers:** 91

**Date of Completion:**
June 2, 2022

**Abstract:**

The next evolution is happening under industry 4.0. For proper D2D communication, it is essential to know the reason for amplitude variation. Most of the channel characterization measurement [5], [8] at mmWave frequency seems not to be able to distinguish between amplitude variations caused by fast fading and NLOS to LOS transitions. Existing RF directional channel characterization measurement method where RF tones are separated in such a fading is uncorrelated can categorize amplitude variation.
In this project, a series of measurements have been performed. Data processing has been done on the collected data to analyze frequency correlation, K-factor, and multi-path spread. Based on data processing, coherence bandwidth is defined.
The measurement results show that coherence bandwidth is higher when both directional receiver and transmitter are in Line of sight(LOS). The coherence bandwidth decreases as the separation between the transmitter and receiver increases in a rich fading channel. Coherence bandwidth decreases as a separation between RF tones increases.

# Preface

This Report is written by group 924 at Nokia Bell Labs during the 9-10th semester of Master programme duration of the project is September 2021 to June 2022. The aim of this study is to define coherence bandwidth for differrent indoor environement condition.

The report is aimed people with knowledge equivalent to Master's focusing on radio communication. The Topic " Directional channel characterization for industrial Robots at mmWave frequencies".

I would like to thank my project supervisors Troels bundgaard sørensen and Poul Olesen.
I would also like to thank Bent Rysgaard, Stig Blucher Brink, and Jan Hviid.

Figures, tables and equations are arranged consecutively according to the chapter's number. Hence, the first figure in chapter one is named Figure 1.1, the second figure Figure 1.2 and so on.

Aalborg University, June 2, 2022

Arun Yadav
<ayadav20@student.aau.dk>

## Abbreviations List

| Abbreviation | Definition |
|---|---|
| AAU | Aalborg University |
| IIOT | Industrial Internet of things |
| MTC | Machine time of communication |
| D2D | Device to device |
| MiR | Mobile Industrial Robots |
| LOS | Line of Sight |
| NLOS | Non-line of Sight |
| SNR | Signal to Noise Ratio |
| PLL | Phased locked loop |
| Tx | Transmitter |
| Rx | Receiver |
| 5G | 5th Generation |
| RBW | Resolution Bandwidth |
| 3GPP | 3rd Generation Partnership Project |
| LTE | Long term evolution |
| IF | Intermediate frequency |
| RF | Radio frequency |
| 3G | 3rd generation |
| LO | Local oscillator |
| CW | Continious wave |
| 3D | Three dimension |
| UE | User equipment |
| TRP | Transmission reception point |
| us | microsecond |
| VSWR | Voltage standing wave ratio |

# Contents

# List of Tables

# List of Figures

# Chapter 1

# Summary

The current industry 4.0 is a step toward achieving advanced industrial production, such as swarm production. Inside the factory, the robots will follow different paths with line of sight(LOS) and non-line of sight (NLOS) propagation, which impacts the directionality of the transmission/reception. To design algorithms for controlling the directional transmission/reception it is important to know the time dynamics of the directional propagation paths in both LOS and NLOS conditions, e.g., for the design of "beam handover" algorithms. It is essential to know the reason for amplitude variation, most of the channel characterization measurement at mmWave frequency [5], [8] seems not to be able to distinguish between amplitude variations caused by fast fading and NLOS to LOS transitions.

The existing measurement method is based on the principle that simultaneously several RF carriers are in the air, and separation between each carrier is chosen in such a way that the fading is uncorrelated between them [20], able to categorize the fast fading and LOS to NLOS transition. In this project, the measurements focus on defining the coherence bandwidth for a range of typical office settings that mimic an industrial environment. The benefit of the new measurement setup presented in this project is that it uses sixteen RF tones, while the existing measurement setup uses only 4 RF tones over a bandwidth. The higher number of RF tones gives more detailed channel characteristics and accurate coherence bandwidth value.

After capturing the data through a series of measurements, data processing has been done on the collected data to analyze frequency correlation, K-factor, multipath spread, field strength, and fading. Based on the data processing, coherence bandwidth for different channel conditions will be defined and provide optimized tone separation for further measurement of the existing measurement technique. Based on the result analysis, the antenna's directionality affects the coherence bandwidth. The receiver contains a switched antenna system of four antennae; the coherence bandwidth is very high for the antenna directed towards the receiver, and antennas that are not directive toward the receiver have less coherence

bandwidth. Coherence bandwidth decreases as the bandwidth separation between RF tones increases. Coherence bandwidth also reduces as the separation between transmitter and receiver increases.

# Chapter 2

# Introduction

The first industrial revolution started with the transition of the handmade product to machines, and machines run by steam and water power. It transformed the iron industry, mining, and textile industry mostly. The second industrial revolution/technological revolution took place around the end of the 19th century to the beginning of the 20th century, and it led to the expansion of railroad and electricity, and the electrification of industry led to mass production. The third industrial revolution, also called digitization, began in the 20th century. It began with digitization and the development of computers and electronic components. Figure 2.1 shows four industrial revolutions. The fourth industrial revolution depends on several technologies such as cyber-physical systems, industrial internet of things(IIOT), and cloud computing to provide flexibility and reliable high-level manufacturing. The rapid development of the electronics industry, information technology, advancement in manufacturing, and increased demand for goods and

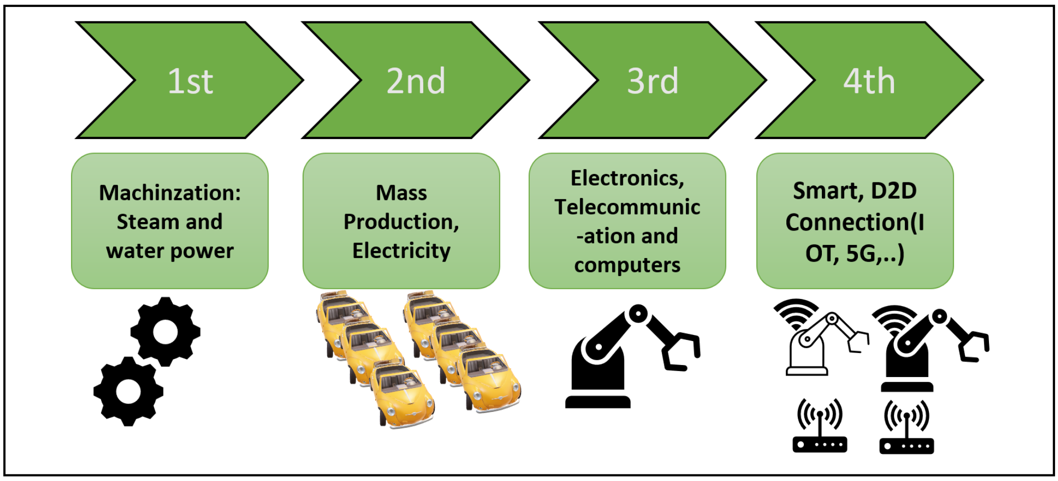


**Figure 2.1:** Four Industrial Revolution

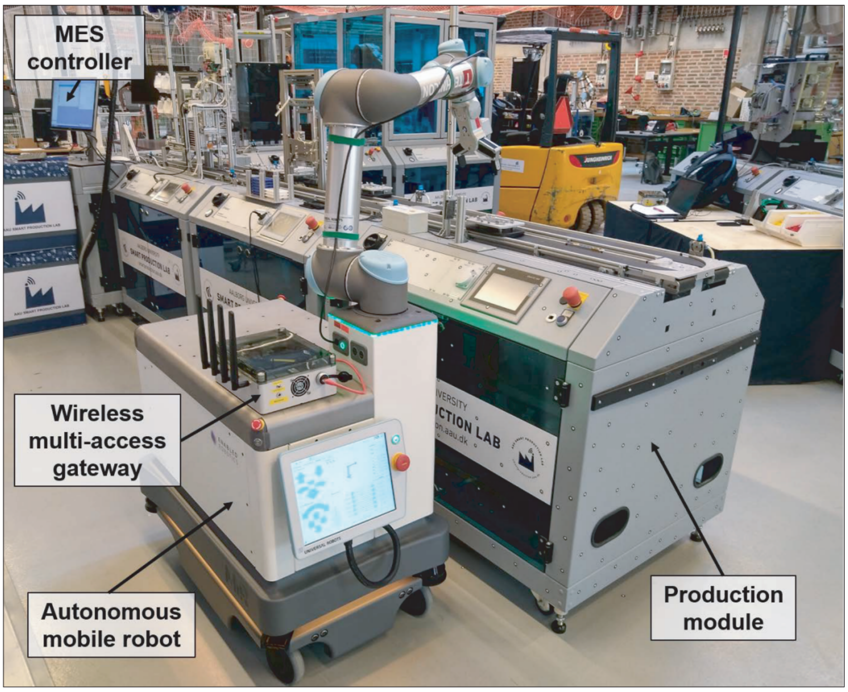


**Figure 2.2:** Automation Factor AAU [22]

products led to the transformation of the current digital sector to intelligent based, referred to as industry 4.0, wireless technologies will replace the cables, and it provides more flexibility and also cost reduction [22], figure 2.2 shows Aalborg University 5G smart production factory focused on the idea of industry 4.0. 5G is a crucial enabler for industry 4.0, and it does have the potential to increase the efficiency of the industries.

Device-to-device communication is categorized into two classes massive MTC (machine type communication) and machine critical MTC. Massive MTC is a large collection of a devices such as sensor with a requirement on coverage zone and efficiency, while machine-critical MTC needs low latency and high reliability. Two significant components for critical machine-type communication are low latency and ultra-reliable communication. Based on the application, the requirement for latency and reliability varies. In terms of delay, some of the most significant contributors to delays are network stack, medium access, signal processing, transmission, and propagation delays [14]. The requirement for reliability and latency is strict in the case of industry 4.0, [14].

## 2.1 Device to Device Communication

The current industry 4.0 is a step toward achieving advanced industrial production, such as swarm production, where small mobile robots are being used for manufacturing. Swarm production will provide high flexibility and reconfiguration to the industry's production process but requires highly robust wireless connectivity in an environment with a high degree of clutter and potentially high density of wirelessly connected robots. 5G wireless communication at mm-wave frequencies is considered a potential candidate for such robot-to-robot communication applications. With the evolution of 5G, it is possible to achieve high reliability and low

| e2e latency | Reliability | Data size | Communication range between devices | No. of devices per factory hall | Machine mobility (indoors) |
|---|---|---|---|---|---|
| Summarized Result | | | | | |
| 1 to 50 ms | 1-10^-6 to 1-10^-9 | 10 to 300 bytes | 2 to 100 m | 10 to 1000 | 0 to 10 m/s |
| Application scenario: Manufacturing processes | | | | | |
| <10ms | 1-10^-9 | <50 bytes | <100m | <1000 | ~1m/s |
| Application scenario: Automated guided vehicles | | | | | |
| 10 to 50 ms | 1-10^-6 to 1-10^-9 | < 300 bytes | ~ 2 m | < 1000 | < 1000 |

**Figure 2.3:** Requirements for wireless factory automation [14]

latency. The requirement for industry 4.0 is ultra-reliable low latency, where correct data need to be delivered within defined latency. Figure 2.3 shows the study done [14] for different types of industrial applications such as manufacturing processes, automated guided vehicles, also general summarized results with a requirement of e2e latency, reliability, data size, communication range between devices, number of devices and machine mobility. In automated industry 4.0, D2D communication plays a crucial role. Device-to-device communication allows robots to communicate without needing an access point; all the devices work collaboratively and increase efficiency.

Robots share collective data with each other who are in proximity, this will reduce the chance of collision among robots and also increase mobility and productivity inside the factory [12]. Robots move randomly and constantly inside the factory; they sense and track surroundings environment and exchange information based on the critical and extended range as shown in figure 2.4. Robots within extended range(re) share mobility and position information that can be used for channel estimation. Within critical range(rc), they share video data that help in movement and provide traffic information.

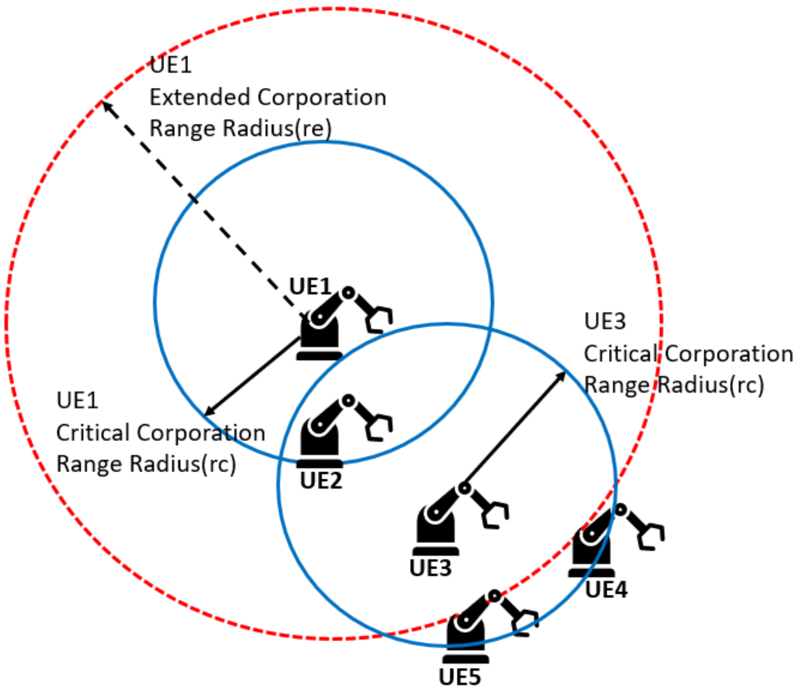


**Figure 2.4:** Device to Device communication [12]

## 2.2 mmWave and Challenges

5G is inevitable for industry 4.0, but the mmWave has disadvantages, such as a smaller coverage range and lower SNR. Larger bandwidth in 5G leads to higher SNR(signal to noise ratio). For mmWave frequencies, the path loss is larger than lower frequency bands, even for free space. At mmWave frequency, the propogating wave are very sensitive to blockage structure due to diffraction around the object in factory environment [3]. There will be a range of complex structures in an industrial environment, which increases the fading, so it is vital for MiR(Mobile Industrial Robots) to have an antenna system with beamforming or directionality capability. A directional antenna system can be an option to improve the SNR and have less fading [5].

## 2.3 Beamforming and Management

Beamforming is formed by using multiple antenna system to produce directional beam. The major advantage of breamforming is reduction in interference, beamforming will provide diversity gain and multiplexing gain. Industrial communica-

tion is quite different that normal communication. Inside the factory there can be several heavy structure, moving robots, and machine which affect the wave propagation and lead to rich fading, using directional antenna system will decrease the path diversity [15] will improve the gain and signal to noise ratio.
Beam management plays important role for mmWave communication, it maintain antenna beam in a direction of importance. In the case of industrial environment, where the channel have rich fading, it is important to find effective direction for beamforming, for proper TRP, UE communication. Study on beammanagement process have been done between TRP-UE have been done [1], it contain three steps. **For mmWave, UE-UE beamforming still under research**.

## 2.4 Channel Effect

In an industrial environment, beam-management will be done based on channel characteristics response. Inside the factory, the robots will follow different paths with line of sight(LOS) and non-line of sight (NLOS) propagation, which impacts the directionality of the transmission/reception. To design algorithms for controlling the directional transmission/reception it is important to know the time dynamics of the directional propagation paths in both LOS and NLOS conditions, e.g., for the design of "beam handover" algorithms.
For example, if robot moved into a non-line sight scenario then it would difficult to share information to other robot. For industry 4.0, effective TRP handover and data sharing among robots plays an crucial role. It is essential to discover the reasons for amplitude variations in the channel. Fast Fading can be handled in the coding and modulation domain. LOS to NLOS transitions also refers as shadowing must be dealt with by redundancy means like Side links, TRP, DAS, or multiple UU connections[20].
Amplitude variations in the RF channel are caused by the movement of devices behind obstacles, around corners, and simply due to changing path loss due to movements in a straight line or rotation. Similar variations should be expected across a relatively large bandwidth when the channel is affected by fast fading and LOS to NLOS transitions.

### 2.4.1 LOS To NLOS Transition and Fading

As discussed in [20] with an example case, the time it takes a device with different beam widths to pass a corner with varying combinations of speed (5 km/h and 70 km/h) could be anything from 4 ms to 1000 ms. This is comparable with amplitude variations caused by fading, and for that reason it is essential to know the exact reason for amplitude variations as the two physical phenomena need to be dealt with using very different means as described above. Fast fading occurs

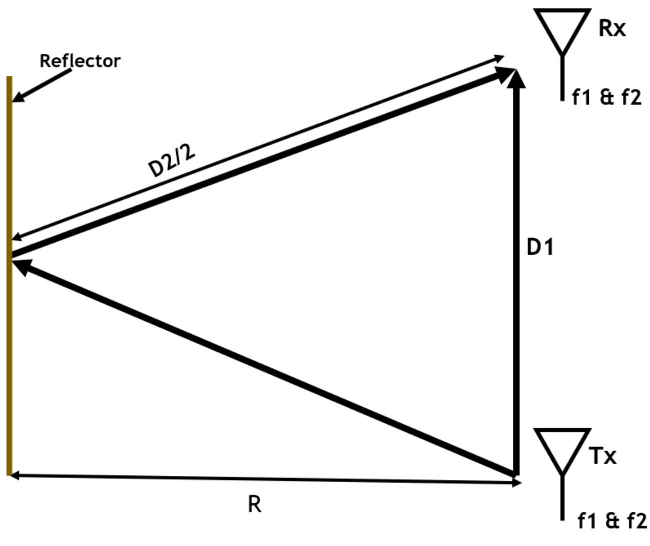


**Figure 2.5:** Direct and reflected component

due to amplitude variation of the RF signal because of multipath components; the received RF signal is a combination of direct and indirect components, and it may amplify when they combine in the same phase and cancel each other if they are out of phase, shows Rayleigh distribution. Figure 2.5 shows that two RF components are in the air, and figure 2.6 shows the plot of the RF signal of corresponding components, the resultant received RF signal is the constructive and destructive addition of two components and deep fades will occur for every half wavelength can be of 10 to 30 dB in the case of fast fading. It is essential to know when fast fading is happening and when LOS to NLOS transition is happening. Both scenarios of amplitude variation can be handled by different techniques.

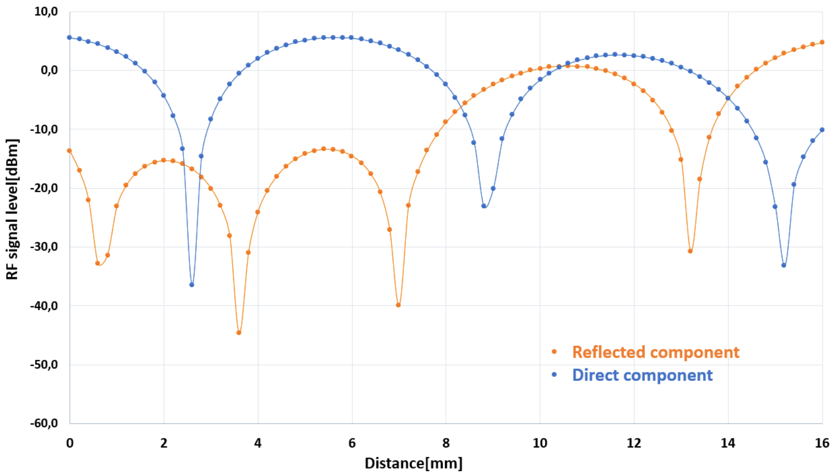


**Figure 2.6:** Direct and Reflected Components

## 2.5 Existing Measurement Setup

The existing measurement setup is based on the principle that simultaneously several RF carriers are in the air, and separation between each carrier is chosen in such a way that the fading is uncorrelated between them [20]. The measurement technique is able to categorize the fast fading and LOS to NLOS transition.
Figure 2.7 shows the basic measurement set-up. On the transmitter side, signal generator generates simultaneously a continuous wave 4 RF tones. Local oscillator generates carrier frequency $f_{lo}$ is added via mixer and then passes into the amplifier, the RF signal is then propagated through the transmitting antenna, all the 4 CW RF signals will be in the air simultaneously.
At the same time, on the receiver side the antenna have access simultaneously to all the 4 RF carriers, but the local oscillator is programmed sequentially to generate local tones corresponding to all four RF signal for down-conversion, after down-coversion the baseband signal will look like as shown in figure 2.8 on oscilloscope.

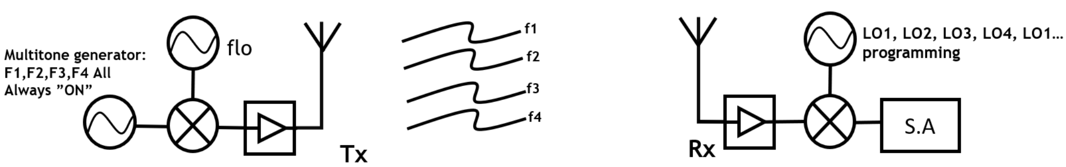


**Figure 2.7:** Block diagram of existing Measurement Setup

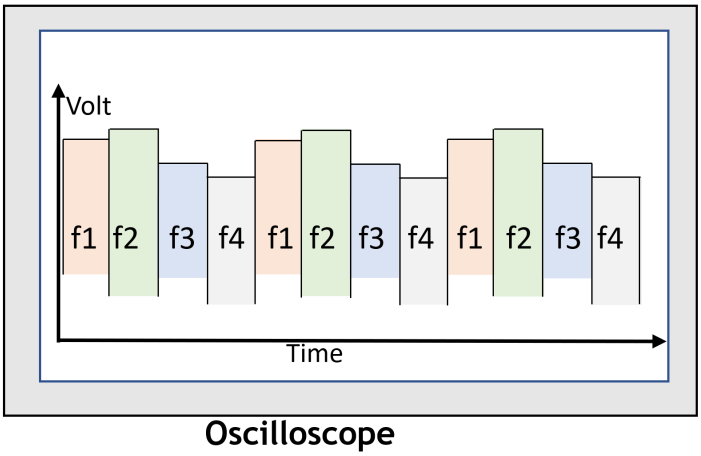


**Figure 2.8:** Video signal plot on Oscilloscope (4 tones, 1Tx and 1Rx)

The benefit of using this measurement technique is that it will provide wideband channel characteristics without using the whole band; hence it will have low SNR.

## 2.6 Thesis outline

The report is organized as follows. Some general information about the background of components of channel models, path loss channel model, and fading in Chapter 3. Chapter 4 introduces the problem statement. Chapter 5 describes the measurement setup in detail. Chapter 6 discusses the detail of data processing. Chapter 7 discusses the measurement results, and finally, chapter 8 presents the conclusion and future work.

# Chapter 3

# Background

## 3.1 Component of Radio Channels

In a communication system, the path loss increases as the separation increases between the Tx(transmitter) and Rx(receiver). Inside the factory, many obstacles such as cluttering machines, metallic structures, corners, etc. affect the propagating RF signal. As shown in the figure 2.2 which contain complex objects which do affect propagating wave, they affect the channel characteristics and lead to fading on the received RF signal.

1. **Diffraction :** Diffraction is a phenomenon where the propagating wave spreads out as they pass the object; it passes the wave even if it is in non-line of sight(means blocked by the object). Huygens's principle states that each wavefront point can be considered as a source point for expanding the wavefront. Transmitter and receiver are a non-line of sight scenario, there can be some edge type of structure as shown in figure 3.1 (example hill, corner wall, etc.), based on **knife edge diffraction** principle it says that propagating wave can reach other side of knife edgy structure. p(r) is loss due to diffraction, h is height between corner and transmitter, receiver(both of them are at same level), $\alpha$ is angle between transmitter and horizontal line from corner. Equation 3.1, $\nu$ is Fresnel–Kirchhoff diffraction parameter, path loss due to knife edge diffraction at distance d* is function of $\nu$ [13]. Study have been done for indoor environment diffraction loss on wooden corner, drywall corner, and plastic board at mmWave frequency [6].

$$\nu = \alpha \sqrt{\frac{2(d^1 + d^2)}{\lambda d^1 d^2}} \tag{3.1}$$

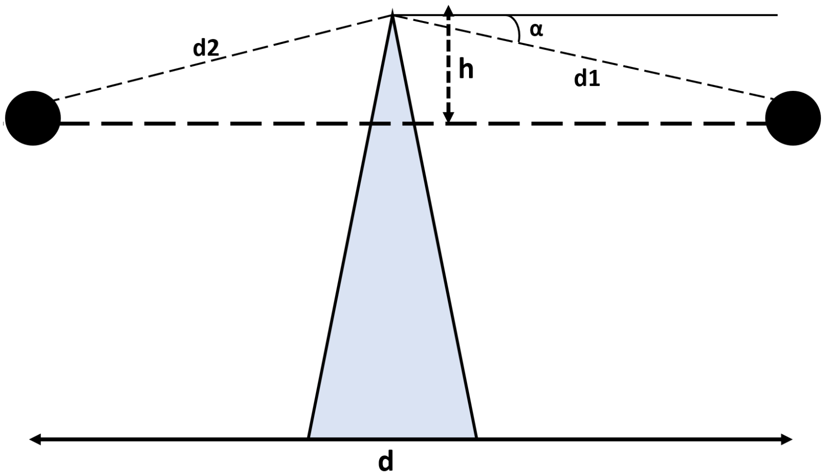


**Figure 3.1:** Knife Edge Diffraction

$$p(r) = \begin{cases} 0 & \nu \leq 0 \\ 20\log_{10}[.5e^{-.95}\nu], & 0 \leq \nu < 1 \\ 20\log_{10}[.4 - \sqrt{.1184 - (.38 - .1\nu)^2}], & -0.8 \leq \nu < 0 \\ 20\log_{10}[.5 - .62\nu], & 1 \leq \nu < 2.4 \\ 20\log_{10}[.25/\nu], & -0.8 \leq \nu > 2.4 \end{cases} \tag{3.2}$$

Based on equation 3.1 and 3.2 diffraction analysis have done.

| $\alpha$ | **Diffraction loss : Corner Wall [dB]** |
|---|---|
| 0 | 0 |
| 10 | -15 |
| 20 | -21.10 |
| 30 | -23.89 |
| 40 | -26.39 |
| 50 | -28.33 |
| 60 | -29.91 |
| 70 | -31.25 |
| 80 | -32.43 |
| 90 | -33.43 |

**Table 3.1:** Diffraction Loss at different angles.

2. **Reflection:** Propagating electromagnetic wave collides with other medium and reflects back with some angle and the phenomena can be referred as reflection. Losses due to reflection vary with respect to medium and propa-

gating angle. Figure 3.2 shows a incident wave at angle $\theta_i$ on a boundary of two dielectric media, part of wave reflected in first media with angle $\theta_i$, and some part is refracted to other media at an angle $\theta_t$. Section 1 of figure 3.2, E-field is parallel to the plane of incidence and in second part of figure the E-field is perpendicular [21]. $E_i$, $E_r$, and $E_t$ are incident, reflected, and transmitted electric fields. The reflection coefficient at the boundary of the two material: $\Gamma_{||}$ for parallel E-field and $\Gamma_{\perp}$ for perpendicular E field. Equation 3.7 calculates Return loss in dB caused by reflection.

$$\Gamma_{||} = \frac{-\epsilon_r \sin\theta_i + \sqrt{\epsilon_r - \cos^2\theta_i}}{\epsilon_r \sin\theta_i + \sqrt{\epsilon_r - \cos^2\theta_i}} \tag{3.3}$$

$$\Gamma_{\perp} = \frac{\sin\theta_i - \sqrt{\epsilon_r - \cos^2\theta_i}}{\sin\theta_i + \sqrt{\epsilon_r - \cos^2\theta_i}} \tag{3.4}$$

$$Er = \Gamma Ei \tag{3.5}$$

$$Et = (1 + \Gamma Ei) \tag{3.6}$$

$$Returnloss[dB] = -20log10(|\Gamma|) \tag{3.7}$$

Based Fresnel reflection formula 3.4, the reflection loss can be calculated, $\epsilon_r$ = 4.7 have been taken in paper [24] for wall. $\epsilon_r$ = 4 [21] for glass.

| $\theta_i$ | **Reflection Loss [dB] : Wall** | **Reflection Loss [dB] : Glass** |
|---|---|---|
| 0 | 0 | 0 |
| 10 | -1.56 | -1.73 |
| 20 | -3 | -3.40 |
| 30 | -4.5 | -4.94 |
| 40 | -5.7 | -6.30 |
| 50 | -6.74 | -7.45 |
| 60 | -7.57 | -8.35 |
| 70 | -8.18 | -9.01 |
| 80 | -8.54 | -9.41 |
| 90 | -8.66 | -9.54 |

**Table 3.2:** Reflection Loss at different angles.

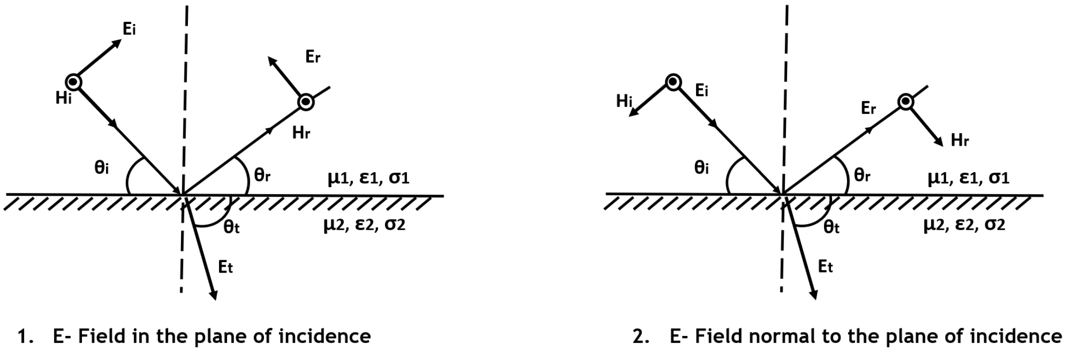


**Figure 3.2:** Frensel Reflection

3. **Scattering:** Scattering is a phenomenon when propagating waves change their path due to irregularity on the structure or surface, it is clearly visible in the figure 3.3 where propagating waves changes their direction of propagation based on irregularity of the structure. The received signal due scattered array 3.8.$\tau$ =$(s^* + s^*)$/c is delay associated with scatterred array. $\sigma$ is radar cross-section of the scattering body, it depends on the roughness and physical property of scatterer. $G_k$ is antenna power gain.

$$r(t) = Re\left\{ \frac{\lambda}{4\pi} \left[ \frac{\sqrt{G_k \sigma u(t-\tau) e^{-j2\pi(s^*+s^*)/\lambda}}}{\sqrt{4\pi} s^* s^*} \right] e^{j2\pi fct} \right\} \tag{3.8}$$

$$P_r dBm = P_t dBm + log10(G_s) + 20log10(\lambda) + 10log10(\sigma) \tag{3.9}$$

$$- 30log10(4\pi) - 20log10(s^*) - 20log10(s^*) \tag{3.10}$$

Equation 3.10 is associated path loss from equation 3.8, $P_r$ and $P_t$ are transmitted and received power [13].

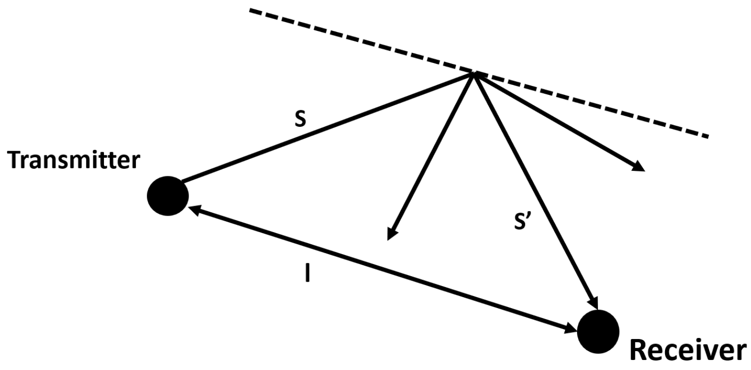


**Figure 3.3:** Scattering

Reflection, diffraction, and scattering are the basic components which affect the propagation of wave in a communication system. These components are important parameter for defining the path loss models, received RF power is normally the most critical parameter predicted by large-scale propagation models established on the impact of reflection, scattering, and diffraction. In the next section several path loss models are discussed.

## 3.2 Path Loss Models

1. **Friis Free Space**
   Consider a scenario in a communication system, the transmitter and receiver pointing at each other, and there is no obstruction between means they are in a line of sight case; based on that received power of the antenna can be calculated [13].

$$P_{\mathrm{R}} = \frac{\lambda^2 G_T P_T G_R}{(4\pi d)^2}, \tag{3.11}$$

$$G_{\mathrm{R}} = \frac{4\pi A_{eR}}{\lambda^2}, \tag{3.12}$$

$$G_{\mathrm{T}} = \frac{4\pi A_{eT}}{\lambda^2}, \tag{3.13}$$

   Where $\lambda$ is the wavelength of propagating wave, $G_T$ and $G_R$ are transmitting and receiving antenna gain, respectively, $P_T$ is transmitted power, $P_R$ is received power, d is a distance between transmitter and receiver, and $A_{eR}$ &

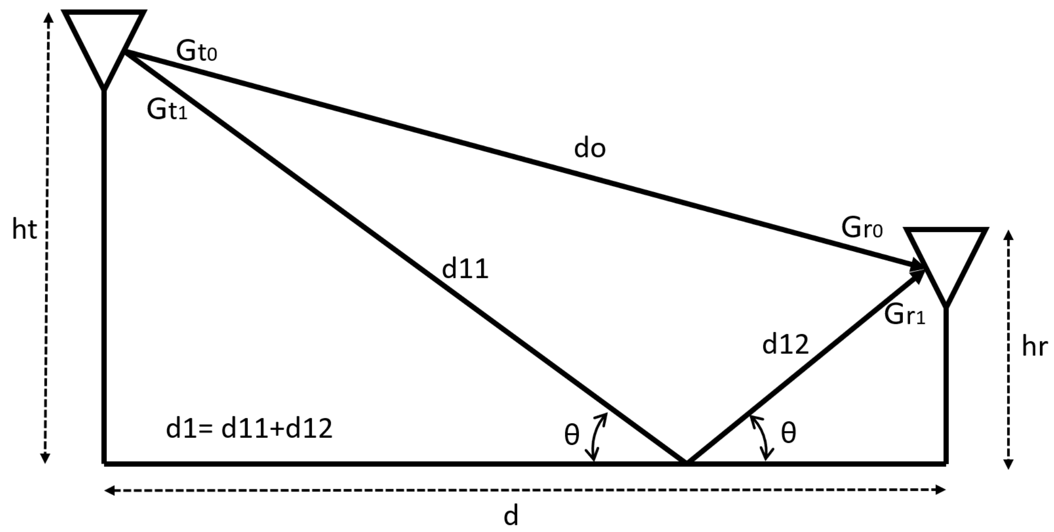


**Figure 3.4:** Two ray model

$A_{eT}$ are an effective area of transmitting and receiving antennas respectively. As the separation between transmitter and receiver increases, the received power decreases by a factor of $1/d^2$ as shown in equation 3.11.

2. **Two Ray/Path Model**
   Two ray model channel model is used when most of mulipath component passed through single reflector(ground), at receiver side it receive components: line of sight and non line of sight. LOS components corresponds which directly through free space and it covers distance do, other components which is multipath comes through reflector(or ground) and it covers a distance( d1 = d11+d12) as shown in figure 3.4, if the transmitted signal is narrow band relative to the delay spread then approximated received power equation will be 3.14, $\Delta\phi$ is the phase difference difference between LOS and reflected component [13].

$$P_{\mathrm{R}} = \left[\frac{\lambda}{4\pi}\right]^2 \left| \frac{\sqrt{G_l}}{l} + \frac{R\sqrt{G_R}\exp^{(-j\Delta\phi)}}{x+x'} \right|^2 \tag{3.14}$$

$$d1 - do = \sqrt{(h_r+h_t)^2 + d^2} - \sqrt{(h_r-h_t)^2 + d^2} \tag{3.15}$$

$$\Delta\phi = \frac{2\pi(d1-do)}{\lambda} \approx \frac{4\pi h_t h_r}{\lambda d} \tag{3.16}$$

$$R = \frac{Sin\theta - Z}{Sin\theta + Z} \tag{3.17}$$

$$Z_v = \epsilon_r - Cos^2\theta / \epsilon_r \tag{3.18}$$

$$Z_h = \epsilon_r - Cos^2\theta \tag{3.19}$$

R is a ground reflection coefficient( $Z_v$ for vertical polarization, $Z_h$ for horizontal polarization)

3. **Path Loss Exponent Models**
Modeling the signal propagation for a range of frequencies and environment is challenging. For general trade-off analysis of the propagation model, it is not essential to add complex parameters. Equations 3.20 is a simplified path loss equation that captures the propagation model over the distance for several cases [13].

$$P_{\mathrm{R}} = P_T K \left[\frac{d_r}{d}\right]^{\alpha} \tag{3.20}$$

where $d_r$ is a reference distance from the transmitting antenna, $\alpha$ is a path loss exponent and K is a constant.

4. **Empirical And Standard Bias Model : In house**
The model is from 3GPP TR 38.901 version 14.3.0 Release 14 [11], $P_{L-LOS}(d_{3d})$ is pathloss in dB for line of sight case and $P_{L-NLOS}(d_{3d})$ for non line of sight case, fc is in GHz and $d_{3d}$ is the distance between transmitter and receiver antenna.

$$P_{L-LOS}(d_{3d}) = 32.4 + 17.3log10(d_{3d}) + 20log10(f_c), 1mt < d_{3d} < 150mt \tag{3.21}$$

$$P_{L-NLOS}(d_{3d}) = 38.3log10(d_{3d}) + 17.3 + 24.90log10(f_c), 1mt < d_{3d} < 150mt \tag{3.22}$$

For path loss models, it is generalized that the path loss also increases as the frequency of operation increases. Industry 4.0, which operates at 5G technology, will have higher path loss than lower-frequency technology.
In a communication system, there is a transmitter and receiver. The propagating wave goes through various types of attenuation based on channel characteristics. The received signal may be affected by the multipath effect, shadowing, path loss, etc. In the next section, fading and its type will be discussed, which will provide a better explanation of channel response.

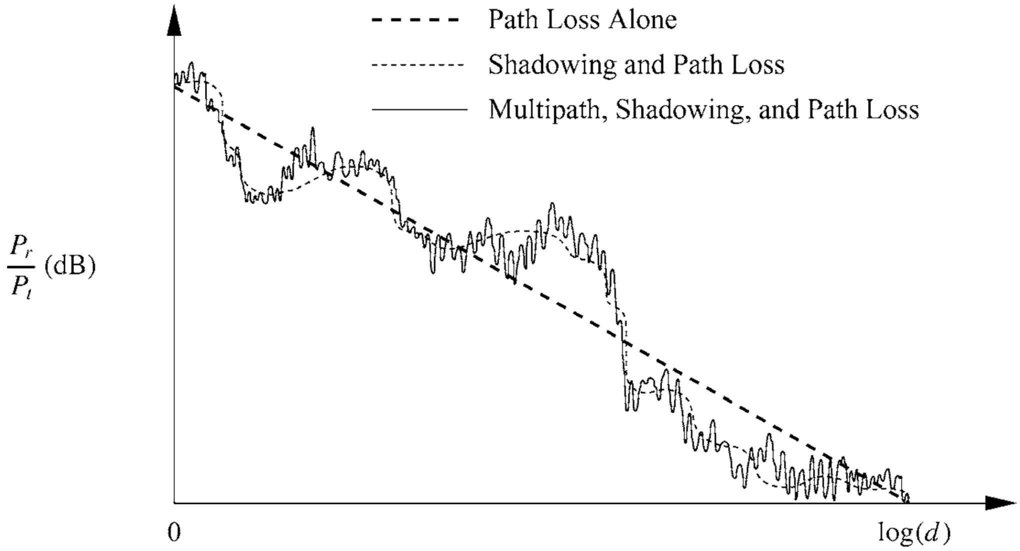


**Figure 3.5:** Components of Radio Channel [13]

## 3.3 Channel Fading

Wireless channel fading can be categorised into two cases: small scale fading and large scale fading, both of the cases are categorised into sub-cases as shown in figure 3.6.

### 3.3.1 Small Scale Fading

Small scale fading occurs due to constructive and destructive interference of multipath radio signal. Small scale fading occurs at wavelength level and is frequency-dependent. Small scale fading can be further categorised into cases.

#### Rician Fading

It include a line of sight and non-line of sight components. Racian K factor can be defined as the ratio of a line of sight components to scattered components. Equation 3.23 expresses Rayleigh pdf distribution, r is the evolope of the recieved RF signal, and $2\sigma^2$ is the pre-detection mean power of the multipath signal. Specular components are the components which only contain line of sight components. If the amplitude of specular components approaches zero, then rician pdf approaches

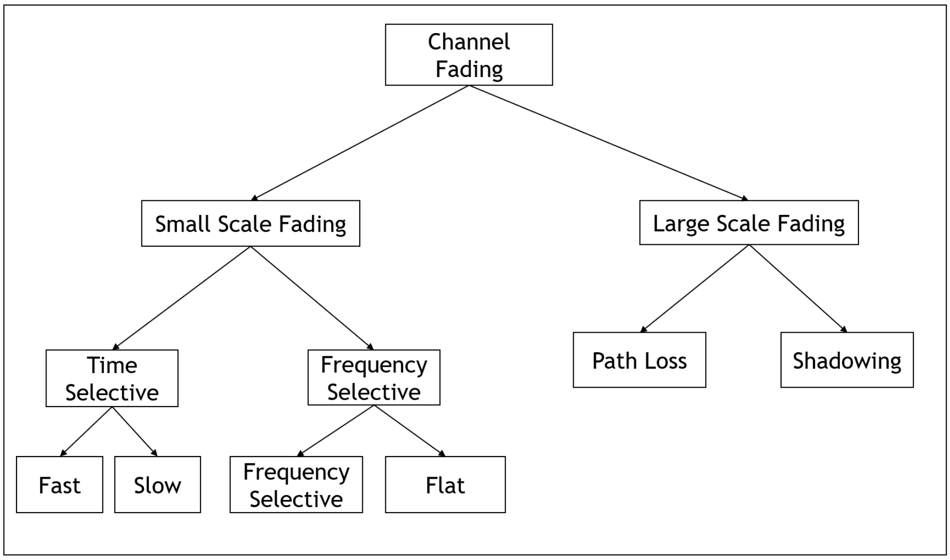


**Figure 3.6:** Fading and there categories

to rayleigh probability distribution function.

$$p(r) = \begin{cases} \frac{r}{\sigma^2} exp\left[-\frac{r^2}{2\sigma^2}\right] & r \leq 0 \\ 0 & otherwise \end{cases} \tag{3.23}$$

#### Rayleigh Fading

It is one of the worst kinds of fading and the reason behind that, it only contains multipath components. Rayleigh fading shows large amplitude fluctuation within a few wavelength distance travel by robot. Most of the time multipath components are in out phase or in-phase, they add up constructively and destructively shows high variation of resultant amplitude.

### 3.3.2 Large Scale Fading

Large-scale fading is caused by attenuation because of wave propagation over distance and diffracting by large objects. Large-scale fading occurs due to path loss and shadowing by large objects such as wall corners, big machines, etc. Large-scale fading occurs while the antenna moves in **20-40 or more wavelengths**. Usually, large-scale fading is frequency-independent.

#### Path Loss

In a scenario of free space signal power level varies by a factor of $1/d^2$, d is the distance between transmitting and receiving antenna [16], for NLOS(non-line of sight) the signal propagation varies by a factor of $1/d^3$ to $1/d^6$ [13].

#### Shadowing

It occurs when a signal is blocked by a big object such wall corner, mountain, building, or some big solid structure. Because of those big structures/objects, it takes time for a signal to pass through that, also called as slow fading. In an industrial factory environment, slow fading can occur, when robot moves around the corner, a signal may be blocked by big mechanical structure, etc [13].

# Chapter 4

# Problem Statement

The next evolution is happening under industry 4.0, which is considered intelligent, cyber-physical, IoT, and device-to-device connection-based. Device-to-device communication allows robots to communicate without needing an access point; all the devices work collaboratively and increase efficiency. 5G is inevitable for industry 4.0, but the mmWave band has some disadvantages, such as range, low SNR. Directional antenna system can be an option to improve the SNR and have less fading. To design algorithms for controlling the directional transmission/reception it is important to know the time dynamics of the directional propagation paths in both LOS and NLOS conditions, e.g., for the design of "beam handover" algorithms. Most of the channel characterization measurement [5], [8] at mmWave frequency seems not to be able to distinguish between amplitude variations caused by fast fading and NLOS to LOS transitions. It is crucial to know the reason for amplitude variation, fast fading which can be handled in the coding and modulation domain, while the transition of a line of sight to non-line sight can be handled by side links, TRP, and multiple UE connections. The existing RF directional channel characterization measurement method 2.5 where RF tones are separated in such a fading is uncorrelated is able to categorise amplitude variation. Next step is to finding coherence bandwidth, correlation between received RF tones, which will be used to defined coherence bandwidth.

## 4.1 Proposed Method

In this project, the focus will be on defining coherence bandwidth under different indoor environmental conditions. Defined coherence bandwidth based on channel characteristics will provide a baseline for frequency tone separation for the existing measurement technique 2.5. The benefit of the new measurement setup presented in this project is that, it uses sixteen RF tones while the existing measurement setup uses 4 RF tones over a bandwidth, principle of this measurement technique is same as existing method defined in section 2.5. Higher the number of RF tones gives more detailed channel characteristics and gives accurate coherence bandwidth value. Detailed data processing analysis will be done on measurement results; parameters like frequency correlation, Kfactor, multipath spread, and field strength response will be analyzed to define the coherence bandwidth.

# Chapter 5

# Measurement Setup

The measurement setup aims to have several RF carriers simultaneously over the air in the range bandwidth, where RF carrier tones are separated in the frequency domain. Correlation between received RF tones can be analyzed at the receiver side, correlation between RF tones will define coherence bandwidth under different channel condition.

The principle of this setup is to have sixteen continuous wave frequency tones, all these sixteen tones will be in the air all the time. At the receiver side each active antenna have access to all sixteen frequency tones at the same time. As shown in the figure 5.1, at transmitter side signal generator generates simultaneously 16 CW

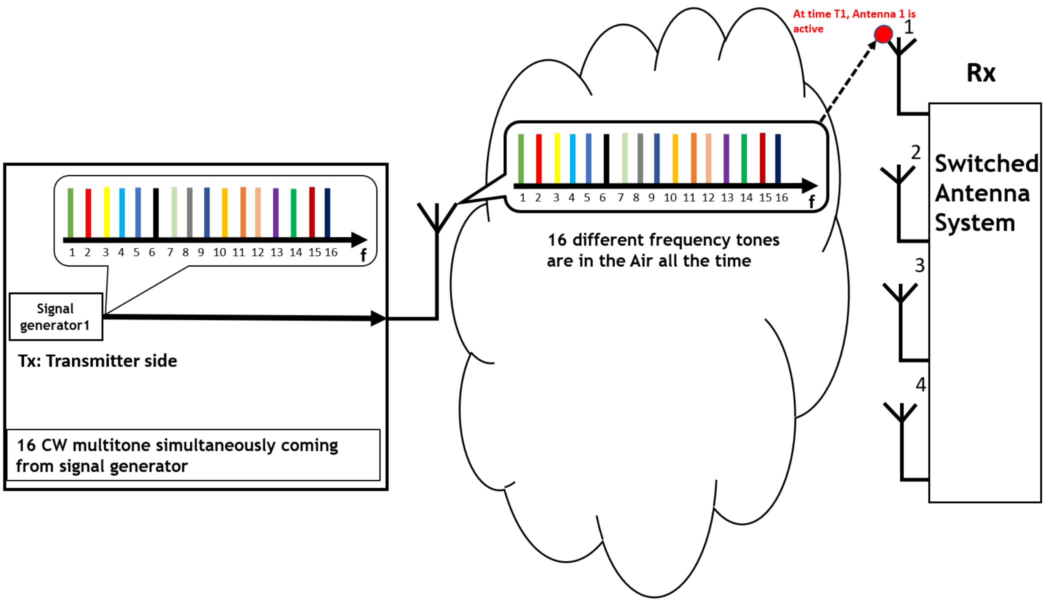


**Figure 5.1:** Measurement Setup diagram

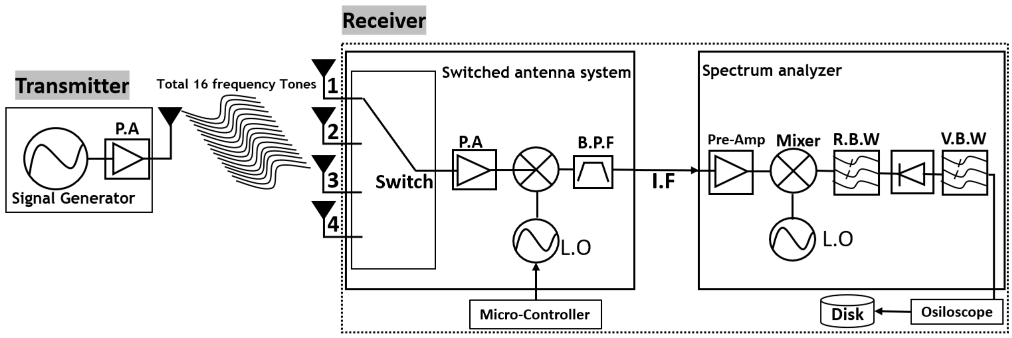


**Figure 5.2:** Block Diagram: Measurement Set-up

multione mentioned in table 5.7. Figure 5.3 shows the spectrum plot of 16 CW rf tones of signal generator.

| Tone | f1 | f2 | f3 | f4 | f5 | f6 | f7 | f8 | f9 | f10 | f11 | f12 | f13 | f14 | f15 | f16 |
|---|---|---|---|---|---|---|---|---|---|---|---|---|---|---|---|---|
| freq[MHz] | 27001 | 27002 | 27003 | 27004 | 27005 | 27006 | 27007 | 27008 | 27009 | 27010 | 27020 | 27030 | 27040 | 27050 | 27060 | 27070 |

**Table 5.1:** 16 CW multione simultaneously generated by signal generator : Tx

As shown in the figure 5.1, at receiver side the antenna will be active sequentially over the time, at a moment antenna 1 is active and it have access to all sixteen frequency tones which are present over the air. Local oscillator is programmed sequentially for sixteen carrier frequency which are used in down conversion of received RF signals. Corresponding 16 carrier frequency generated by local oscillator mentioned in table 5.2.

| Tone | f1 | f2 | f3 | f4 | f5 | f6 | f7 | f8 | f9 | f10 | f11 | f12 | f13 | f14 | f15 | f16 |
|---|---|---|---|---|---|---|---|---|---|---|---|---|---|---|---|---|
| freq[MHz] | 22001 | 22002 | 22003 | 22004 | 22005 | 22006 | 22007 | 22008 | 22009 | 22010 | 22020 | 22030 | 22040 | 22050 | 27060 | 22070 |

**Table 5.2:** 16 carrier frequency generated by local oscillator : Rx

At receiver side as shown in figure 5.2, switched antenna system consist of four antenna. All the sixteen frequency tones will be in the air all the time, as shown in figure 5.1, antenna 1 is active and it have access to all sixteen frequency tones. All the antennas will get active sequentially over time based on antenna selection switch and activation time is defined by total duration of sixteen tones, detailed discussion antenna selection and tone generation have been discussed in appendix A.4. Received RF signal from active antenna will pass into mixer for downconversion where carrier frequencies corresponds to tones( F + $\triangle$fj, j is 1 to 16) of defined duration feeded by local oscillator sequentially over time into mixer and downconverted IF output. Spectrum analyzer(set at zero span with lower resolution bandwidth(RBW)) takes IF output from mixer, and then video signal from spectrum analyzer passed into oscilloscope. Digital oscilloscope have been used to

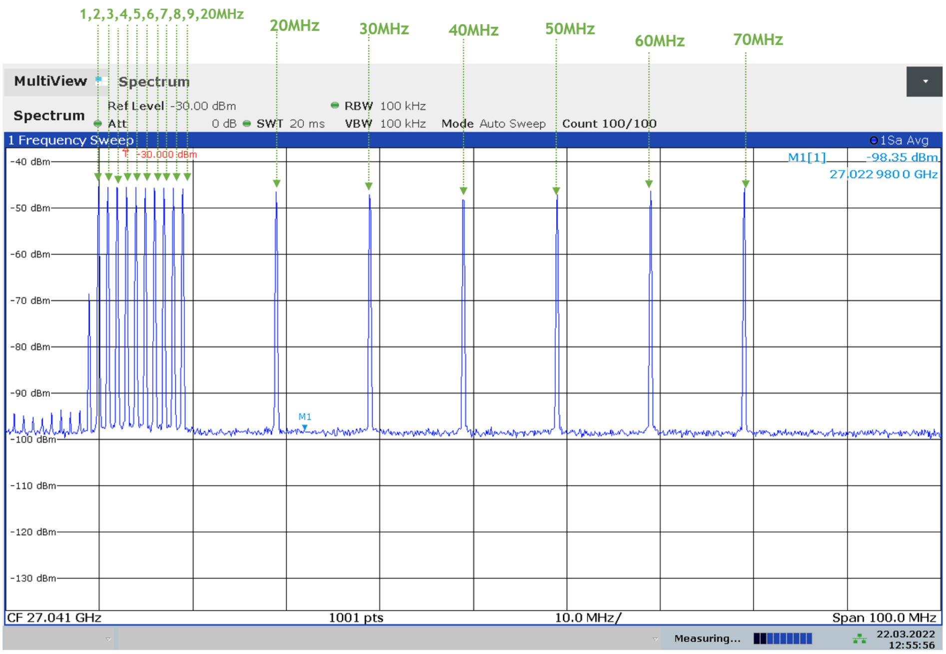


**Figure 5.3:** Spectrum Plot of Signal Generator

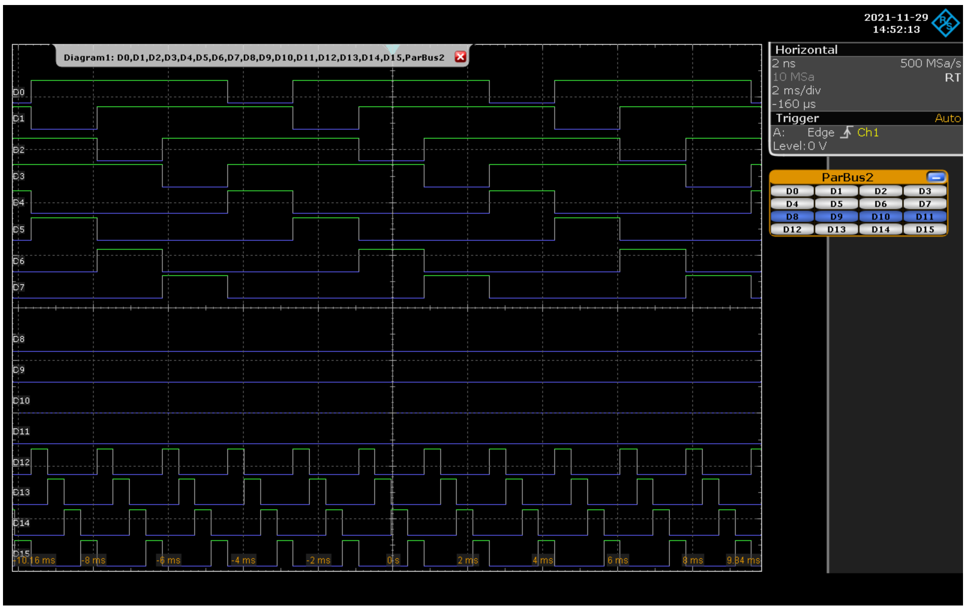


**Figure 5.4:** Digital Oscilloscope


**Figure 5.5:** Measurement Setup : location 1

capture and save the data in video signal format from spectrum analyzer. GPIO pins of raspberry pi corresponding to antenna selections have also been saved into analog channel of oscilloscope as shown in figure 5.4 to track the jittering effect, antenna selection bits will helpful in data processing.
The benefit of the measurement method presented in this section is that, it uses sixteen RF tones while other existing measurement technique presented in the section 2.5 uses 4 RF tones over a bandwidth, higher the number of RF tones gives more detailed channel characteristics and gives accurate coherence bandwidth value. Also using higher number of RF tones will provide wideband channel characteristics which is suitable for 5G.

## 5.1 Instrument Settings adjustment for Measurement Setup

### 5.1.1 Resolution Bandwidth

Based on the requirement from figure 5.6, total number of antennas at receiver side is 4(A), per tone duration is 400us(T) with 16 tones, robot moves with speed of 0.1m/s and total distance covered by robot is 5.12mm (0.1*N*T*A) over a cycle which is less than half wavelength. For one cycle of downconversion, the channel state will be the same if the distance traveled by robot is less than half the wavelength. If robot travels less than half wavelength in one cycle then it easy to visual the fast fading.
At the receiver side, spectrum analyzer is set on zero span with specified resolution bandwidth. Equation 5.1 show that lower resolution bandwidth leads to the

| MiR Speed(V) | Number of tones(N) | Each Tone Duration(T) | Number of antenna(A) | Distance travelled by MiR(d)= V*N*T*A | Min. Sampling time = 5.4mm / V |
|---|---|---|---|---|---|
| 0.1m/s | 4 | 400us | 4 | 0.64mm | 0.054s |
| 0.2m/s | 4 | 400us | 4 | 1.28mm | 0.027s |
| 0.3m/s | 4 | 400us | 4 | 1.92mm | 0.018s |
| 0.1m/s | 8 | 400us | 4 | 1.28mm | 0.054s |
| 0.2m/s | 8 | 400us | 4 | 2.56mm | 0.027s |
| 0.2m/s | 16 | 400us | 4 | 5.12mm | 0.018s |

**Figure 5.6:** Timing Table

lower noise floor, and it will provide more dynamic channel characteristics [20], but resolution bandwidth(RBW) need not to be lower than 1/2*T(tone duration) because the time response of filter start increasing beyond tone duration and it will be difficult to separate the tones in time domain analysis. Figure 5.7 shows resolution bandwidth analysis with four tones for four cases: case 1 with 3MHz, case 4 with 100KHz, case 2 with 10KHz and case 2 with 5KHz resolution bandwidth. It has been observed that for case 2 and 3 tone separation is not clear in time domain due to wide time response of IF filter which is comparable to tone duration, higher the resolution bandwidth narrower the time response of IF filter. It is important to find a balanced value of resolution bandwidth(RBW) with consideration of tone duration and noise floor.

$$NoiseFloor(dBm) = 10log(KTB), \tag{5.1}$$

where, K = Boltmann's constant (1.38$X10^{-23}J/K$; T = temperature (in degrees Kelvin); and B = bandwidth in which the noise is measured (in Hz).

### 5.1.2 Multi-tone Pattern

Multitones will provide channel information over the band and considered as wideband measurement, more the number of tones over the band lead to more detailed channel information over the band. Separation between each tone is chosen in such a way that frequency correlation can be calculated with 1MHz step size for 1 to 69MHz bandwidth, single antenna is transmitting all sixteen tones simultaneously.

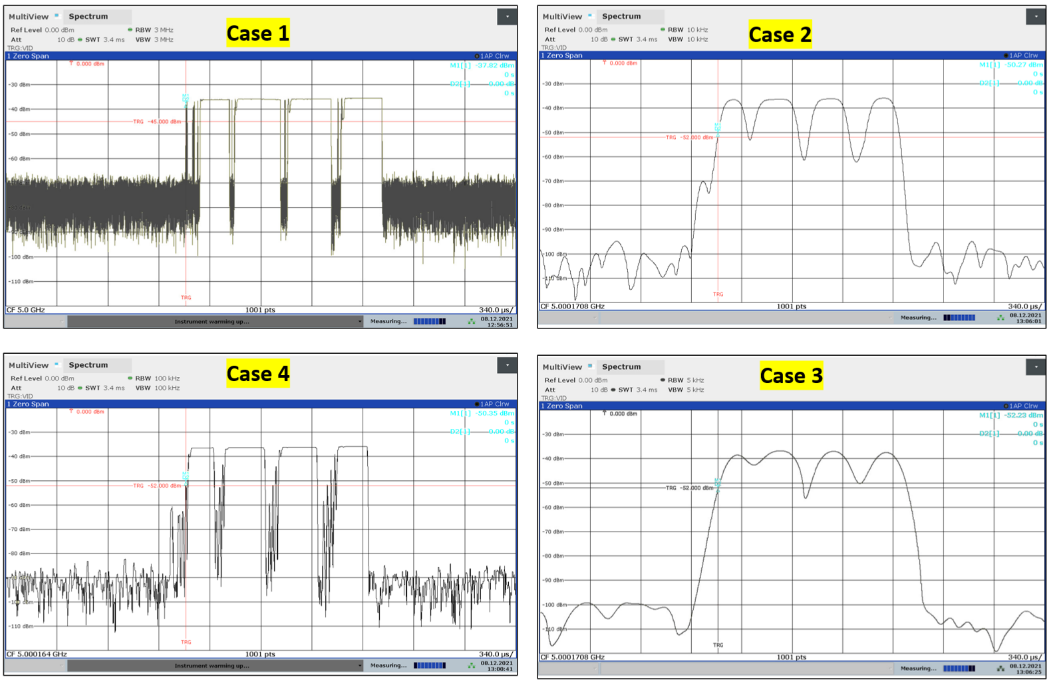


**Figure 5.7:** Resolution Bandwidth Analysis

## 5.2 Link Budget Analysis: Friis Free-space Pathloss, calculated

| | 1.3mt | 12mt | 16mt | 20mt | 30mt | Unit |
|---|---|---|---|---|---|---|
| Source/per CW frequency tones | -6.91 | -6.91 | -6.91 | -6.91 | -6.91 | dBm |
| Cable | -6.55 | -6.55 | -6.55 | -6.55 | -6.55 | dB |
| Tx Antenna Gain | 25 | 25 | 25 | 25 | 25 | dBi |
| | | | | | | |
| Friis Free-Space pathloss | -63.5 | -83 | -85.5 | -87.4 | -90.93 | dB |
| | | | | | | |
| Rx Antenna gain | 9.5 | 9.5 | 9.5 | 9.5 | 9.5 | dBi |
| Rx: front end and down converter | -1.5 | -1.5 | -1.5 | -1.5 | -1.5 | dB |
| Cables and Combiner | -8.4 | -8.4 | -8.4 | -8.4 | -8.4 | dB |
| Received Power | -52.39 | -71.70 | -74.20 | -76.60 | -79.10 | dBm |

**Table 5.3:** link Budget

- At transmitter side as mentioned in table 5.3, signal generator is able to feed around 8.64dbm of RF power and that is futher divided in sixteen tones(-6.91dBm/per tone).

- The cable connected from output port of signal generator to horn antenna have cable loss of -6.55dBm,
- As shown in in table 7.21, friis free space path loss have about -63.50dBm path loss at 1.3 mt and at 30 mt its about -90.93dbm.
- At receiver side, switched antenna system with four antennas spaced 90 degree with each other, the front-end for receiver configuration have almost -1.5 dbm gain.
- Reiceved power detected on spectrum analyzer at 1.3mt is -50.09 and -76.90 at 30mt.

## 5.3 Test equipment for Coherence Bandwidth Measurement

| **Brand** | **Name** | **Model** |
|---|---|---|
| Rohde Schwarz | Signal Generator | SMW200A |
| Rohde Schwarz | Spectrum Analyzer | FSW |
| Rohde Schwarz | Oscilloscope | RTO2064 |
| A-INFOMW | Octave horn antenna | LB-180400-25-C-KF |
| Raspberry Pi | Microcontroller | 4 |
| Rohde Schwarz | RF cables | |

**Table 5.4:** The used test equipment for the experiment.

| Model | LB-180400-25-C-KF |
|---|---|
| Frequency Range(GHz) | 18-40GHz |
| Gain(dBi) | 25 Typ |
| Polarisation | Linear |
| 3dB Beamwidth(deg): E-plane | 12-5 |
| 3dB Beamwidth(deg): H-plane | 13-7 |
| Cross Pol. Isolation(dB) | 40 Typ. |
| VSWR | 1.5:1 Typ. |

**Table 5.5:** Specification of transmitter antenna used in case 1 [2]

Figure 5.8 shows 2d radiation pattern of receiver antenna system which have been used in measurement. It contain 4 antennas, placed 90 degree to each other. All four antennas are controlled by sequential switching. Under ideal channel condition, the isolation between antenna 1 and 3, 2 and 4 is approximately 28.5dB, also the isolation between antenna 1 and 2, 3 and 4 is 27.5dB [19].

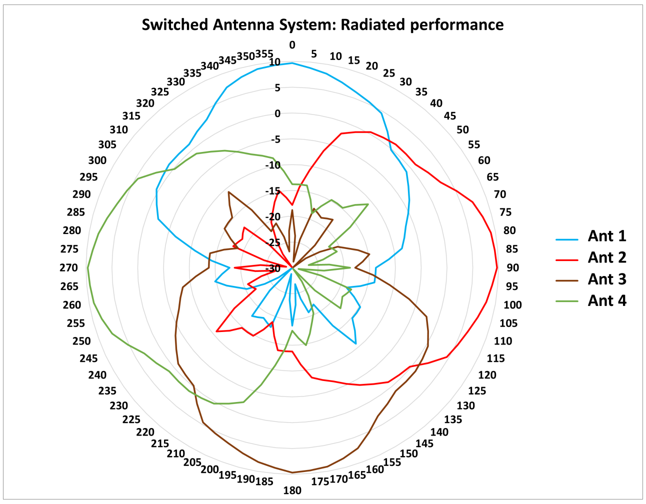


**Figure 5.8:** Switched Antenna System Radiation Pattern [19] : Receiver

### 5.3.1 Signal Generator Settings

| Supply RF power level | Supplied RF power/per tone | Gain per tone | Phase Shift |
|---|---|---|---|
| 8.64dBm | -6.91dBm | Same gain | zero phase shift |

**Table 5.6:** Signal Generator Settings

### 5.3.2 Oscilloscope and Spectrum Analyzer Settings

| Spectrum Analyzer | | | | | | | |
|---|---|---|---|---|---|---|---|
| Reference level | Range | Attenuation | Pre-Amplifier | Resolution bandwidth | Sweep time | Trigger | Baseband Frequency |
| -30dBm | 100dB | 0 | On | 100KHz | 20ms | Free run mode | 5.000177GHz |
| **Oscilloscope Settings** | | | | | | | |
| Video signal | Sampling rate | Channel 1 | Channel 2 | Channel 3 | Channel 4 | Single sweep | Data format |
| [Range = 0 to 1] volt | 100Ksample/sec | Rin : DC 50 Ω | Rin : DC 1 MΩ | Rin : DC 1 MΩ | Rin : DC 1 MΩ | avoid blind time | CSV |

**Table 5.7:** Oscilloscope and Spectrum Analyzer Settings

**The average noise floor which is at -114.40dBm and Average(Minimum hold[Noise Floor]) is between -128dBm to -142 dBm of the spectrum analyzer**.

### 5.3.3 Measurement Procedure

1. Transmitter side: Enable 16 tones with customised tone separation with respect to center frequency(27GHz) on signal generator and connect the output cable to antenna input port.

2. Receiver side: For down conversion of received signal(16 tones), corresponding 16 carrier frequency is generated in same order as TX side.

3. Receiver side: For down conversion of received signal(16 tones), corresponding 16 carrier frequency is generated in same order as TX side.

4. Set transmitter in position, depending on the specific case.

5. Start the single sweep of the Oscilloscope, and start moving the robot.

6. Once single sweep is done, Oscilloscope will stop capturing the data.

7. To save and export the captured single sweep data: Go to save option.

8. Save option –> Waveform –> Enable time stamp, select the CSV format and start exporting the data to specified location.

9. Change the transmitting Antenna –> Repeat the steps 4-8.

10. Data processing.

# Chapter 6

# Data processing

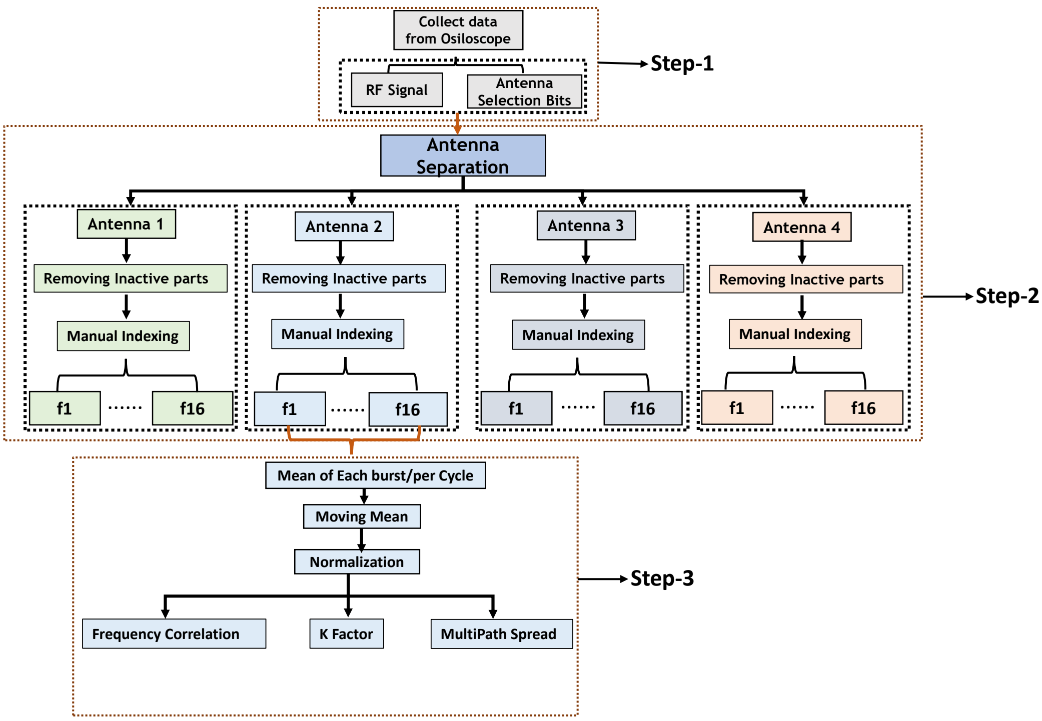


**Figure 6.1:** Block Diagram for Data Processing

The aim of data processing is visualization of collected data which will help in defining the coherence bandwidth. Figure 6.1 shows block diagram of data processing, it contains 3 main steps. As discussed in measurement setup chapter, oscilloscope is used to store the data. The output of the oscilloscope is stored in the time domain form(video signal), and therefore the time domain characteristics can be directly plotted. The data processing aims to calculate the frequency correlation,

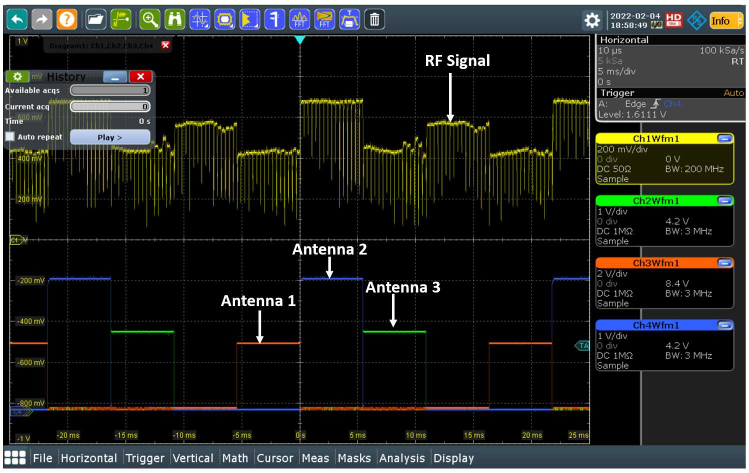


**Figure 6.2:** RF signal with antenna selection bits : Digital Oscilloscope

Multipath spread, and K factor. Based on the value of frequency correlation, the coherence bandwidth will be defined for each antenna. Figure 6.1 shows the block diagram of data processing for each step.

### 6.0.1 Step 1 : Antenna Separation

- Collect the video time signal with a corresponding logic bit(antenna selection) from the oscilloscope. Antenna selection logic bits will be helpful in separating the RF signal corresponding to each RX antenna of a switched antenna system, switching between antennas happening sequentially with a defined duration of 400us.

- RTO 2064 has four analog channels: channel one is connected with a spectrum analyzer for processing of video signal, remaining three-channel are connected with three antennas( antenna selection bit) out of 4. Figure 6.2 shows RF signal with antenna selection bits response plot on oscilloscope.

- **Volt(Video Signal) to dBm Conversion:** Given RefrenceLevel=-30dBm and milliVolt/division = 100. Video Signal from spectrum analyzer is 0 volt = -130 dBm and 1 volt = -30dBm. Equation 6.1 is conversion formula for volt( video signal) to dBm.

$$Antenna_{i_{dBm}} = ReferenceLevel + 10^4 * (Antenna_{i_{volt}} - 1)/(milliVolt/division) \tag{6.1}$$

- **dBm to mmWatt Conversion:**

$$Antenna_{i_{mWatt}} = 10^{(Antenna_{i_{dBm}}/10)} \tag{6.2}$$

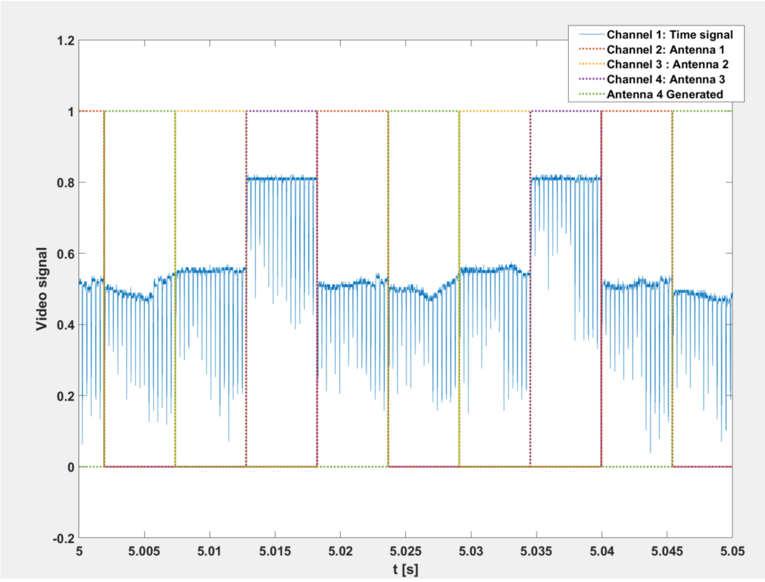


**Figure 6.3:** Video time signal and corresponding logic bits of antennas

- As shown in figure 6.2 only antenna(1, 2, and 3) bits are captured because of constraints on the number of ports on an oscilloscope, bits corresponding to antenna 4 selection will be generated by the inactive bits('0') of the common part of antenna 1, 2 and 3: which correspond active duration of antenna 4. Figure 6.3 shows analog time signal(channel 1), and the remaining 3 channels correspond to digital antenna selection bits and generated bits for antenna 4.

- $Rx_i$(i=1, 2, 3 and 4) which corresponds to logic bits of antenna selection. Time signal(RF signal) response of $Antenna_i = [videosignal]. * [Rx_i]$ as shown in figure 6.4, In the same way response of each antenna is generated as shown in column 6, 7, 8, and 9 of figure 6.4.

- As shown in figure 6.5, each antennas are active periodically and it means there will be break points which corresponds to inactive state of antenna where Rx1, Rx2, Rx3 and Rx4 logic are 0 as shown in table 6.4 column 2, 3, 4, and 5. For frequency correlation calculation break points need to be removed in defined order for each antenna for each cycle( [One cycle] = [Number of antenna]*[Number of tones]*[Tone duration] ). Figure Table 6.1 shows antenna 1 response after removing the break points( where antenna 1 is inactive) and stacking each cycle in column for each antenna.

| Video signal | Rx1 logic | Rx2 logic | Rx3 logic | Rx4 logic | Time signal*Rx1= Antenna 1 response | Time signal*Rx2= Antenna 2 response | Time signal*Rx3= Antenna 3 response | Time signal*Rx4= Antenna 4 response |
|---|---|---|---|---|---|---|---|---|
| f1 (Rx1) | 1 | 0 | 0 | 0 | f1 (Rx1) | 0 | 0 | 0 |
| : | : | : | : | : | : | : | : | : |
| f16 (Rx1) | 1 | 0 | 0 | 0 | f16 (Rx1) | 0 | 0 | 0 |
| f1 (Rx2) | 0 | 1 | 0 | 0 | 0 | f1 (Rx2) | 0 | 0 |
| : | : | : | : | : | : | : | : | : |
| f16 (Rx2) | 0 | 1 | 0 | 0 | 0 | f16 (Rx2) | 0 | 0 |
| f1 (Rx3) | 0 | 0 | 1 | 0 | 0 | 0 | f1 (Rx3) | 0 |
| : | : | : | : | : | : | : | : | : |
| f16 (Rx3) | 0 | 0 | 1 | 0 | 0 | 0 | f16 (Rx3) | 0 |
| f1 (Rx4) | 0 | 0 | 0 | 1 | 0 | 0 | 0 | f1 (Rx4) |
| : | : | : | : | : | : | : | : | : |
| f16 (Rx4) | 0 | 0 | 0 | 1 | 0 | 0 | 0 | f1 (Rx4) |
| f1 (Rx1) | 1 | 0 | 0 | 0 | f1 (Rx1) | 0 | 0 | 0 |
| : | : | : | : | : | : | : | : | : |
| f16 (Rx1) | 1 | | | | f16 (Rx1) | 0 | : | 0 |
| : | : | : | : | : | : | : | : | : |

**Figure 6.4:** Antenna response generation

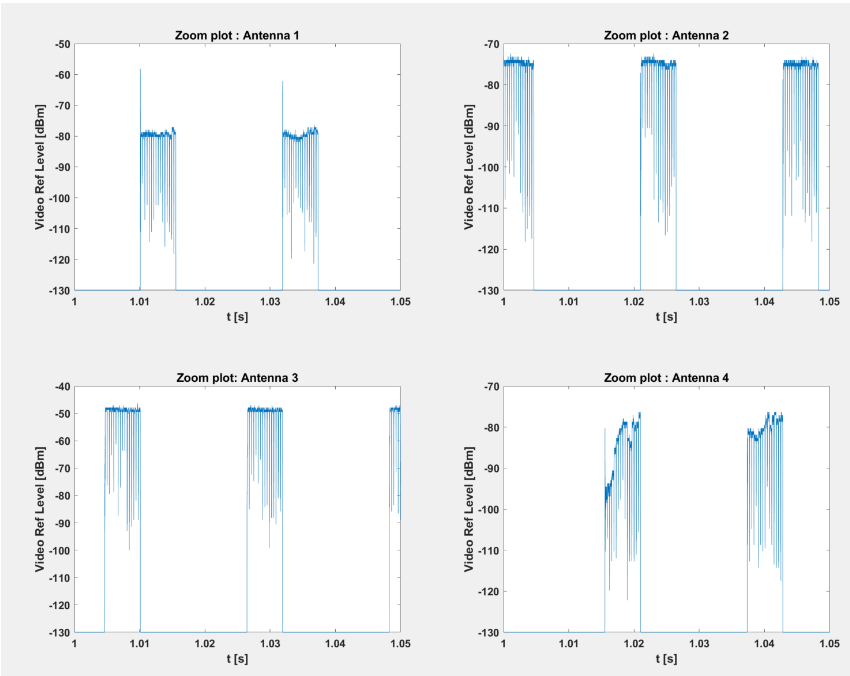


**Figure 6.5:** Time response after time grating

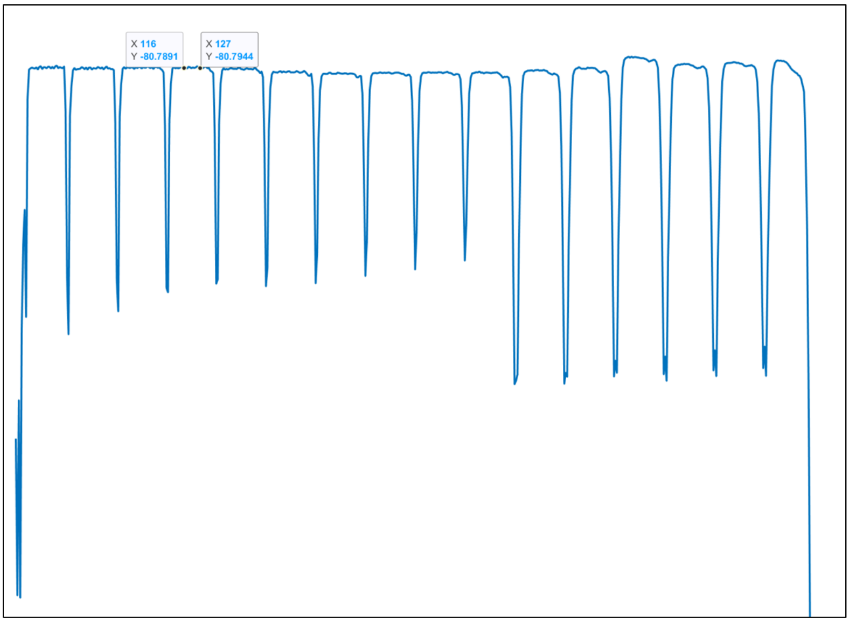


**Figure 6.6:** Manual indexing of RF tones : Tone tracker

| Cycle 1 | Cycle 2 | ........ | Cycle N-1 | Cycle N |
|---|---|---|---|---|
| f1(Rx1) | f1(Rx1) | f1(Rx1) | f1(Rx1) | f1(Rx1) |
| f2(Rx1) | f2(Rx1) | f2(Rx1) | f2(Rx1) | f2(Rx1) |
| f3(Rx1) | f3(Rx1) | f3(Rx1) | f3(Rx1) | f3(Rx1) |
| : | : | : | : | : |
| : | : | : | : | : |
| f15(Rx1) | f15(Rx1) | f15(Rx1) | f15(Rx1) | f15(Rx1) |
| f16(Rx1) | f1(Rx1) | f16(Rx1) | f16(Rx1) | f16(Rx1) |

**Table 6.1:** Table after break point removed from Antenna 1(Rx1) response

### 6.0.2 Step 2: Frequency Separation

- For frequency correlation calculation, further each tones of corresponding antenna need to separated, which is done based on manual observation. As we know all the cycles which contain jittering affect(discussed in A.2) already have been removed, so choosing manual index for each RF tone is correct way, and they periodically follow same order for the cycle. Example shown in figure 6.6 with the help markers for frequency tone 4(f4).
- Once all the sixteen tones of corresponding antenna are separated, each tone have burst of 7 data points per cycle which is chosen manual indexing. $P_{f_i}(t_i)$ is power envelope response of frequency tone $f_i$ per cycle (each cycle contain

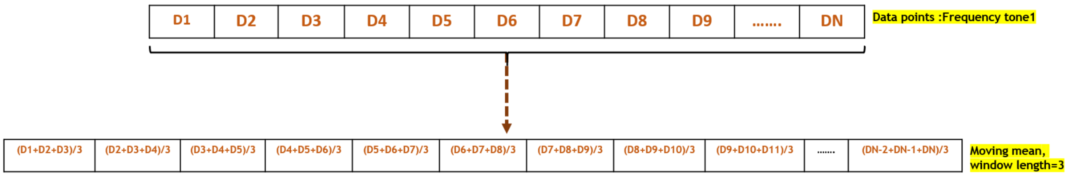


**Figure 6.7:** Example case for moving mean calculation with window length of 3

seven data points per tone(i)), unit can be in dBm or mmWatt. $P_{f_i}(tc)$ is the average of all data points per cycle for f(i) frequency tone, similarly for all the tones.

$$P_{f_i}(tc) = \frac{1}{7}\sum_{i=1}^{7} P_{f_i}(t_i)) \tag{6.3}$$

- Next step after averaging the burst. Moving average of each tones is calculated, as shown in figure 6.7 with example case, where data points of frequency tone is transformed into moving mean with window length(K=3). In general window length(k) need to be in between 20*lamda to 40*lamda( wavelength of center frequency), to track the shadowing affect only [23]. Top section of figure 6.8, trace with black colour is moving mean of separated frequency tone, orange and blue plot shows normalized field strength in dBm and mmWatt respectively. $\overline{P_{f_i}(tc)}$ is moving mean of frequency tone $f_i$. $P_{f_i}\hat{(}tc)$ is normalized response of $P_{f_i}(tc)$ with respect to $\overline{P_{f_i}(tc)}$, referred as normalized field strength.

$$\overline{P_{f_i}(tc)} = \frac{1}{K}\sum_{i=1}^{K} P_{f_i}(tc)) \tag{6.4}$$

$$P_{f_i}\hat{(}tc) = \frac{P_{f_i}(tc)}{\overline{P_{f_i}(tc)}} \tag{6.5}$$

### 6.0.3 Step 2 : Evaluation Matrixes

- Frequency correlation is defines the statistical relationship between two frequency components response, it can be in term of amplitude, phase, or both.

$$F(P_{f_i}\hat{(}tc), P_{f_i}\hat{(}tc)) = \frac{1}{N-1}\sum_{i=1}^{N}\left(\frac{P_{f_i}\hat{(}tc) - \mu_{P_{f_i}\hat{(}tc)}}{\sigma_{P_{f_i}\hat{(}tc))}}\right)\left(\frac{P_{f_j}\hat{(}tc)) - \mu_{P_{f_j}\hat{(}tc)}}{\sigma_{P_{f_j}\hat{(}tc)}}\right) \tag{6.6}$$

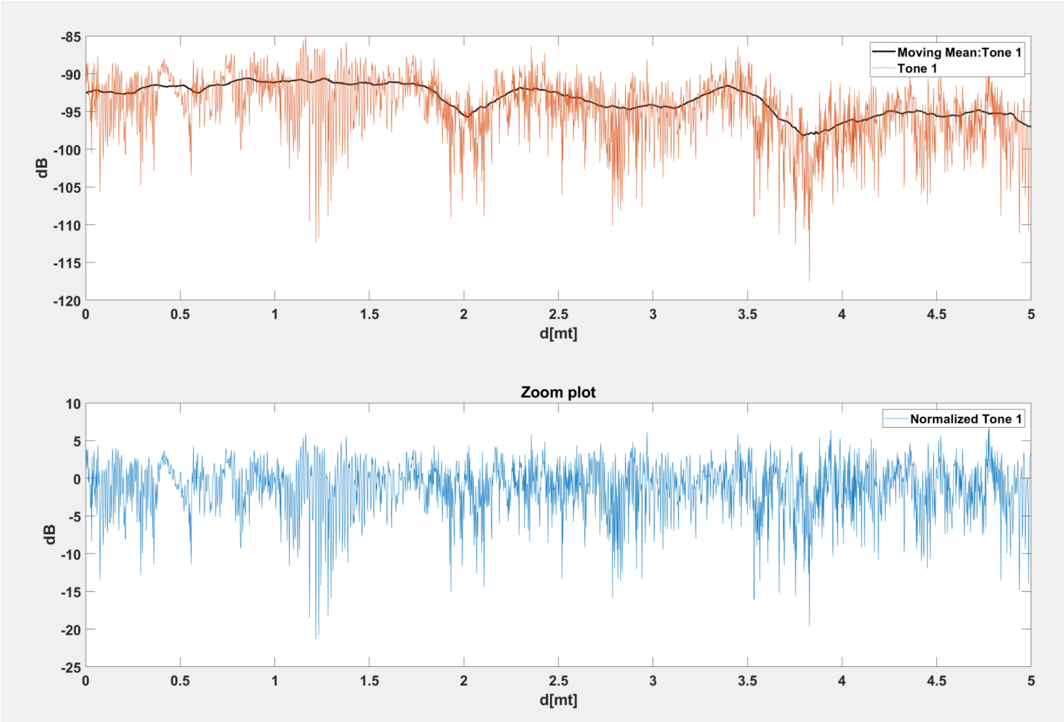


**Figure 6.8:** Normalized field strength and moving mean of frequency Tone 1

$F(P_{f_i}\hat{(tc)}, P_{f_j}\hat{(tc)})$ is frequency correlation between normalized field strength response of two frequency tones $P_{f_i}\hat{(tc)}$ and $P_{f_j}\hat{(tc)}$ [17]. $\mu_{P_{f_i}\hat{(tc)}}$ and $\sigma_{P_{f_i}\hat{(tc)}}$ are mean and variance of $P_{f_i}\hat{(tc)}$, $\mu_{P_{f_j}\hat{(tc)}}$ and $\sigma_{P_{f_j}\hat{(tc)}}$ are mean and variance of $P_{f_j}\hat{(tc)}$.

- In a communication system, all the propagating wave does not reach directly to receiver, propagating wave comes under affect of reflection, diffraction, and reflection which makes them multipath components. MS is the Multipath Spread between two frequency tones, based on analysis done in paper [4], two frequency tones are separated by f [Hz] of bandwidth. $P_{f_i}\hat{(tc)}$ and $P_{f_j}\hat{(tc)}$ are envelopes of two carriers which corresponds to normalized field strength calculated in step 8. Equation 6.10 is normalized field strength difference between two frequency tones, and multipath spread can be calculated with equation 6.9, $f_i - f_j$ = f is frequency separation between two components.

$$dP_f\hat{(tc)} = \frac{P_{f_i}\hat{(tc)} - P_{f_j}\hat{(tc)}}{f} \approx \frac{dP_f(tc)}{df} \tag{6.7}$$

$$MS = \frac{1}{\pi\alpha}\sqrt{\frac{\overline{dP_f(tc)^2}}{\overline{P_{f_j}\hat{(tc)}^2}}} \tag{6.8}$$

- pdf($P_{f_i}(tc)$) is rician distribution of the frequency tone $f_i$, $\mu_{P_{f_j}(tc)}$ and $\sigma_{P_{f_j}(tc)}$ is mean and variance of rician distribution of $P_{f_i}(tc)$ respectively.

$$pdf(P_{f_i}(tc)) = \frac{P_{f_i}(tc)}{\sigma_{P_{f_i}(tc)}{}^2} exp\left[-\frac{P_{f_i}(tc)^2}{2\sigma_{P_{f_i}(tc)}{}^2}\right] \tag{6.9}$$

K-factor estimate is the ratio of specular power(from direct path) to scattered power(from indirect path) [9].

$$Kfactor = \frac{(\mu_{P_{f_i}(tc)})^2}{(\sigma_{P_{f_i}(tc)})^2} \tag{6.10}$$

## 6.1 Measurement for Sanity Check

### 6.1.1 Noise Floor Test

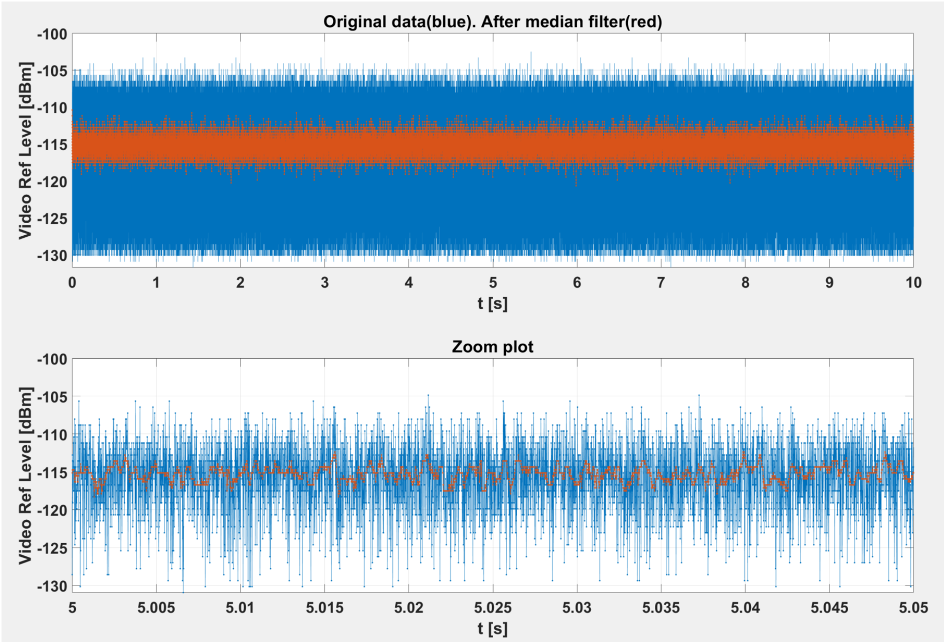


**Figure 6.9:** Noise Floor Testing, average noise floor = 114.40 dBm

To know the reference level of your measurement, its important to find out the lower limit, and it will be helpful to perform the sanity check on the measurements results. For the noise floor test, the transmitter is turned off through signal generator that means the Tx antenna is not transmitting any waves, while at the receiver side the process is normal such as PLL is generating carrier frequency tones and downconversion taking place, also the settings of spectrum analyzer and oscilloscope are same.
Figure 6.9 shows power level of 10 second captured data's, its clearly visible that noise power level varies between -105 to 130 dBm shows by blue plot and average power level shown by orange plot at around -115dBm. Figure 6.10 shows frequency correlation plot, K factor, and multipath spread plot, frequency correlation are below 0.2, K factor is between 0 to 2.5 over the whole frequency band of 1 to 69MHz. Multipath spread(max approximately 210ns) decreases as the bandwidth increases.

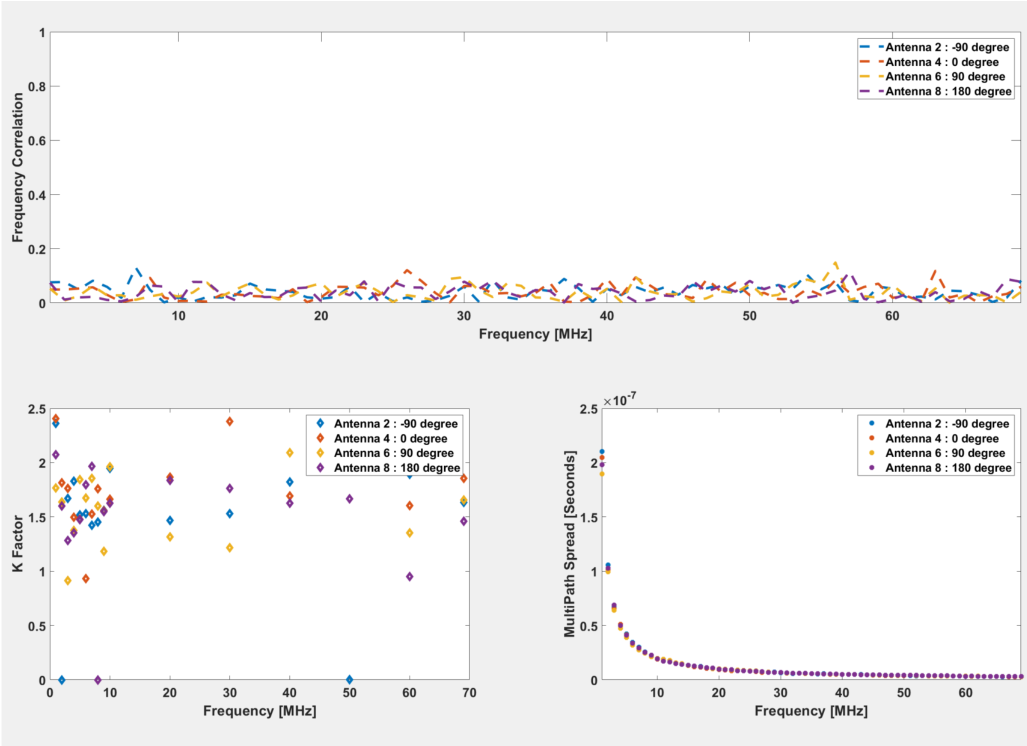


**Figure 6.10:** Frequency Correlation : Noise floor Testing

### 6.1.2 Conducted Testing

Similar to noise floor test, conducting test is also used for sanity check on the real measurements, In conducted testing the output port of signal generator(Tx) is directly connected via coax cable to the input port of spectrum analyzer that means there no channel effect on the measurement, and it provide over all affect of Rx and Tx instruments, setting of Tx and Rx instruments are same as real measurement setup. Figure 6.11 shows power level(dBm) over a period of 10 seconds, only antenna 6 is active remaining antennas are inactive, but because of the coupling affect the antenna 4 have also strength of around -95dBm, but we are focusing only one antenna that is antenna 6 which shows stable power level around -55dBm over all 16 sixteen frequency.

Figure 6.12 shows frequency correlation estimation, K factor and multipath spread for all antennas, frequency correlation is below 0.1 over the frequency band, K factor factor for antenna 6 it lies between 140-150, approximately 50 for antenna, while remaining antennas are are close 0 over the band. Multipath spread(max approximately 178ns) decreases as the bandwidth increases.

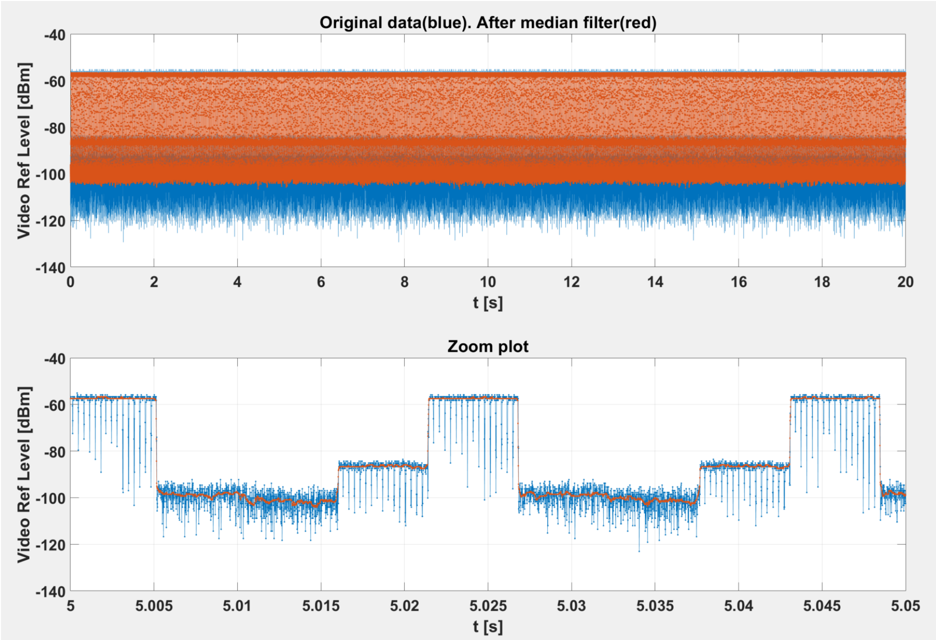


**Figure 6.11:** Conducted Testing, average noise floor = 114.40 dBm

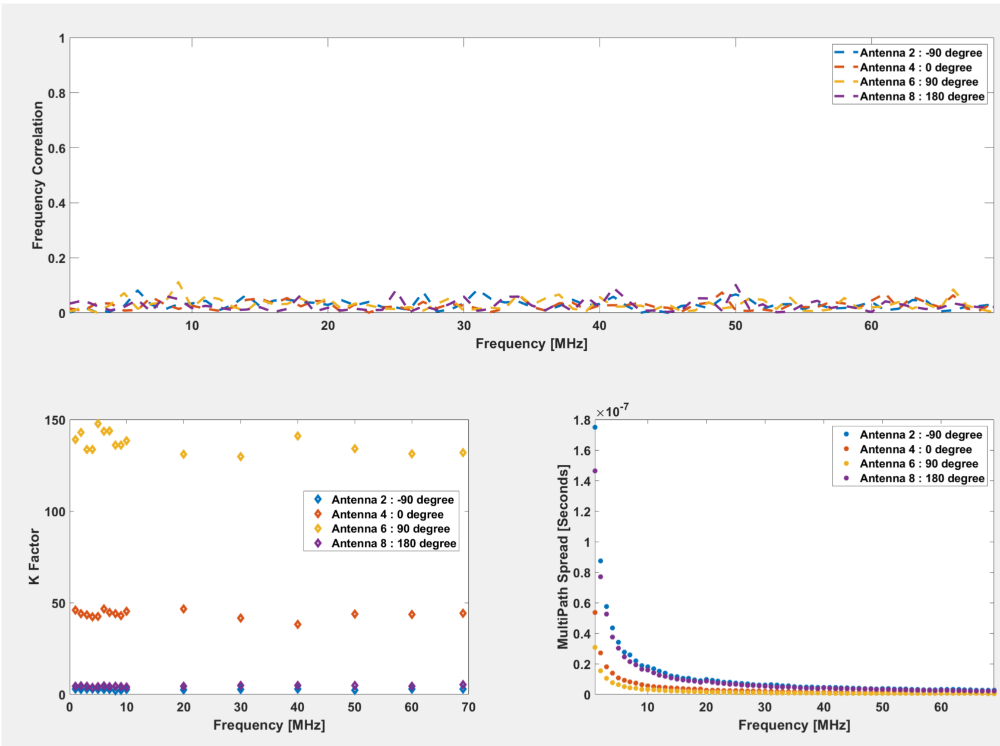


**Figure 6.12:** Frequency Correlation : Conducted Testing

# Chapter 7

# Results

In this project, a series of measurements have been performed under different indoor environments condition. A total of four measurements have been done under indoor environmental conditions in a typical office setting that mimics an industrial environment. As discussed in the data processing section, the collected measurement data have been analyzed. Based on data processing, the coherence bandwidth has been defined for each measurement.
On the receiver, a switched antenna system has been used, which contains four antennae, the Tx setup is stable, and the Rx setup is moving with the help of a human hand( He[Arun] is always standing in front of the antenna 8). The orientation of antenna may change for each measurement depend location. Orientation of each antenna from each measurement have mentioned in table 7.1.
For each measurement, field strength plot of **frequency tone 1** (one of tone out 16 RF tones) and **moving mean of frequency tone 1** also included in the result, also include friis free space, and indoor : 3GPP TR 38.901 model path loss plots [11] with respect to current measurement set-up.
Plot like frequency correlation, K-factor, and multipath spread are analyzed. Based on the plots from each measurement, coherence bandwidth will be defined for each antenna from switched antenna system.

| Measurement Number | Antenna 1 | Antenna 2 | Antenna 3 | Antenna 4 |
|---|---|---|---|---|
| 1 | NLOS | LOS | NLOS | NLOS |
| 2 | NLOS | LOS | NLOS | NLOS |
| 3 | NLOS | NLOS | NLOS | NLOS |
| 4 | NLOS | LOS | NLOS | NLOS |

**Table 7.1:** Antenna Orientation for Each Measurement

## 7.1 Measurement 1

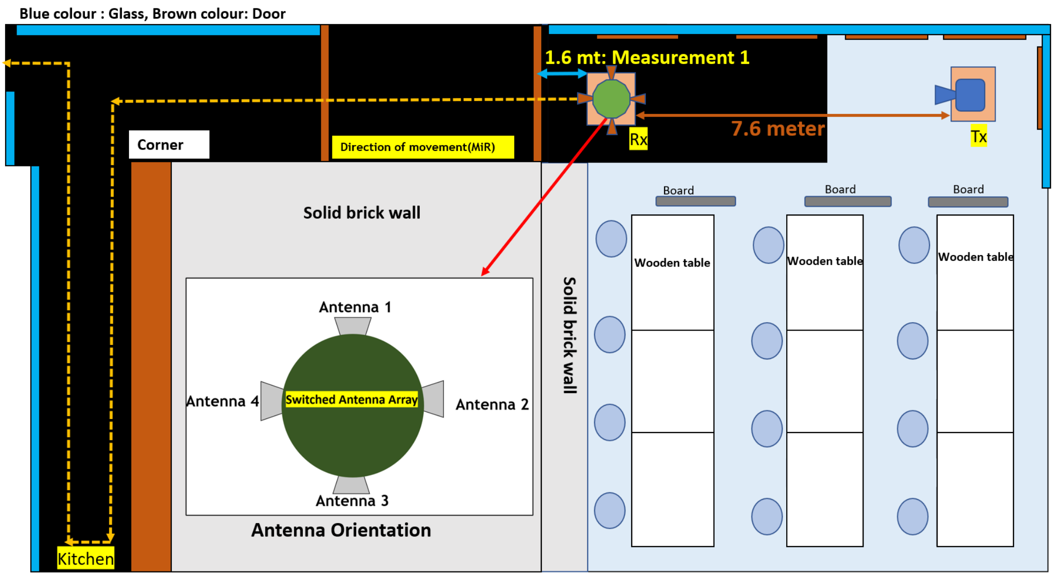


**Figure 7.1:** Identified path for Robot : Measurement 1

Each Rx antenna have a different orientation. As mentioned in the table 7.1 antenna 1 is NLOS, antenna 2 is LOS, antenna 3 is NLOS, and antenna 4 is NLOS with respect to transmitter. Rx switched antenna system will provide omnidirectional coverage of the indoor environment. Map of the measurement 1 shown in figure7.1, at the start of measurement distance between RX-TX is 7.6 mt. Rx moves 1.6 meter during measurement 1.

- Figure plot 7.2 shows field strength plot for antenna 1, 3, and 4. Friis free space 1 and LOS : 3GPP model 4 is approximately 20-25 dB higher than **moving mean: frequency tone1** curve. Antenna 1, 3, and 4 are in non-line of sight. Losses such as diffraction, reflection, and scattering, which have been not included in the friis space and LOS : 3GPP model.

  Antenna 1 and 3 are in non-line of sight with respect to transmitter, hence they are receiving reflected component. Distance between transmitter and receiver is 7.6 mt, based on observation the approximated angle of incidence is 40 degree, then the reflection will be -6.30 dBm based on table 3.2 and gain of the point where reflection component will strike is approximately -5dB, which lead to approximately 22dB drop in field strength with respect friis free space and LOS : 3GPP model. As clearly shown in plot 7.2, **moving mean of tone 1** also have dropped approximately 20-25 dB.

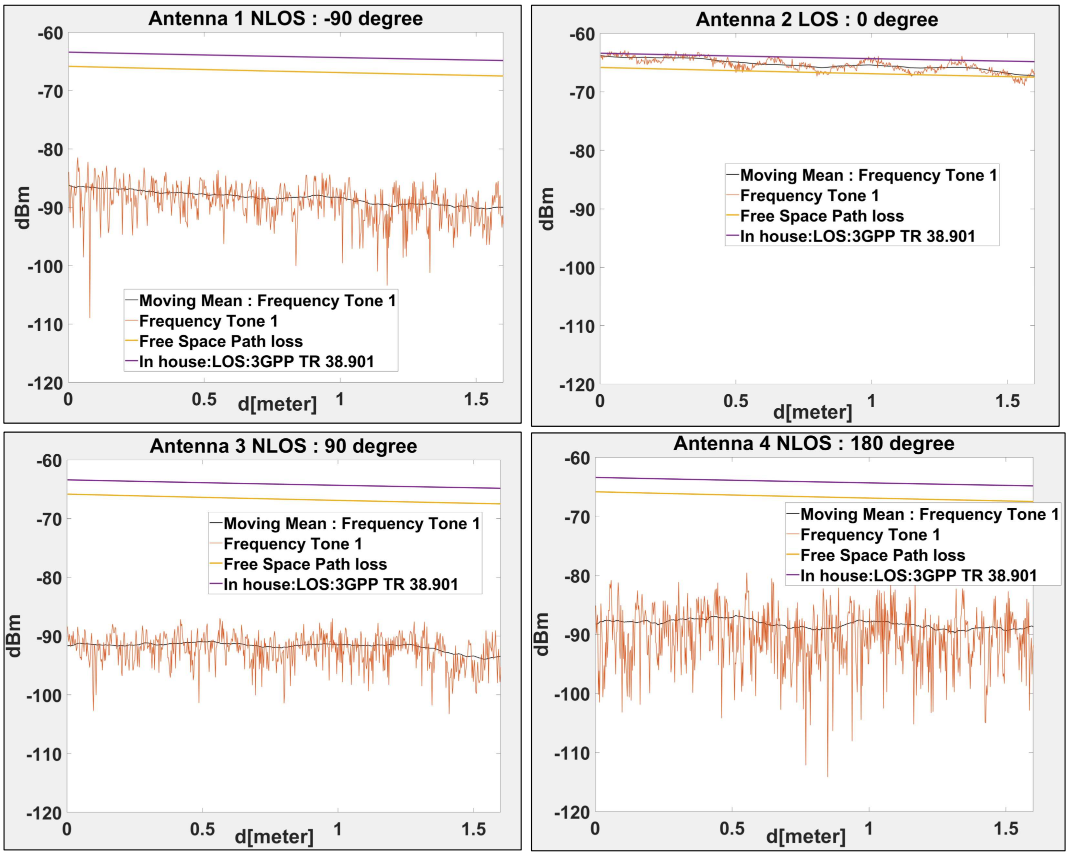


**Figure 7.2:** Field Strength plot [dBm], average noise floor = 114.40 dBm

Antenna 2 (LOS) field strength curves closely follow the friis free space and LOS: 3GPP model 7.2, and there are not many losses due to reflection, diffraction, and scattering because most of the rf received signals are direct components. Antenna 4 is exactly 180 degrees from antenna 2, and it will receive direct components but on its back lobe. Isolation between antenna 2 and 4 is approximately 27.5dB. Also, the difference in strength level between antenna 2 and 4 is approx 25 dB, which is also clearly visible from plot 7.2.

- Figure 7.3 shows the plots of frequency correlation. Antenna 1(NLOS) frequency correlation is around 0.8 for the first 10MHz, drops to 0.6 at 20MHz, 0.4 at 30MHz, and then drops to 0.2 at 69MHz. Antenna 2(LOS) shows a high-frequency correlation of more than 0.6 over the band of 0 to 69MHz. Antenna 3(NLOS) frequency correlation is above 0.4 for bands 0 to 13MHz and then drops to 0.1 for higher frequency bands. Antenna 4(NLOS) frequency correlation is above 0.4 over the band 0 to 50 MHz and drops to 0.3 at 69MHz.

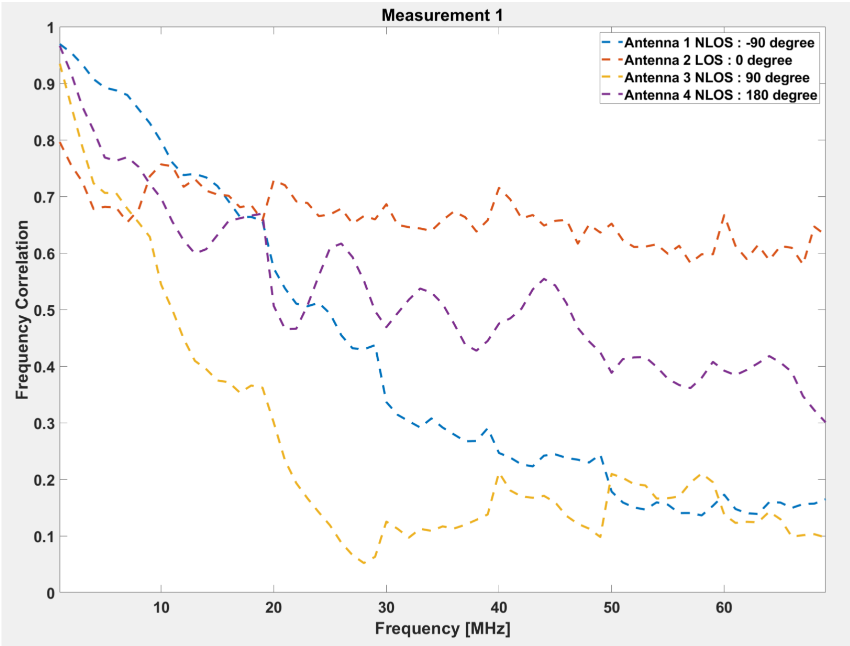


**Figure 7.3:** Frequency Correlation : Measurement 1

- Figure 7.4 shows the K factor plot. K factor is approximately 6-9 for antenna 2(LOS)over the band and mostly receives direct components. For antennas 1, 3, and 4, the k-factor is approximately zero, and this makes sense as we are mostly getting multipath components directly from the glass.

- Figure 7.5 shows a multipath spread plot; for all the antennae, the multipath-spread decreases as the frequency separation increases.

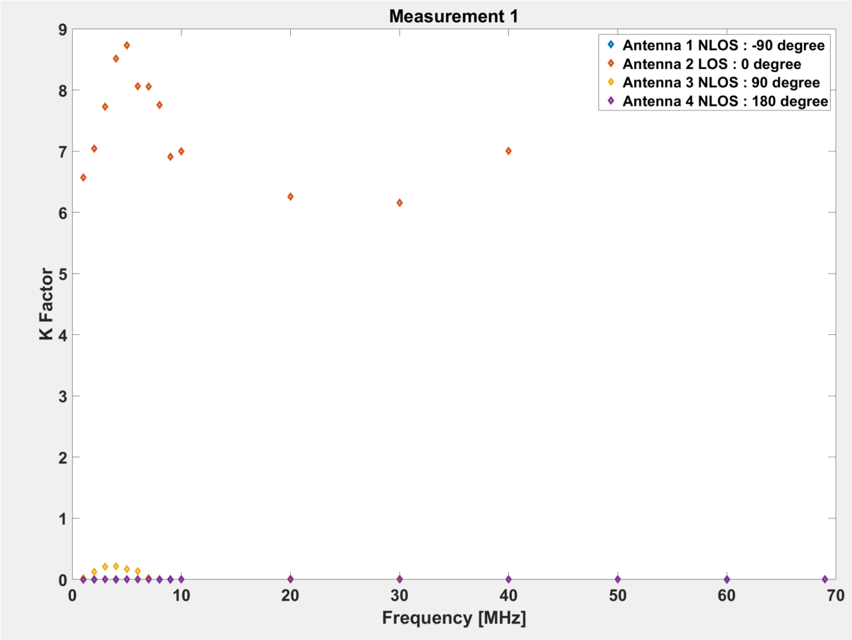


**Figure 7.4:** K-factor: Measurement 1

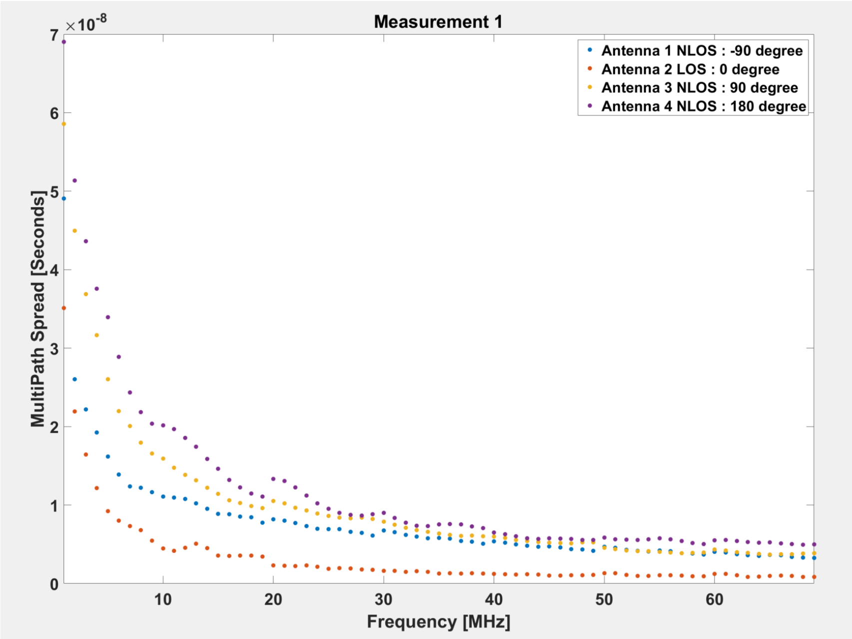


**Figure 7.5:** Multi-Path Spread: Measurement 1

## 7.2 Measurement 2

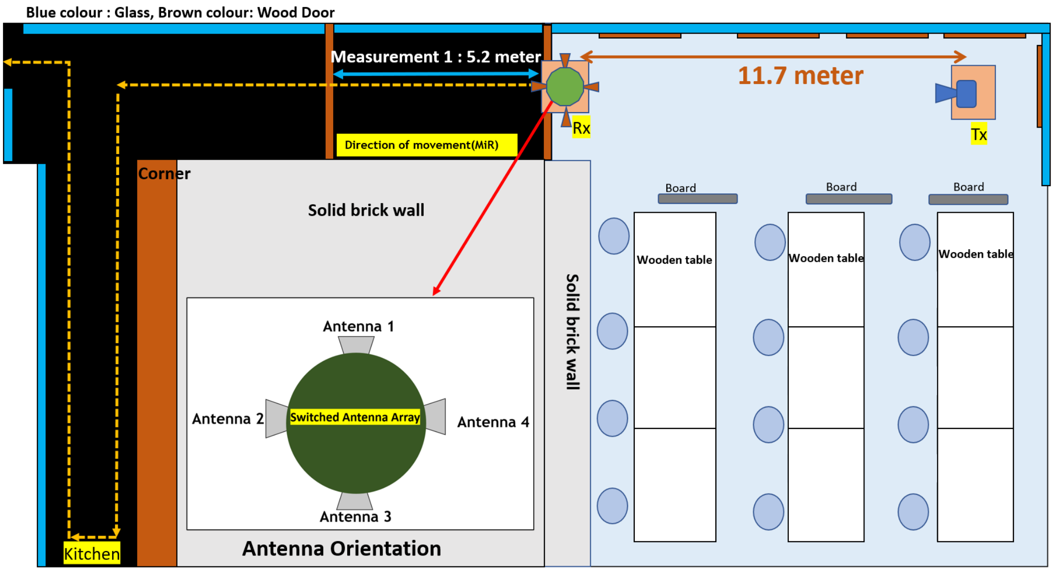


**Figure 7.6:** Identified path for Robot : Measurement 2

Each Rx antenna have a different orientation. As mentioned in the table 7.1 antenna 1 is NLOS, antenna 2 is LOS, antenna 3 is NLOS, and antenna 4 is NLOS with respect to transmitter. Map of the measurement 2 shown in figure 7.6, at the start of measurement the distance between reciever and transmitter is 11.7mt. Rx moves 5 meter during measurement 2.

- Field strength plot 7.7 shows field strength plot for antenna 1, 3, and 4, friis space and LOS : 3GPP model is approximately 20-30 dB higher than **moving mean frequency tone1** curve. Antenna 1, 3, and 4 are in non-line of sight, and it includes a type of loss such as diffraction, reflection, and scattering, which have been not included in the friis free space and LOS : 3GPP model.
  Antenna 2 (LOS) field strength curves closely follow the friis free space and LOS: 3GPP model 7.7, and there are not much loss due to reflection, diffraction, and scattering because most of the received signals are direct components. Antenna 4 is exactly 180 degrees from antenna 2, and it will receive direct components but on its back lobe. Isolation between antenna 2 and 4 is approximately 27.5dB. Also, the difference in strength level between antenna 2 and 4 is approx 25 dB, which is also clearly visible from plot 7.7.
  Antenna 1 and 3 are in non-line of sight from transmitter, hence they are receiving reflected component. Distance between receiver and transmitter is 11.7mt, based on observation the angle of incidence is 30 degree, lead to

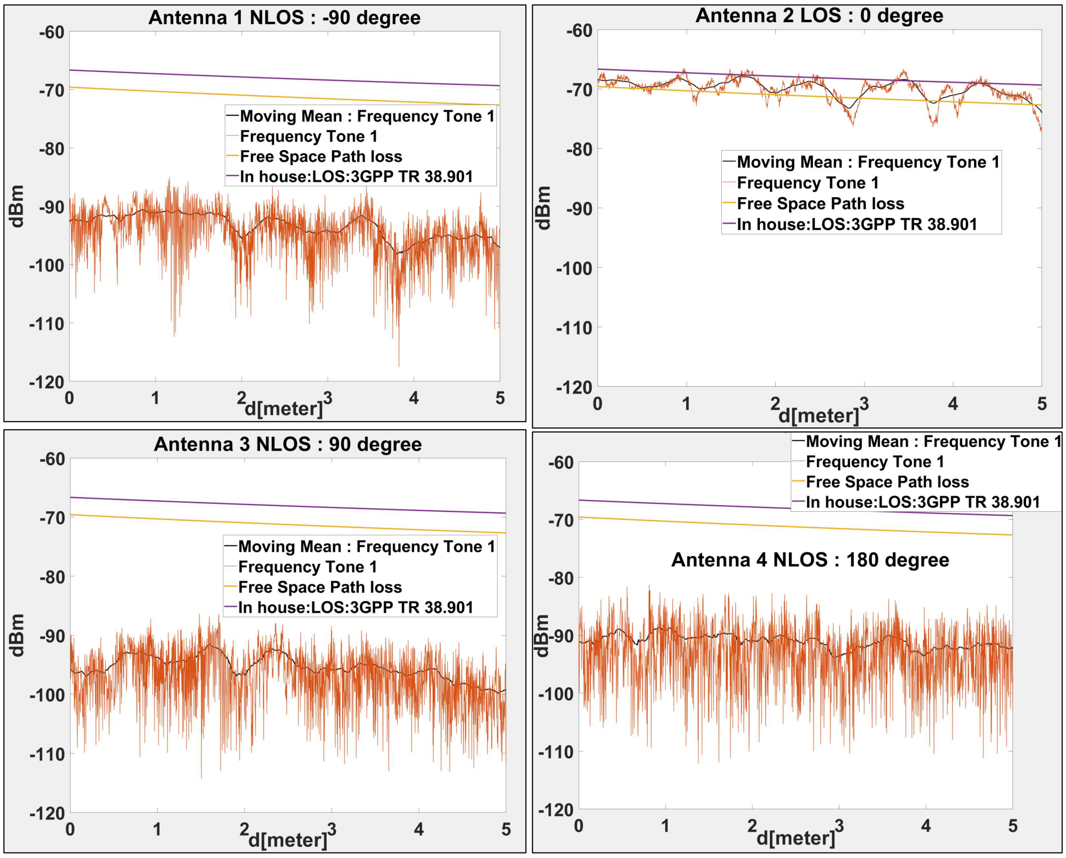


**Figure 7.7:** Field Strength plot [dBm], average noise floor = 114.40 dBm

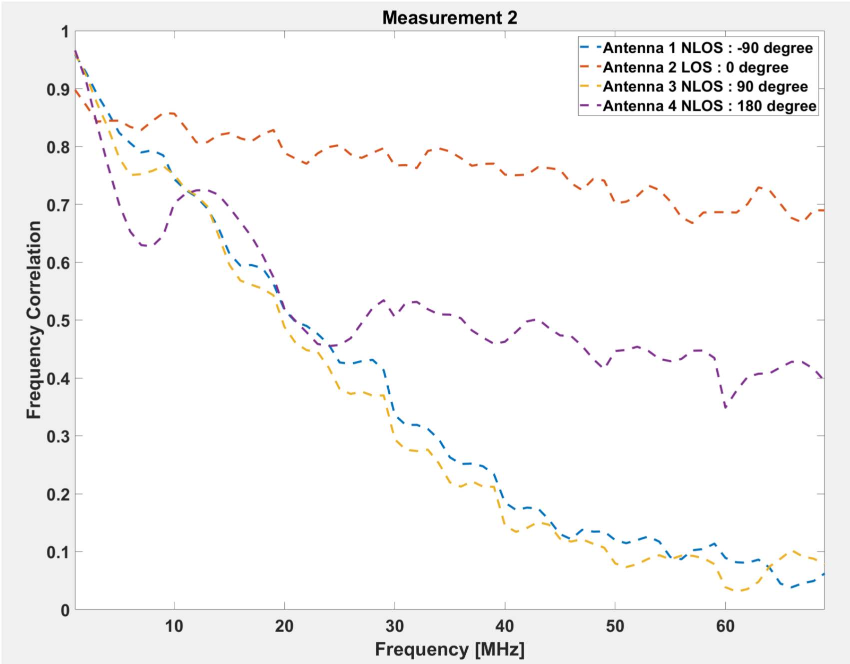


**Figure 7.8:** Frequency Correlation : Measurement 2

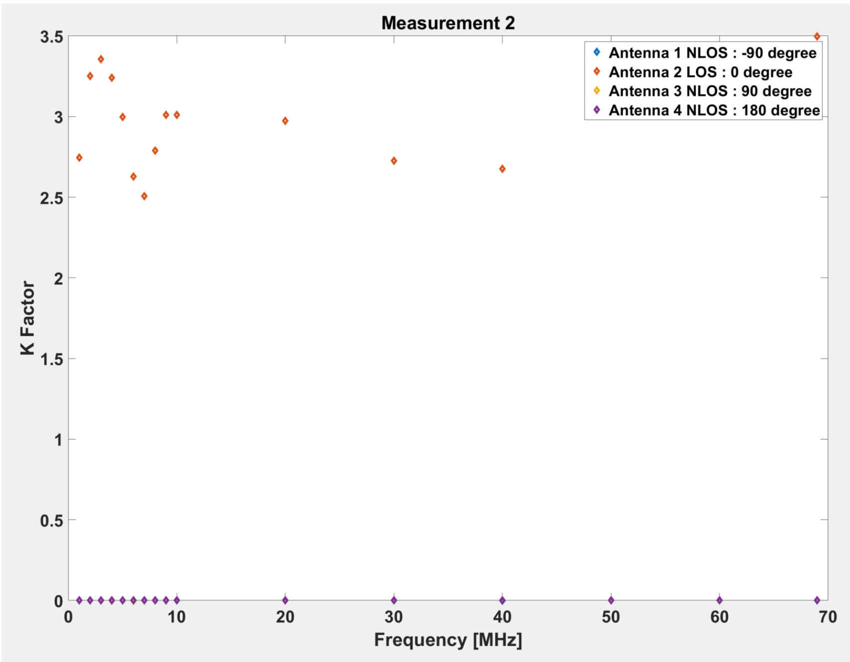


**Figure 7.9:** K-factor : Measurement 2

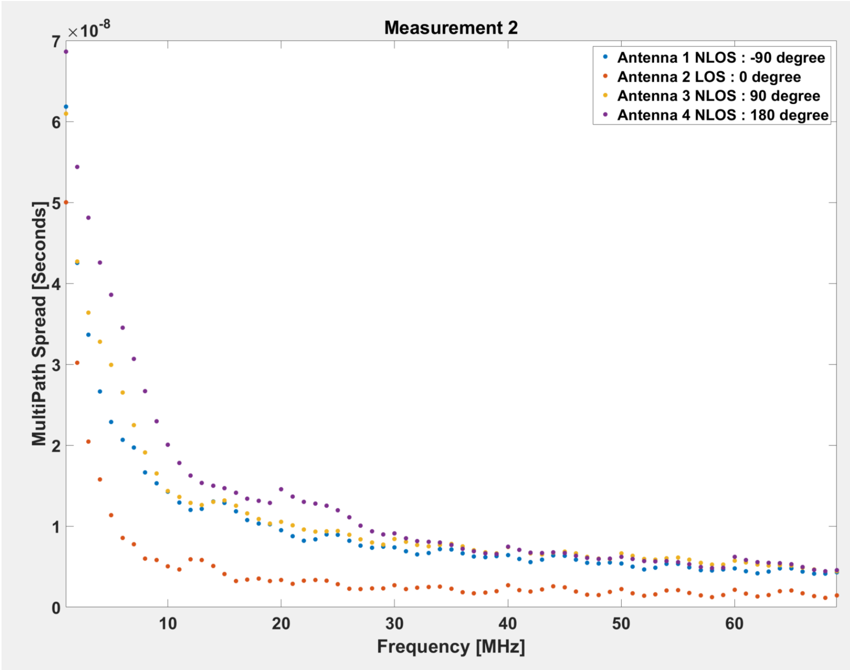


**Figure 7.10:** Multi-path Spread : Measurement 2

reflection loss of -4.5dB based on table 3.2 and gain of the point where reflection component will strike is -5dB approx, which lead to approximately 20 dB drop in field strength with respect friis free space and LOS : 3GPP model. As clearly shown in plot 7.7, **moving mean of tone 1** also have drop approximately 20-25dB.

- Figure 7.8 shows the plots of frequency correlation. Antenna 1(NLOS) frequency correlation is around 0.8 for the first 10MHz, drops to 0.48 at 20MHz, 0.3 at 30MHz, and then drops to 0.1 at 69MHz. Antenna 2(LOS) shows a high-frequency correlation of more than 0.65 over the band of 0 to 69MHz. Antenna 3(NLOS), frequency correlation is above 0.4 for bands 0 to 13MHz and then starts dropping to 0.1 for higher frequency bands. Antenna 3(NLOS) frequency correlation is above 0.4 over the band 0 to 60 MHz and further drops to 0.3 at 69MHz.

- Figure 7.9 shows the K factor plot. K factor is approximately 2.5 to 3.5 for antenna 2 over the band, which is in LOS and primarily receives direct components. For antennae 1, 3, and 4, the k-factor is approximately zero, and this makes sense as we are mostly getting multipath components directly from the glass.

- Figure 7.10 shows a multipath spread plot; for all the antennae, the multipath-spread decreases as the frequency separation increases.

## 7.3 Measurement 3

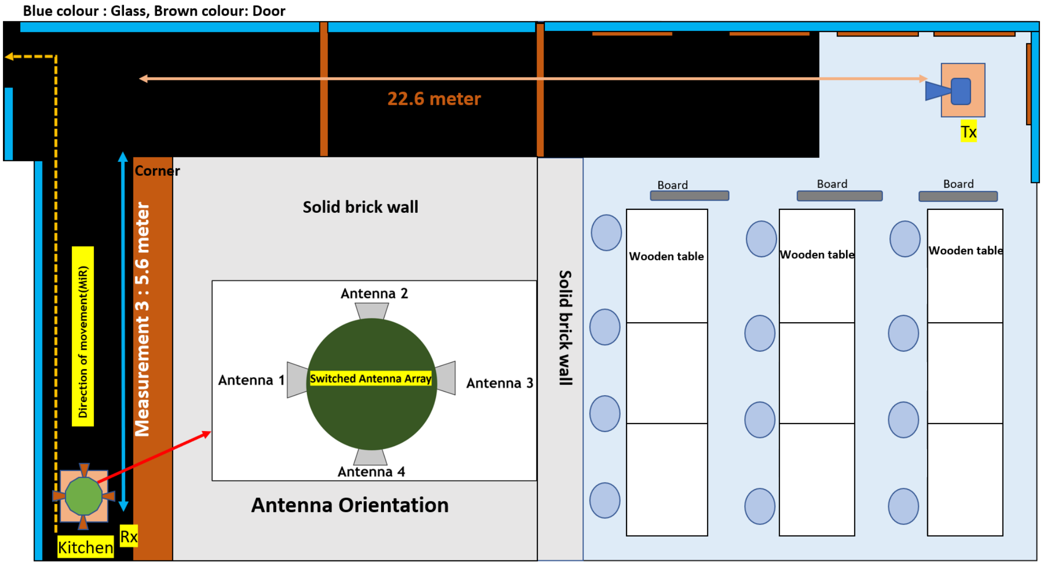


**Figure 7.11:** Identified path for Robot : Measurement 3

Each Rx antenna have a different orientation. As mentioned in the table 7.1 antenna 1 is NLOS, antenna 2 is NLOS, antenna 3 is NLOS, and antenna 4 is NLOS with respect to transmitter. Map of the measurement 3 shown in figure 7.11, at the start of measurement distance between RX-TX is 28.2 meter. Rx moves 5.6 meter during measurement 3.

- Figure 7.12 shows field and normalized field strength plot with one of the tone for each antenna also includes friis free space and LOS: 3GPP path loss models. Antenna 1, 2, 3, and 4 are in non-line of sight, they includes a type of losses such as diffraction, Reflection, and scattering, which have been not included in the friis free space and LOS: 3GPP model.
  The receiver is in the kitchen; all the antennas are in non-line of sight scenarios. Based on the map 7.11, the propagating waves come under the effect of Reflection and diffraction. The reflection and diffraction losses have been calculated at mmWave frequency in section 3.1. All the antennas in NLOS, hence they will receive multipath components. Based on map 7.11, there is one corner that leads to diffraction and several Reflection. Inside the kitchen(NLOS), based on observation $\alpha$ = 10 degrees( diffraction on corner wall), $\theta_i$ = 40 degrees at least two reflections which leads to a loss of approximately 30dB, and that makes sense from path loss plot 7.12 for friis free space and LOS: 3GPP model.

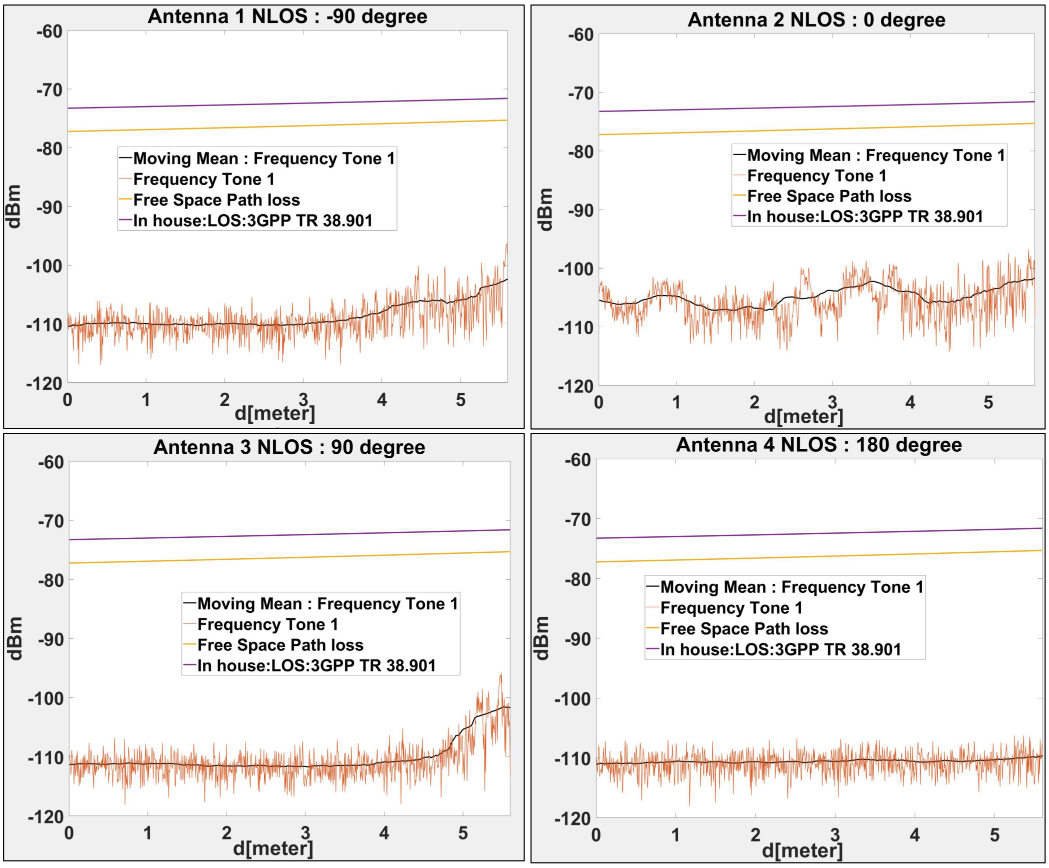


**Figure 7.12:** Field Strength plot [dBm], average noise floor = 114.40 dBm

- Figure 7.13 shows the plots of frequency correlation. Antenna 1(NLOS) frequency correlation is above 0.4 for the first 4MHz, drops to 0.1 over the band 6 to 69MHz. Antenna 2 (LOS) shows a frequency correlation above 0.4 for the first 4MHz; further, it jumps between 0.35 and 0.1 over the band 6 to 69MHz. Antenna 3 (NLOS) frequency correlation is below 0.4 over the whole band of 0 to 69Mhz. Antenna 4(NLOS)frequency correlation is below 0.1 over the band 0 to 69 MHz.

- Figure 7.14 shows K factor plot, for antenna 1, 2, 3, and 4 the k-factor is approximately zero and this makes sense as we are mostly getting multipath components directly from the glass.

- Figure 7.15 shows multipath spread plot, for all the antenna the multipath-spread decreases as the frequency separation increases.

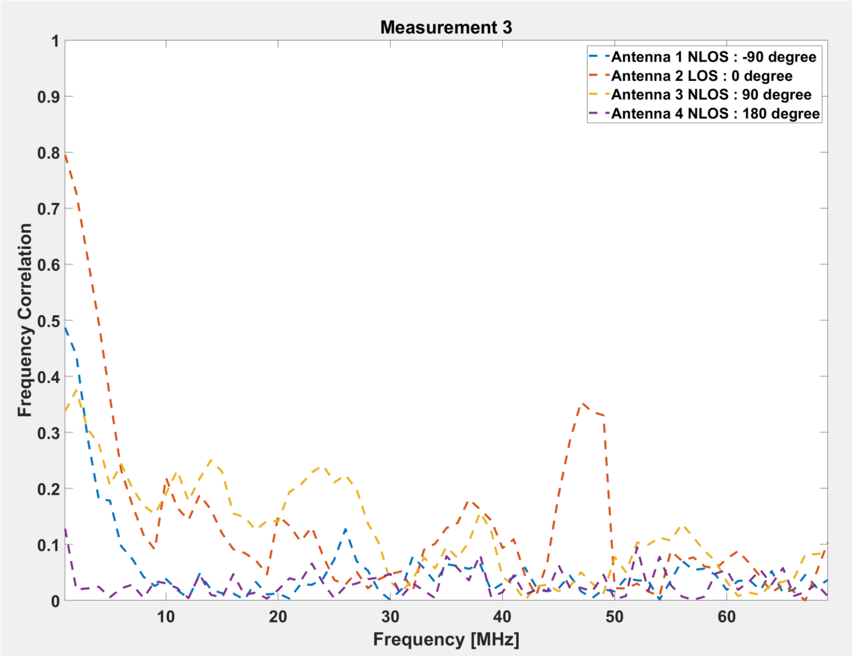


**Figure 7.13:** Frequency Correlation : Measurement 3

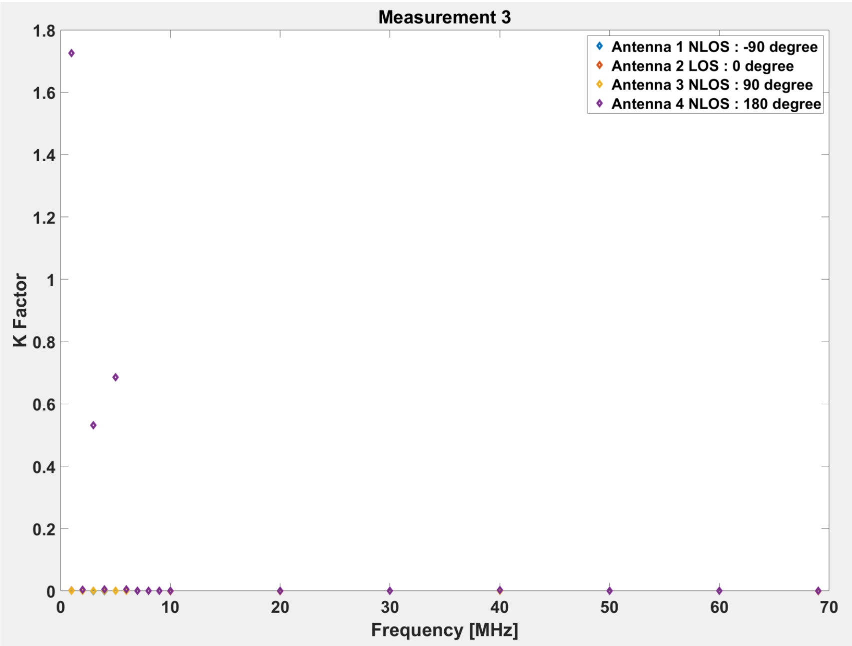


**Figure 7.14:** K-factor : Measurement 3

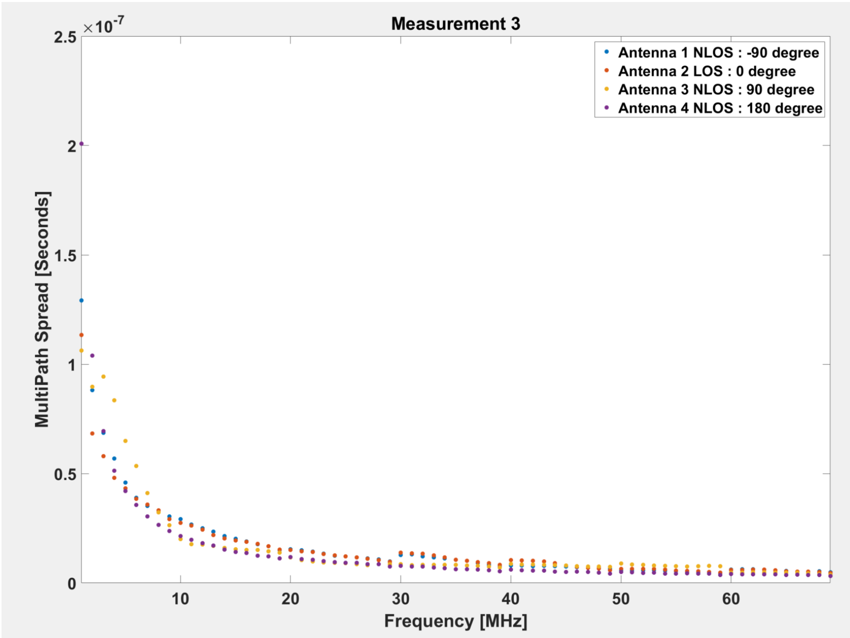


**Figure 7.15:** Multi-path Spread: Measurement 3

## 7.4 Measurement 4

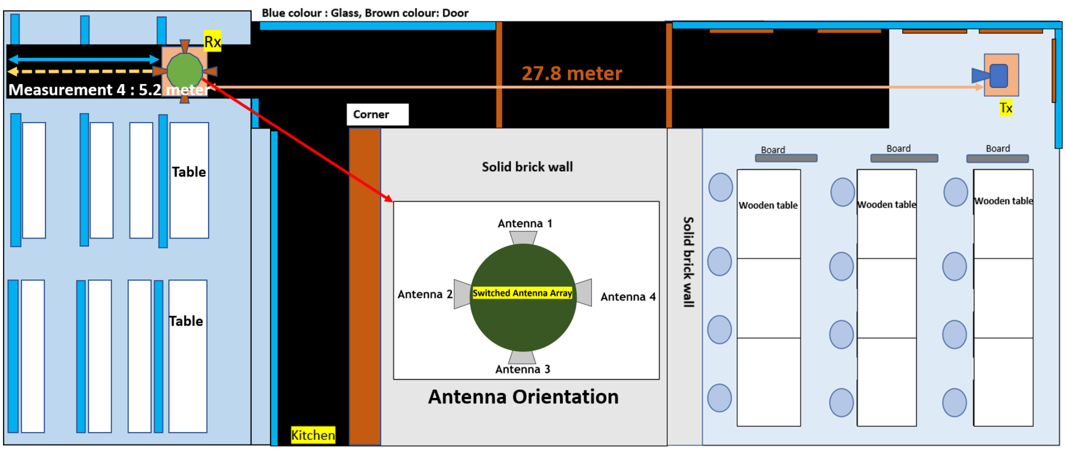


**Figure 7.16:** Identified path for Robot : Measurement 4

Each Rx antenna have a different orientation. As mentioned in the table 7.1 antenna 1 is NLOS, antenna 2 is LOS, antenna 3 is NLOS, and antenna 4 is NLOS with respect to transmitter. Map of the measurement 4 shown in figure 7.16, at the start of measurement distance between RX-TX is 27.8 meter. Rx moves 5.2 meter during

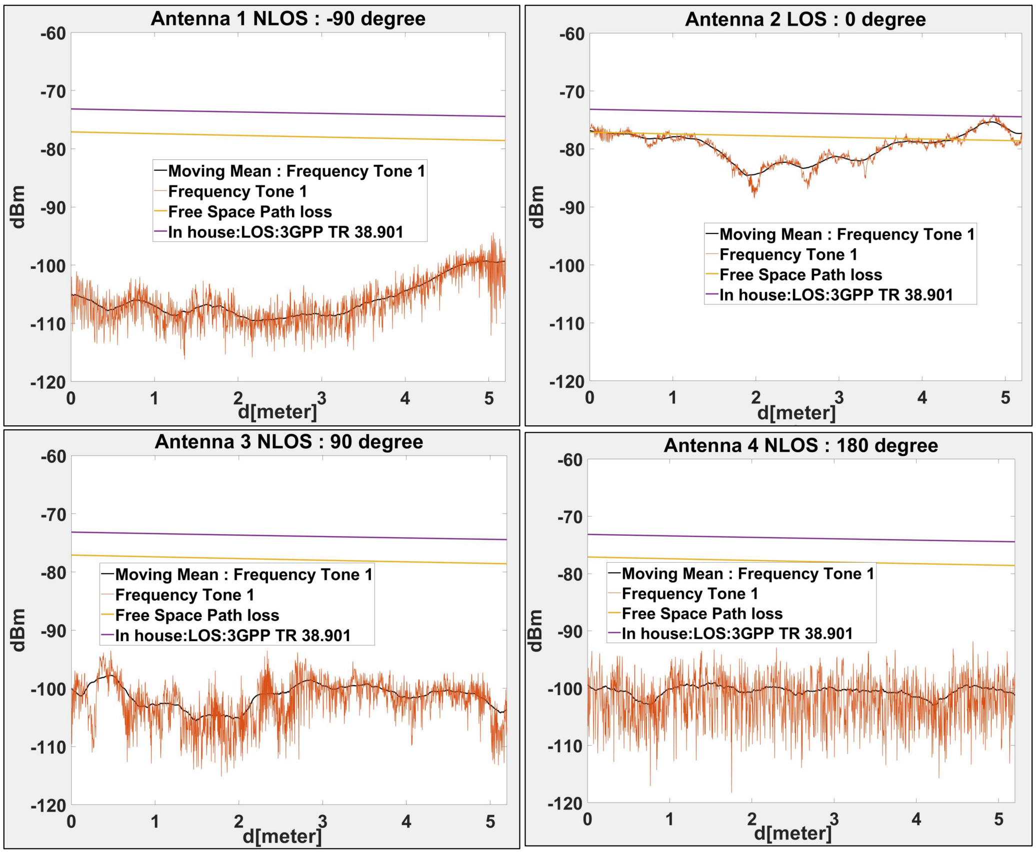


**Figure 7.17:** Field Strength plot [dBm], average noise floor = 114.40 dBm

measurement 4.

- Field strength plot 7.17 shows field strength plot for antenna 1, 3, and 4, friis space and LOS : 3GPP model is approximately 20-35 dB higher than frequency tone1 curve. Antenna 1, 3, and 4 are in non-line of sight, and it includes a type of loss such as diffraction, reflection, and scattering, which have been not included in the friis space and LOS : 3GPP model.
  Antenna 2 (LOS) field strength curves closely follow the friis free space and LOS: 3GPP model 7.17, and there are not many losses due to reflection, diffraction, and scattering because most of the received signals are direct components. Antenna 4 is exactly 180 degrees from antenna 2, and it will receive direct components but on its back lobe. Isolation between antenna 2 and 4 is approximately 27.5dB. Also, the difference in strength level between antenna 2 and 4 is approx 25 dB, which is also clearly visible from plot 7.17.
  Antenna 1 and 3 are in non-line of sight from transmitter, hence they are receiving reflected component. Distance between transmitter and receiver is

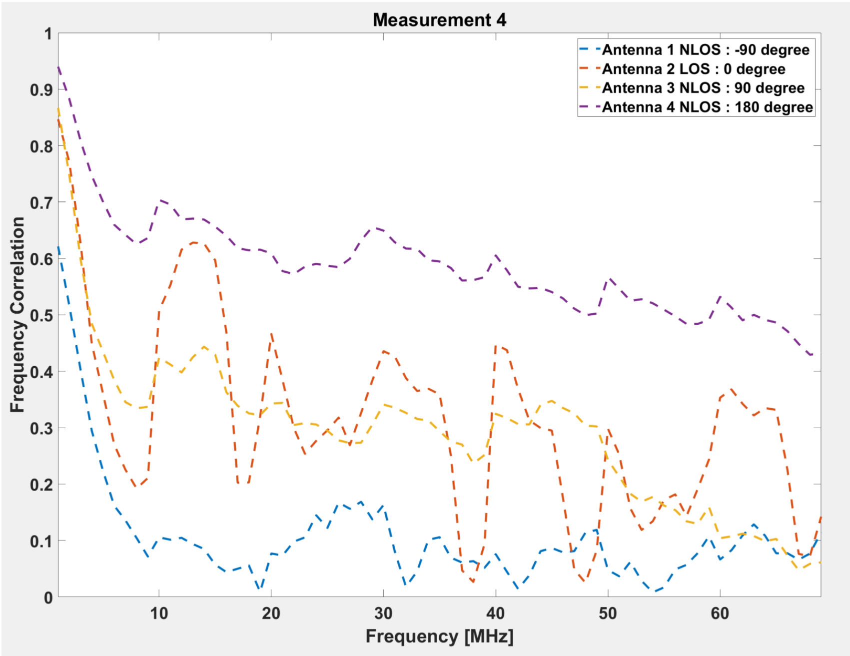


**Figure 7.18:** Frequency Correlation : Measurement 4

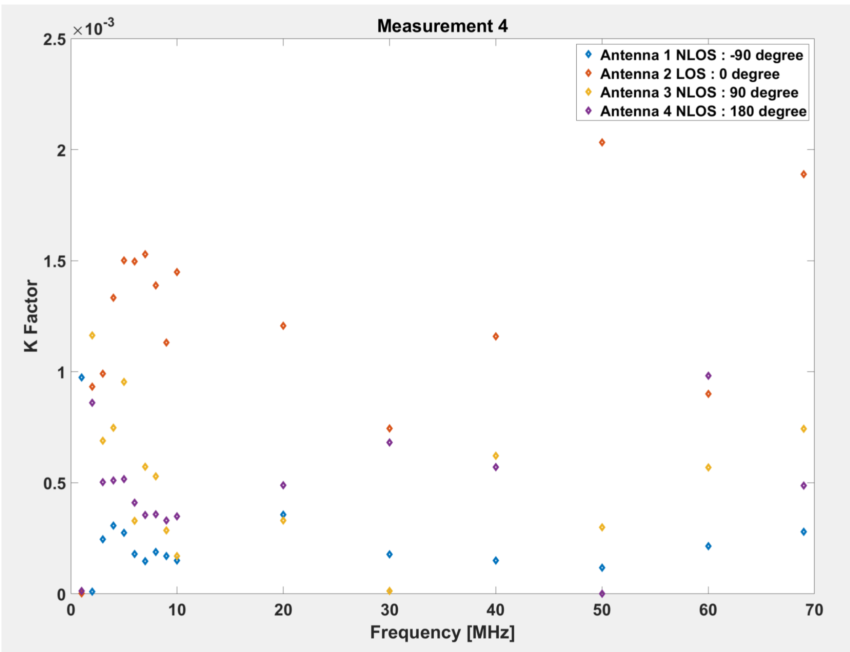


**Figure 7.19:** K-factor : Measurement 4

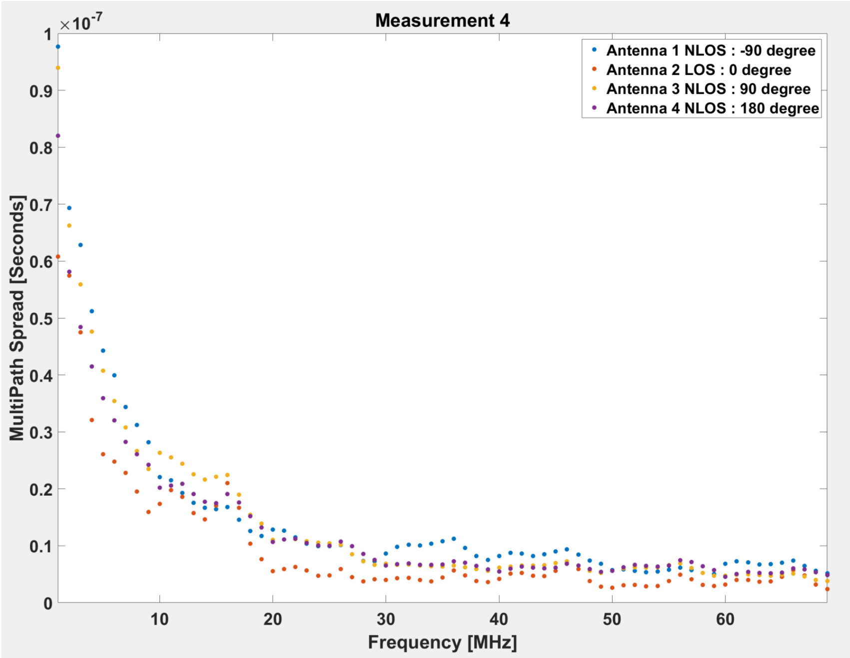


**Figure 7.20:** Multi-path Spread : Measurement 4

27.8mt, based on observation the angle of incidence is 20 degree( for diffraction), also consider two reflection(rich channel) which lead to loss of -6.8 dB based on table 3.2 and gain of the point where reflection component will strike is -0 dB approx, which lead to approximately 26 dB drop in field strength with respect friis free space and LOS : 3GPP model. As clearly shown in plot 7.17, moving mean of tone 1 also have dropped approximately 25-30dB.

- Figure 7.18 shows the plots of frequency correlation. Antenna 1(NLOS)frequency correlation is above 0.4 for the first 3MHz and drops to 0.2 or below for the remaining frequency tones. Antenna 2(LOS) frequency correlation is above 0.4 for the first 3MHz, it jumps around over the remaining frequency bands. Antenna 3(NLOS) frequency correlation jumps between 0.2 to 0.6 over the frequency band. Antenna 4(NLOS)frequency correlation is above 0.4 over the band 0 to 69 MHz.
- Figure 7.19 shows K factor plot, for antenna 1, 2, 3, and 4 the k-factor is approximately zero and this makes sense as we are mostly getting multipath components directly from the glass.
- Figure 7.20 shows multipath spread plot, for all the antenna the multipath-spread decreases as the frequency separation increases.

## 7.5 Result Summary

| Rx Antenna | Average Power level [dBm] | K Factor | Coherence Bandwidth[MHz] |
|---|---|---|---|
| 2 | -115 | 1-2.5 | 0 |
| 4 | -115 | 1-2.5 | 0 |
| 6 | -115 | 1-2.5 | 0 |
| 8 | -115 | 1-2.5 | 0 |

**Table 7.2:** Noise Floor Test [6.9]

| Rx Antenna | Average Power level [dBm] | K Factor | Coherence Bandwidth[MHz] |
|---|---|---|---|
| 2 | -103 | 2 | 0 |
| 6 | -60 | 150 | 0 |
| 8 | -103 | 2 | 0 |

**Table 7.3:** Conducted Test [6.11]

Table 7.2 and 7.3 provides idea about noise level and instrumental affect on the frequency correlation, K factor, and multipath spread calculation. RF tones that show a correlation above 0.4 can be considered as part coherence bandwidth.

**Measurement 1**

The plot from Figure 7.3 shows the frequency correlation for measurement 1, and the map of the measurement one is shown in 7.1. For a line sight antenna 2, the frequency correlation is high compared to the non-line of sight antennas. Antenna 2 mostly receives direction components, and it has less fading A.3 which leads to high-frequency correlation. For antennas 1 and 3, channel characteristics are almost the same; due to that, they have a similar frequency correlation over the band. Based on table 7.4, an antenna with a line of sight view has higher coherence bandwidth.

**Measurement 2**

The plot from Figure 7.8 shows the frequency correlation for measurement 2, and the map of the measurement one is shown in 7.6. For a line sight antenna 2, the frequency correlation is high compared to the non-line of sight antennas. Antenna 2 mostly receives direction components, and it has less fading A.4 which leads to high-frequency correlation. For antennas 1 and 3, channel characteristics are almost the same; due to that, they have a similar frequency correlation over the band. Based on table 7.4, an antenna with a line of sight view has higher coherence bandwidth.

| Measurement 1 | | | | |
|---|---|---|---|---|
| Rx Antenna | Rx Orientation | Average Power level [dBm] | K Factor | Coherence Bandwidth[MHz] |
| 1 | -90 degree(NLOS) | -88 | 0 | 27 |
| 2 | 0 degree(LOS) | -65 | 6-9 | 69 |
| 3 | +90 degree(NLOS) | -90 | 0 | 18 |
| 4 | 180 degree(NLOS) | -87 | 0 | 48 |
| **Measurement 2** | | | | |
| Rx Antenna | Rx Orientation | Average Power level [dBm] | K Factor | Coherence Bandwidth[MHz] |
| 1 | -90 degree(NLOS) | -92 | 0 | 27 |
| 2 | 0 degree(LOS) | -70 | 2.5-3.5 | 69 |
| 3 | +90 degree(NLOS) | -95 | 0 | 18 |
| 4 | 180 degree(NLOS) | -90 | 0 | 69 |
| **Measurement 3** | | | | |
| Rx Antenna | Rx Orientation | Average Power level [dBm] | K Factor | Coherence Bandwidth[MHz] |
| 1 | -90 degree(NLOS) | -110 | 0 | 0 |
| 2 | 0 degree(NLOS) | -105 | 0 | 0 |
| 3 | +90 degree(NLOS) | -110 | 0 | 0 |
| 4 | 180 degree(NLOS) | -110 | 0 | 0 |
| **Measurement 4** | | | | |
| Rx Antenna | Rx Orientation | Average Power level [dBm] | K Factor | Coherence Bandwidth[MHz] |
| 1 | -90 degree(NLOS) | -105 | 0 | 3 |
| 2 | 0 degree(LOS) | -80 | 0 | 4 |
| 3 | +90 degree(NLOS) | -100 | 0 | 5 |
| 4 | 180 degree(NLOS) | -100 | 0 | 69 |

**Table 7.4:** Coherence Bandwidth Table, average noise floor = 114.40 dBm

### Measurement 3

The plot from Figure 7.13 shows the frequency correlation for measurement 3, map shown in 7.11. Based on the map, all the antennas are in NLOS, the received signal is close to the noise floor, frequency correlation is very low and almost the same as the noise floor test case. All the antennas have the same random fading as shown in plot A.1. Based on table 7.4, all antennas have almost zero coherence bandwidth.

### Measurement 4

The plot from Figure 7.18 shows the frequency correlation for measurement 4, and the map of the measurement one is shown in 7.16. For a line sight antenna 2, the frequency correlation is high compared to the non-line of sight antennas. Antenna 2 mostly receives direction components, and it has less fading as shown in plot A.6, which leads to high-frequency correlation. For antennas 1 and 3, channel characteristics are almost the same; due to that, they have a similar frequency correlation over the band. As shown in figure A.6, for antenna 4(NLOS) the fading correlation is very high, lead to larger coherence bandwidth.

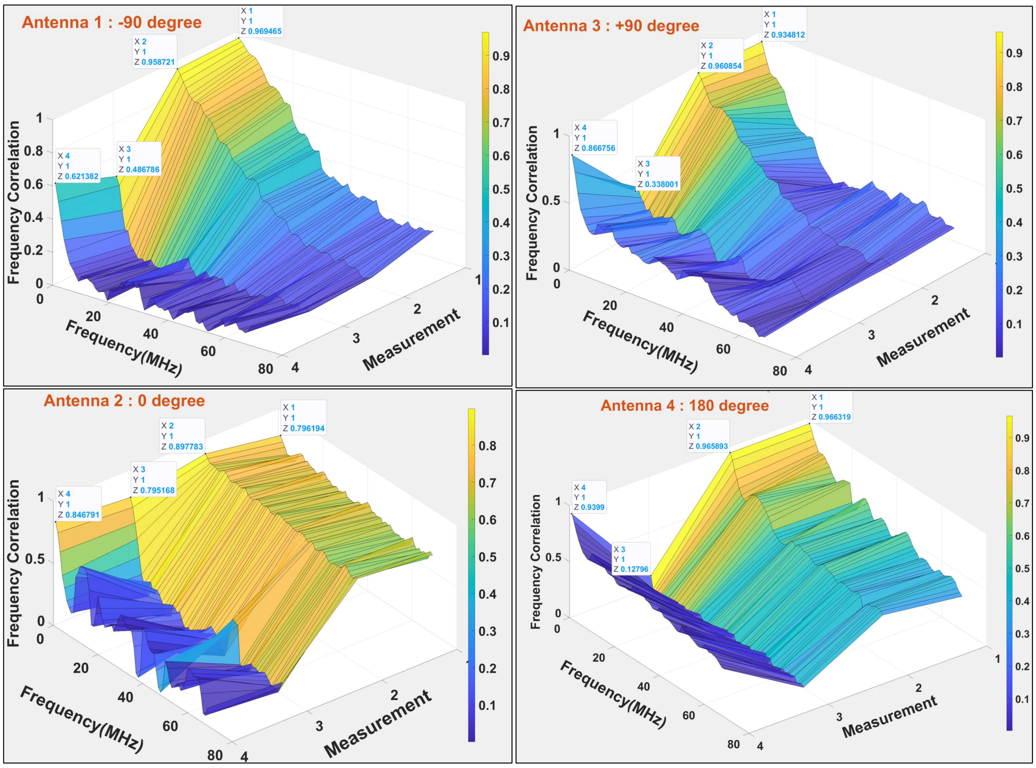


**Figure 7.21:** 3D Frequency Correlation plot

## 7.6 3D Correlation Plot

Figure 7.21 shows a 3D plot of frequency correlation with combined four measurement campaigns. Axis representation; X-axis represent measurement number(i = 1 to 4), y-axis represent frequency[MHz], and Z-axis represent frequency correlation. It is visible that frequency correlation is very high for all antennas which have a line of sight view toward transmitter. Also as the distance increases, the frequency correlation decreases. Measurement 3, which is done inside the kitchen area have lowest frequency correlation, that makes sense because all antennas response close to noise floor. For measurement 4, the setup comes more into a line of sight with the transmitter, and frequency correlation increases.

# Chapter 8

# Conclusion

Millimeter-wave frequencies are very sensitive to the propagation environment; hence it important to find channel characteristics in different environmental conditions, based on that decision can be made. In this project, a series of measurements in the complex indoor environment has been performed, and collected time signals have been analyzed for frequency correlation, K factor, multipath spread, K factor, field strength, and normalized field strength. Based on result analysis coherence bandwidth is defined under different channel characteristics.
A total of four measurements have been under indoor environmental conditions in a typical office setting that mimics an industrial environment. Antenna 1 is in non-line of sight during all the measurements, for measurement 1, 2, and 4 coherence bandwidth is 27, 27, and 3 MHz respectively, measurement 3 response is almost same as noise floor result due to that coherence bandwidth is 0. Antenna 1 is in line of sight during all the measurements(1, 2, and 4), for measurement 1, 2, and 4 the coherence bandwidth is 69, 69, and 4 MHz respectively, measurement 3 response is almost same as noise floor result due to that coherence bandwidth is 0. Antenna 3 is in non-line of sight during all the measurements, for measurement 1, 2, and 4 coherence bandwidth is 18, 18, and 5 MHz respectively, measurement 3 response is almost same as noise floor result due to that coherence bandwidth is 0. Antenna 4 is in non-line of sight during all the measurements, for measurement 1, 2, and 4 coherence bandwidth is 48, 48, and 69 MHz respectively, measurement 3 response is almost same as noise floor result due to that coherence bandwidth is 0. Results show that coherence bandwidth is drastically dropped to zero in the kitchen area, equivalent to noise floor measurement. Usually, as the distance between transmitter increases the coherence bandwidth decreases. The coherence bandwidth is very high for antenna which is directed towards to receiver, and for antennas which are not directive toward receiver are having fairly less coherence bandwidth. The frequency correlation drops as the bandwidth separation increases between RF tones. Multipath spread also follows the same trend as frequency cor-

relation. In comparison to previous measurement where 4 RF tones have, but in this measurement total sixteen tone have used over a defined bandwidth, more the number of RF tones more detailed channel characteristics and gives accurate coherence bandwidth value. The path loss models like friis free space and LOS : 3GPP model closely fallow the field strength response of corresponding RF tones for antenna with line of sight view, after introducing losses like diffraction and reflection, the path loss models closely fallow Normalized field strength response of antenna with non-line sight view.

### 8.0.1 Future Work

Now the coherence bandwidth is defined for different indoor channel environment. Defined coherence bandwidth will be used further for tone separation on existing measurement technique[20] with more stable signals sources, reduction in resolution bandwidth to around 10 kHz, more number of RF carrier, and investigate the range limitations with such setting. Output power, noise figure and loss of the microwave components needed for such measurement setup is quite relaxed due to the very low measurement bandwidth that can be used making method practical and easy to implement. The method can potentially be used for channel characterization at much higher frequencies and bandwidths as envisioned for 6 G and other new and future systems. Thorough interpretation and evaluation of the captured data with the aim to fully understand the timing aspects of LOS to NLOS transitions as well as more in depth investigation of how different types of antennas affect the RF channel properties in indoor environments should be done. Additional measurement campaigns should be planned to investigate this in dept. **In reference to present work, the future possible measurement method are listed in appendix A.3**.

# Bibliography


[1] 3GPP. *Study on New Radio Access Technology—Physical Layer Aspects, document TR 38.802, V14.1.0, 3GPP, Jun. 2017*. Accessed on 31-05-2022. URL: http://ftp.3gpp.org/.

[2] A-info. *Octave horn antenna*. Accessed on 08-02-2022. URL: http://www.ainfoinc.com.cn/en/p_ant_h_om.asp.

[3] Yusra Banday, Ghulam Rather, and Gh Rasool Begh. "Effect of atmospheric absorption on Millimeter Wave (mmWave) frequencies for 5G Cellular Networks". In: *IET Communications* 13 (Feb. 2019). DOI: 10.1049/iet-com.2018.5044.

[4] P. Bello. "Some Techniques for the Instantaneous Real-Time Measurement of Multipath and Doppler Spread". In: *IEEE Transactions on Communication Technology* 13.3 (1965), pp. 285–292. DOI: 10.1109/TCOM.1965.1089133.

[5] Dmitry Chizhik et al. "Path Loss and Directional Gain Measurements at 28 GHz for Non-Line-of-Sight Coverage of Indoors With Corridors". In: *IEEE Transactions on Antennas and Propagation* 68.6 (2020), pp. 4820–4830. DOI: 10.1109/TAP.2020.2972609.

[6] Sijia Deng, Geoge R. MacCartney, and Theodore S. Rappaport. "Indoor and Outdoor 5G Diffraction Measurements and Models at 10, 20, and 26 GHz". In: *2016 IEEE Global Communications Conference (GLOBECOM)*. 2016, pp. 1–7. DOI: 10.1109/GLOCOM.2016.7841898.

[7] Analog devices. *ADF4371*. URL: https://www.analog.com/media/en/technical-documentation/data-sheets/adf4371.pdf.

[8] Jinfeng Du Dmitry Chizhik et al. "Reliable 28 GHz Propagation Models for 90% Coverage in Factories". In: ().

[9] Athanasios Doukas and Grigorios Kalivas. "Rician K Factor Estimation for Wireless Communication Systems". In: *2006 International Conference on Wireless and Mobile Communications (ICWMC'06)*. 2006, pp. 69–69. DOI: 10.1109/ICWMC.2006.81.

[10] Embedded. *Jitter considerations when matching timing solutions to your applications*. URL: https://www.embedded.com/jitter-considerations-when-matching-timing-solutions-to-your-applications/.

[11] ETSI. *5G; Study on channel model for frequencies from 0.5 to 100 GHz*. URL: https://www.etsi.org/deliver/etsi_tr/138900_138999/138901/14.03.00_60/tr_138901v140300p.pdf.

[12] C. Santiago Morejón García et al. "Cooperative Resource Allocation for Proximity Communication in Robotic Swarms in an Indoor Factory". In: *2021 IEEE Wireless Communications and Networking Conference (WCNC)*. 2021, pp. 1–6. DOI: 10.1109/WCNC49053.2021.9417544.

[13] Andrea Goldsmith. "Path Loss and Shadowing". In: *Wireless Communications*. Cambridge University Press, 2005, 27â€"63. DOI: 10.1017/CBO9780511841224.003.

[14] Bernd Holfeld et al. "Wireless Communication for Factory Automation: an opportunity for LTE and 5G systems". In: *IEEE Communications Magazine* 54.6 (2016), pp. 36–43. DOI: 10.1109/MCOM.2016.7497764.

[15] Abdul Jabbar et al. "Millimeter-Wave Smart Antenna Solutions for URLLC in Industry 4.0 and Beyond". In: *Sensors* 22.7 (2022). ISSN: 1424-8220. DOI: 10.3390/s22072688. URL: https://www.mdpi.com/1424-8220/22/7/2688.

[16] Keysight. *Fading*. URL: https://rfmw.em.keysight.com/wireless/helpfiles/n5106a/about_fading.htm.

[17] Matlab. *Correlation Coefficient*. Accessed on 08-02-2022. URL: https://se.mathworks.com/help/matlab/ref/corrcoef.html.

[18] Raspberry Pi. *Getting started with Raspberry Pi*. URL: https://projects.raspberrypi.org/en/projects/raspberry-pi-getting-started.

[19] Kim Nielsen Poul Olesen. "Channel characterization method". In: (2020). DOI: InternaldocumentNokia.

[20] Stig Brink Poul Olesen Kim Nielsen and Bent Rysgaard Jan Hviid. "Channel characterization method". In: (2020). DOI: InternaldocumentNokia.

[21] Theodore S Rappaport. *Wireless communications: Principles and practice*. English (US). 2nd. Prentice Hall communications engineering and emerging technologies series. Includes bibliographical references and index. Prentice Hall, 2002. ISBN: 0130422320.

[22] Ignacio Rodriguez et al. "5G Swarm Production: Advanced Industrial Manufacturing Concepts Enabled by Wireless Automation". In: *IEEE Communications Magazine* 59.1 (2021), pp. 48–54. DOI: 10.1109/MCOM.001.2000560.

[23] David de la Vega et al. "Generalization of the Lee Method for the Analysis of the Signal Variability". In: *IEEE Transactions on Vehicular Technology* 58.2 (2009), pp. 506–516. DOI: 10.1109/TVT.2008.926214.

[24] Yunchou Xing et al. "Indoor Wireless Channel Properties at Millimeter Wave and Sub-Terahertz Frequencies". In: *2019 IEEE Global Communications Conference (GLOBECOM)*. 2019, pp. 1–6. DOI: 10.1109/GLOBECOM38437.2019.9013236.

# Appendix A

# Appendix A name

## A.1 Detailed Results of Each Measurement Campaigns

### A.1.1 Noise Floor Test [6.1.1]

In figure A.1 fading(normalized field strength) have been analysed for all the antennas with four frequency tones(1, 2, 30 and 70MHz) each, all the four antennas have almost similar fading which comes from instrument affect at receiver side( Tx is turned off) which is in range -6 to +6 dB.

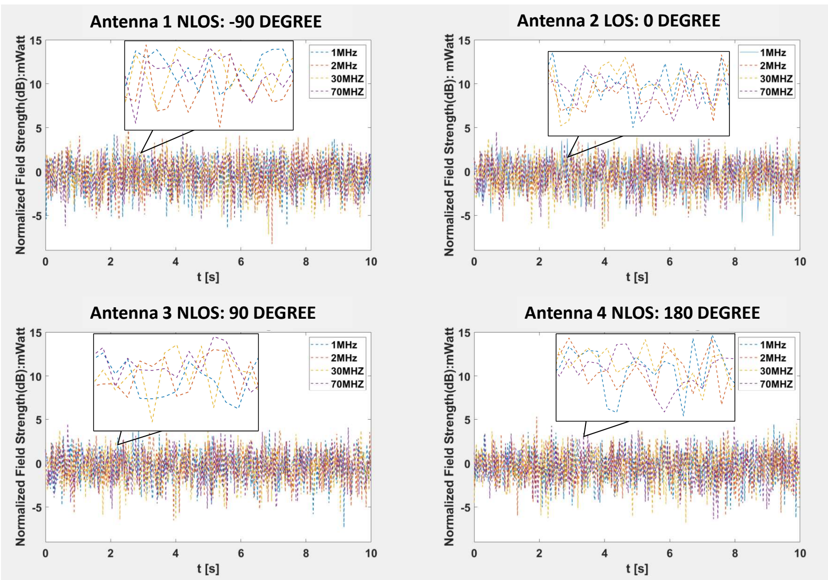


**Figure A.1:** Normalized Field Strength[dB]: Noise Floor

### A.1.2 Conducted Testing [6.11]

Figure A.2 shows the normalized field strength for all the antennas, for antenna 2 and 3 the received power level is above noise floor and they have fading within -1 to 1 dB which is equivalent to quantisation affect of spectrum analyzer and digital oscilloscope, while for remaining antenna 2 and 8 they are similar to noise floor test.

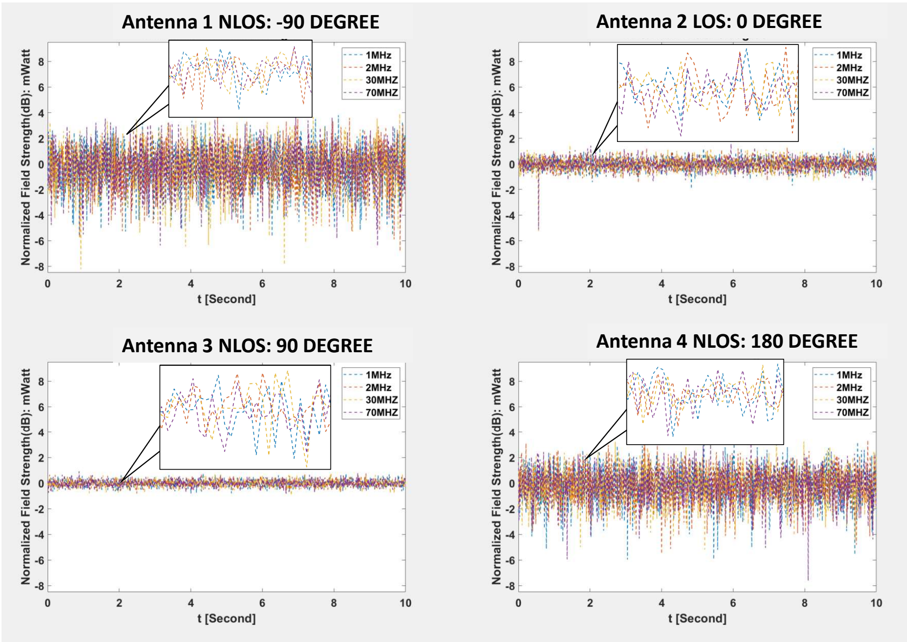


**Figure A.2:** Normalized Field Strength[dB]: Conducted Testing

### A.1.3 Measurement 1 [7.1]

Figure A.3 shows the normalized field strength/fading for corresponding 1, 2, 30, and 70MHz frequency tones for each antenna, all the frequency is centered around 27GHz. Antenna 1(NLOS) shows fading over the moving distance. It varies between -15dB to 5dB; also, the zoomed view of the corresponding case shows that 1 and 2MHz tones coincide with each other, and 30MHz tone also closely follows 1 and 2MHz, higher frequency tone like 70MHz is uncorrelated with the remaining tones. Antenna 2(LOS) primarily receives direct components, so it does not have a much-fading effect, and it is visible from the fading plots as they are within -1 to +1dB, which means they strictly follow each other. Antenna 3(NLOS), the fading is within the range of -5 to 14 dB, and zoomed view of the corresponding case shows that 1 and 2MHz tones coincide. However, higher frequency tone like 30 and 70MHz is uncorrelated with the remaining tones. Antenna 4(NLOS) does not receive direct components, and fading plot varies from -10 to 25 dB, the zoomed view of the corresponding case shows that 1 and 2MHz tones coincide with each other, and 30MHz tone also closely follows 1 and 2MHz tones, but higher frequency tone like 70MHz is uncorrelated with remaining tones.

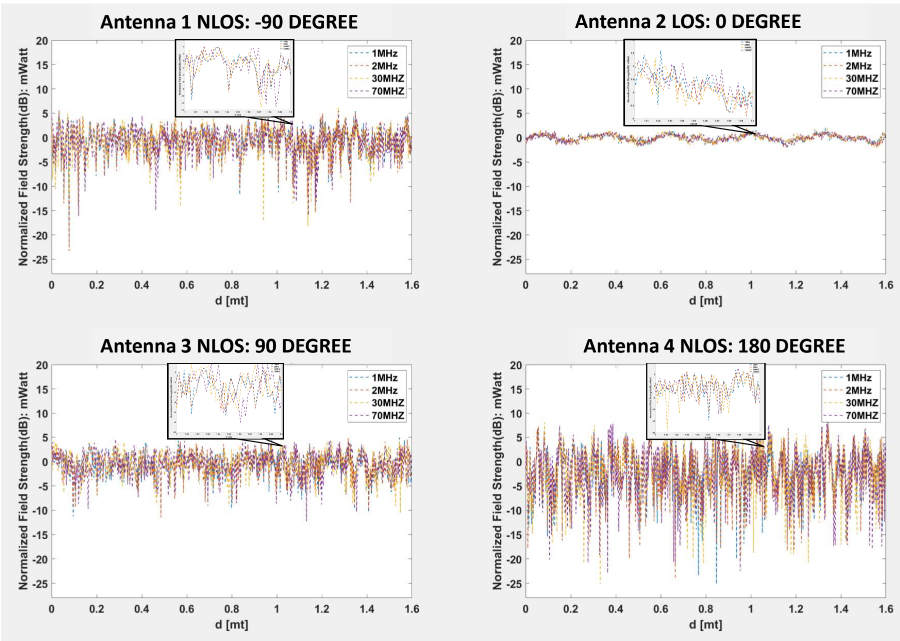


**Figure A.3:** Normalized Field Strength [dB] of Rx Switched antenna system

### A.1.4 Measurement 2 [7.6]

Figure A.4 shows the normalized field strength/fading for corresponding 1, 2, 30, and 70MHz frequency tones for each antenna, all the frequency is centered around 27GHz. Antenna 1(NLOS) shows fading over the moving distance. It varies between -5dB to 25dB; also, the zoomed view of the corresponding case shows that 1 and 2MHz tones coincide with each other, and 30MHz tone also closely follows 1 and 2MHz, higher frequency tone like 70MHz is uncorrelated with the remaining tones. Antenna 2(LOS) primarily receives direct components, so it does not have a much-fading effect, and it is visible from the fading plots as they are within -2 to +4dB, which means they strictly follow each other. Antenna 3(NLOS), the fading is within the range of -5 to 20dB, and zoomed view of the corresponding case shows that 1 and 2MHz tones coincide. However, higher frequency tone like 30 and 70MHz is uncorrelated with the remaining tones. Antenna 4(NLOS) does not receive direct components, and fading plot varies from -10 to 25 dB, the zoomed view of the corresponding case shows that 1 and 2MHz tones coincide with each other, and 30MHz tone also closely follows 1 and 2MHz tones,.

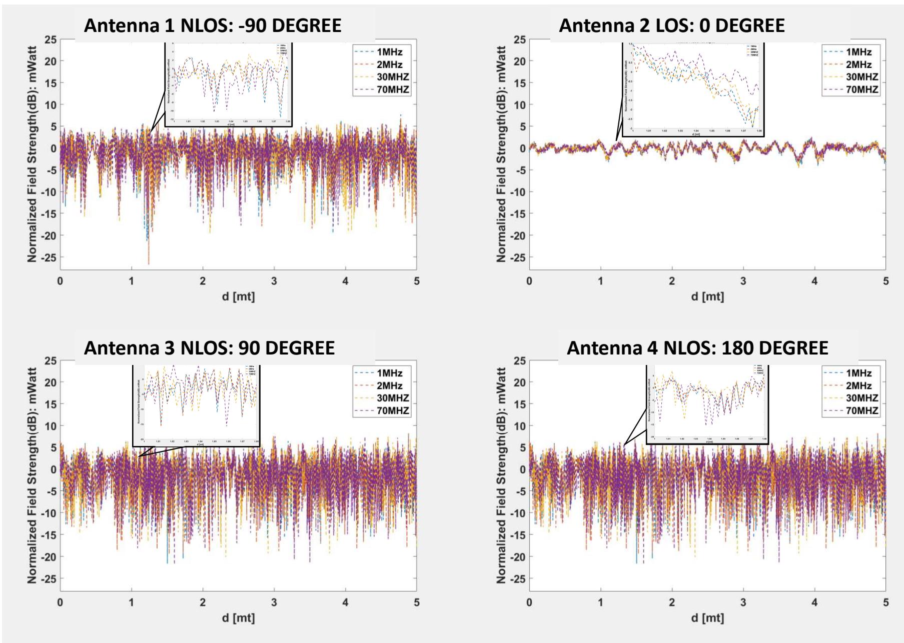


**Figure A.4:** Normalized Field Strength [dB] of Rx Switched antenna system

### A.1.5 Measurement 3 [7.11]

Figure A.5 shows the normalized field strength/fading for corresponding 1, 2, 30, and 70MHz frequency tones for each antenna. Antenna 1(NLOS) shows fading over the moving distance, and it varies between -15dB to 5dB, fading range increasing as the Rx trolley moves inside the kitchen; the zoomed view of the corresponding case shows that 1, 2, 30, 70MHz tones are uncorrelated and the reason behind that we are almost close noise floor. Antenna 2(NLOS), fading of antenna 4 varies between -15 to 5 dB; it increases as we move inside the kitchen; the zoomed view of the corresponding case shows that 1, 2, 30, and 70MHz tones are uncorrelated, and the reason behind that we are almost close noise floor. Antenna 3(NLOS), the fading is within the range of -5 to 14 dB, and also the zoomed view of the corresponding case shows that 1, 2, 30, and 70MHz tones are uncorrelated, and the reason behind that we are almost close noise floor. Ante(NLOS) does not receive direct components, and fading plot varies from -15 to 5 dB; the zoomed view of the corresponding case shows that 1, 2, 30, and 70MHz tones are uncorrelated, and the reason behind that we are almost close noise floor. On the noise floor, things get more randomized, and the instrument quantization effect also comes into play.

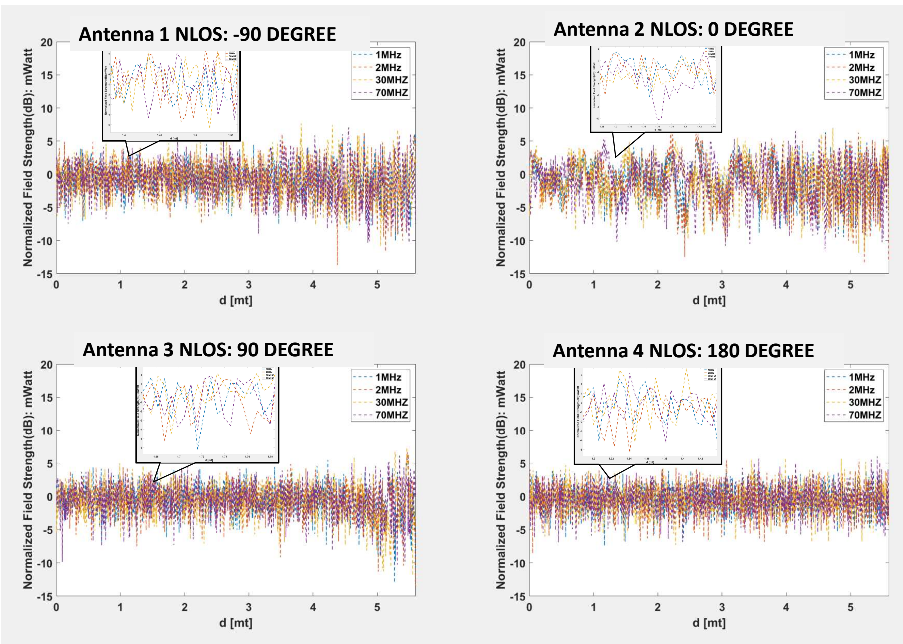


**Figure A.5:** Normalized Field Strength [dB] of Rx Switched antenna system

### A.1.6 Measurement 4 [7.16]

Figure A.6 shows the normalized field strength/fading for corresponding 1, 2, 30, and 70MHz frequency tones for each antenna. Antenna 1(NLOS) shows fading over the moving distance, and it varies between -10dB to 5dB over the distance of 4.6 mt then further it increases to -15 to 5dB and decreases till 5.2 mt; also, the zoomed view of the corresponding case shows that 1 and 2MHz tones follow each other, but higher frequency tones like 30 and 70MHz are uncorrelated with remaining tones. Antenna 2(LOS) is visible from the fading plots as they are within -5 to +5dB most of the time; there is no pattern among the tone. For antenna 3(NLOS), the fading is within the range of -5 to 15 dB, and zoomed view of the corresponding case shows that 1 and 2MHz tones coincide with each other, but higher frequency like 30 and 70MHz are uncorrelated with remaining tones. Antenna 4(NLOS) does not receive direct components, and fading plot varies from -18 to 7 dB, and also, the zoomed view of the corresponding case shows that 1 and 2MHz tones coincide with each other also the remaining tones fallow each other.

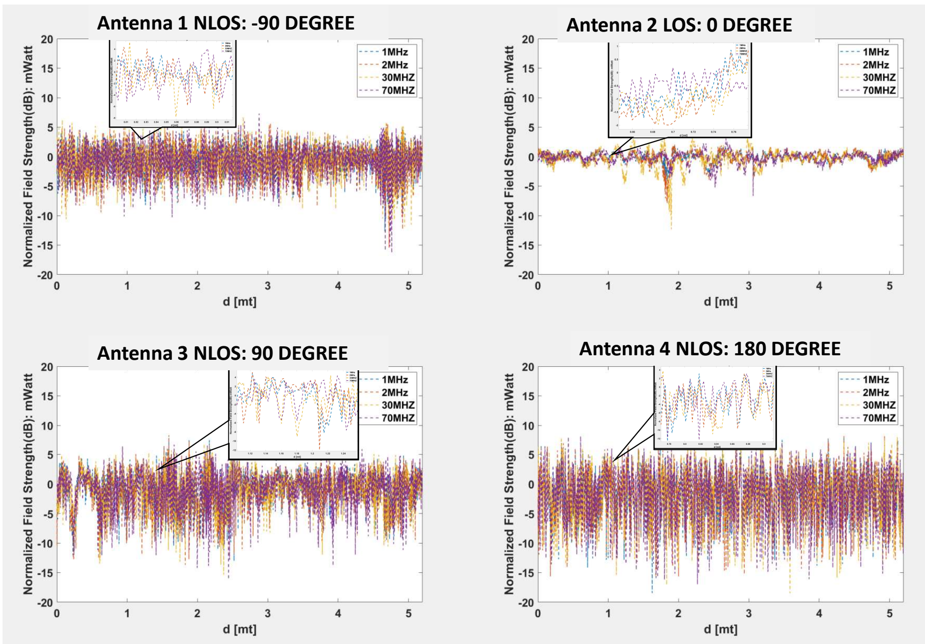


**Figure A.6:** Normalized Field Strength [dB] of Rx Switched antenna system

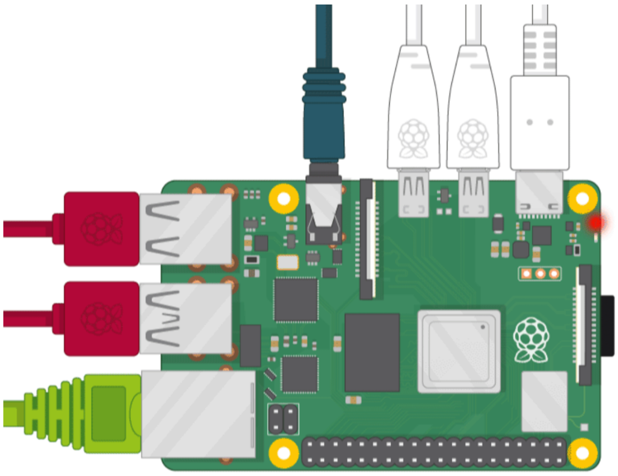

**Figure A.7:** Raspberry Pi 4 [18]

## A.2 Jittering Affect in Raspberry Pi4

Most intelligent products, such as computers, cell phones, industrial robots, etc., all have crystal oscillators embedded inside the product. These crystal oscillators or clock is the system's heartbeat; they provide a stable digital clock signal. Each product has a different frequency band, and the requirement is based on the used case. Based on where the products are being used in the case industry, the medical requirement for jittering is very strict. In contrast, in other products, such as audio, video, and smart home, the requirement for jittering and stability of clock signal is not strict. Jittering refers to a phenomenon when a digital signal has a short variation from its ideal position in time, as shown in figure A.8. Jittering mainly occurs due to intrinsic noise of oscillators or other disturbances such as thermal noise, vibration, and interference between the electronic components. Jittering can be categorized into two cases random noise and deterministic noise. Random noise cannot be predicted, and it is always there, and mainly it occurs due to thermal noise, shot noise, etc., while deterministic jitter is called bounded jitter; if all the components of the setup are known, then jitter can be predicted.
Raspberry pi four has been used in the measurement setup to control the phase lock loop to generate frequency tones. Raspberry pi also has some jitter effects; the data processing section has discussed the jittering effect issue.

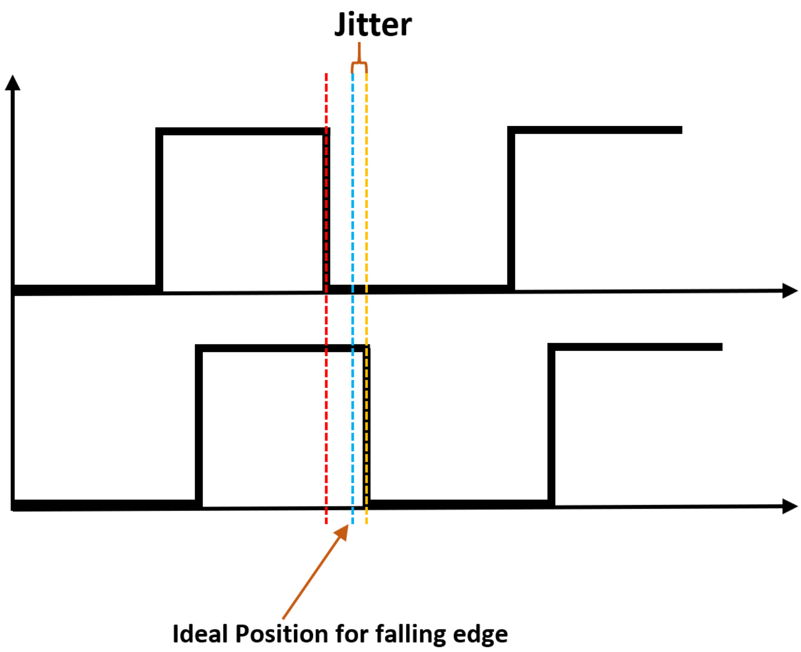


**Figure A.8:** Shows the deviation of digital signal from it ideal position due to jitter [10]

## A.3 Possible Future Measurement Setups

### Measurement Setup 1

The principle of this setup is to have four continuous and independent frequency tone (F1, F2, F3, F4), and all these four tones will be in the air all the time. At the receiver side each active antenna have access to all four frequency tones at the same time.

1. As shown in the figure A.9, at transmitter side signal generator generates simultaneously four CW multione of different frequency and feeded into transmitting antenna.

2. All the four frequency tones(F1, F2, F3, F4) will be in the air all the time.

3. As shown in the figure A.9, at receiver side all the antenna will be active sequentially over the time, at a moment antenna 1 is active and it have access to all four frequency tones which are present over the air.

4. At receiver, raspberry pi is programmed for four carrier frequency and based on that it configure LO1 and LO2 to generate four carrier frequency which are used in down conversion of received signals at 5GHz(IF).

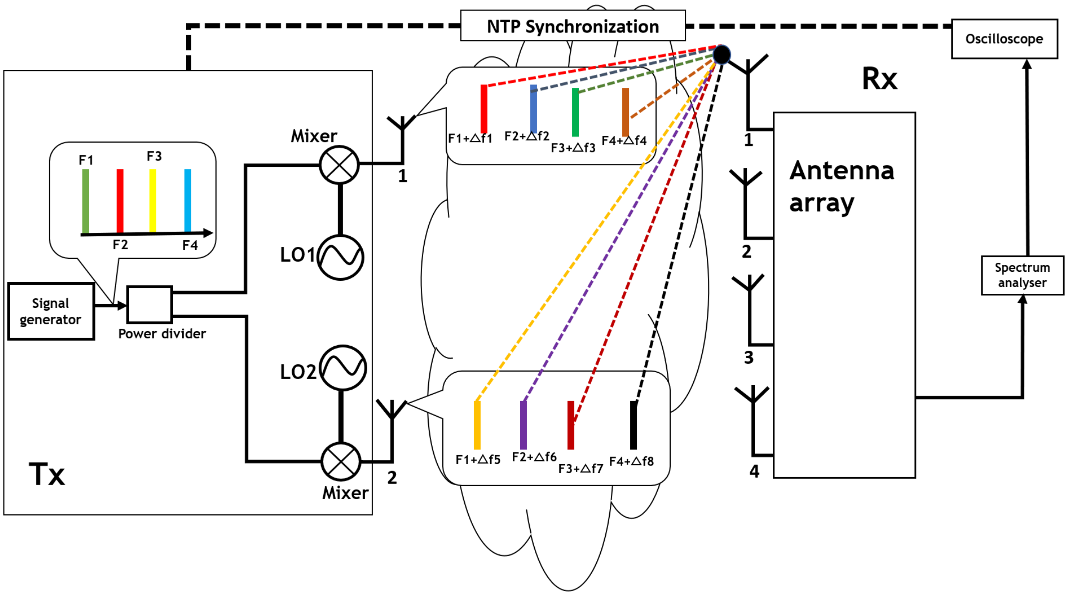


**Figure A.9:** Measurement Setup-1(4 tones, 1Tx and 4Rx)

5. Figure A.11 shows receiver set up, `ANT_SEL` pin is used to select between four pair of antenna(`1_2`, `3_4`, `5_6` and `7_8`), `TX_SEL` pin is used to configure the selected antenna as Rx or Tx, `PA_ON` pin is used to enable the power amplifier for Transmitting antenna between each pair(`1_2`, `3_4`, `5_6` and `7_8`).

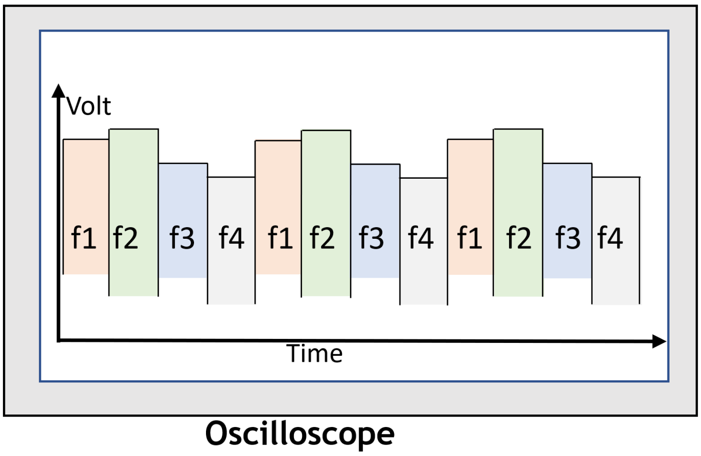


**Figure A.10:** Video signal plot on Oscilloscope (4 tones, 1Tx and 4Rx)

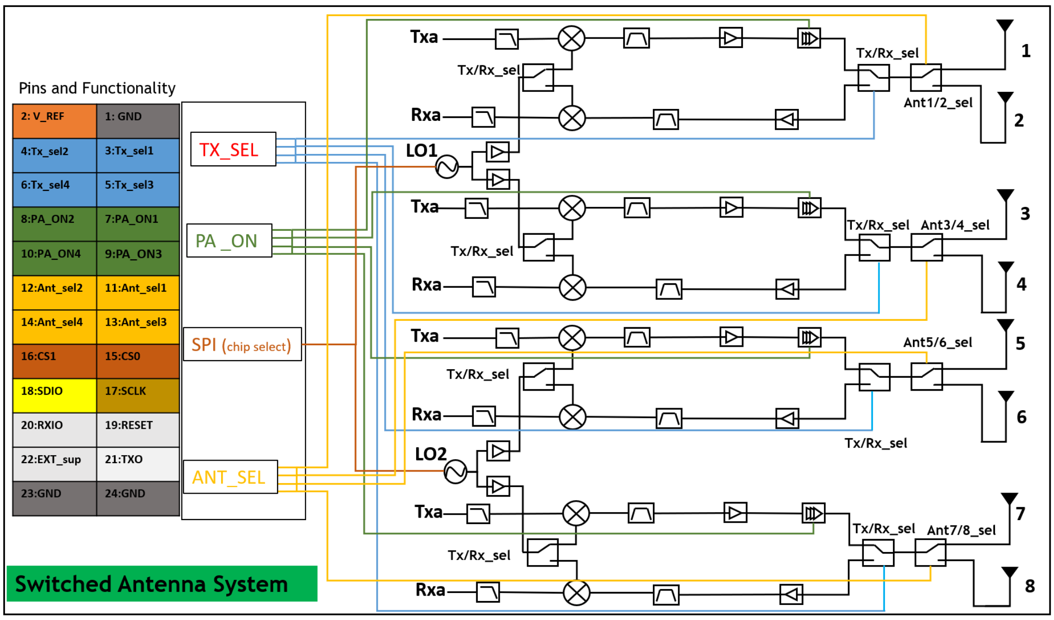


**Figure A.11:** Receiver Setup of Switched Antenna System

| | Antenna1(Reciever1) | Anttenna3(Reciever2) | Antenna5(Reciever3) | Antenna7(Reciever4) |
|---|---|---|---|---|
| PA1 | 0 | 0 | 0 | 0 |
| PA2 | 0 | 0 | 0 | 0 |
| PA3 | 0 | 0 | 0 | 0 |
| PA4 | 0 | 0 | 0 | 0 |
| TX_sel1 | 0 | 1 | 1 | 1 |
| TX_sel2 | 1 | 0 | 1 | 1 |
| TX_sel3 | 1 | 1 | 0 | 1 |
| TX_sel4 | 1 | 1 | 1 | 0 |
| Ant_sel1 | 1 | 0 | 0 | 0 |
| Ant_sel2 | 0 | 1 | 0 | 0 |
| Ant_sel3 | 0 | 0 | 1 | 0 |
| Ant_sel4 | 0 | 0 | 0 | 1 |
| CS1 | 1 | 1 | 0 | 0 |
| CS2 | 0 | 0 | 1 | 1 |

**Figure A.12:** Bit selection for receiver mode : Switched Antenna System

### Measurement Setup 2

The principle of this setup is to have eight continuous and independent frequency tone( Fi + △fi, where i is 1 to 8), and all these eight tones will be in the air all the time. At the receiver side each active antenna have access to all eight frequency tones at the same time.

1. As shown in the figure A.13, at transmitter side signal generator generates simultaneously four CW multitone and then pass into programmed local oscillators LO1 and LO2.

2. Local oscillators transforms 4 tones(from signal generator) into pair of four tones as shown in figure A.15, antenna 1 transmit first pair of four tones and antenna transmit pair second pair of four tones.

3. As shown in the figure A.13, at receiver side all the receiving antenna will be active sequentially over the time, at a moment antenna 1 is active and it have access to all eight frequency tones which are present over the air.

4. At receiver, raspberry pi is programmed for eight carrier frequency and based on that it configured the LO1 and LO2 to generate eight carrier frequency which are used in down conversion of received signals.

5. Figure A.11 shows receiver set up, `ANT_SEL` pin is used to select between four pair of antenna(`1_2`, `3_4`, `5_6` and `7_8`, `TX_SEL`) is used to configure the antenna as Rx or Tx between each pair(`1_2`, `3_4`, `5_6` and `7_8`, `TX_SEL`) pin, `PA_ON` is used to enable the power amplifier for Transmitting antenna for each pair(`1_2`, `3_4`, `5_6` and `7_8`).

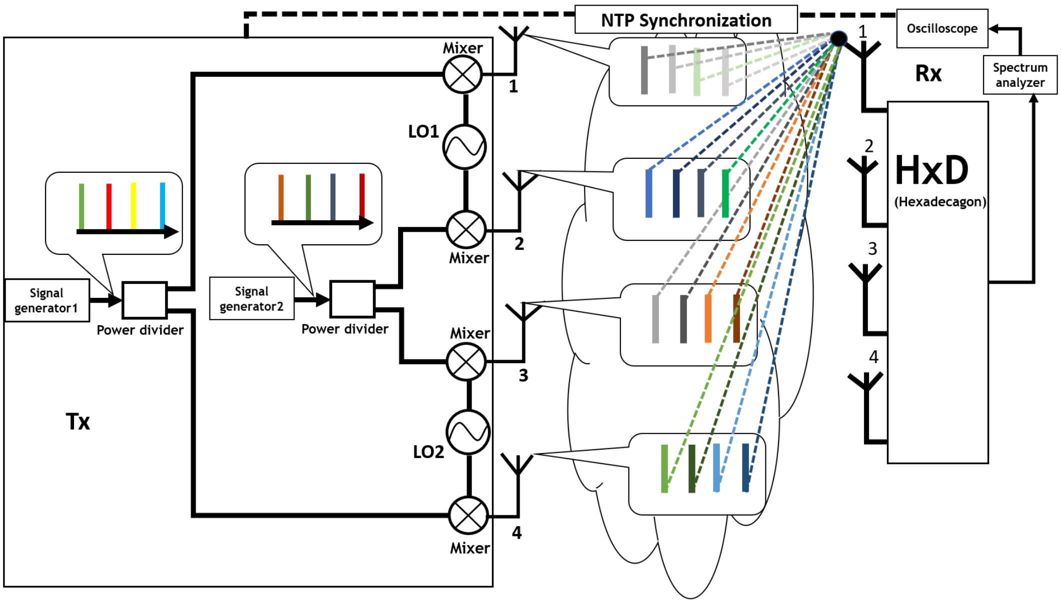


**Figure A.13:** Measurement Setup-2(8 tones, 2Tx and 4Rx)

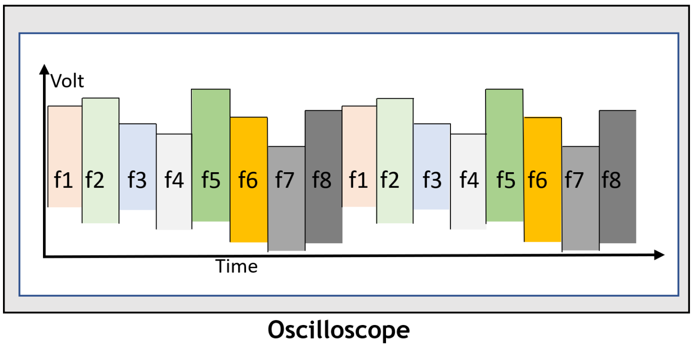


**Figure A.14:** Video signal plot on Oscilloscope (8 tones, 2Tx and 4Rx)

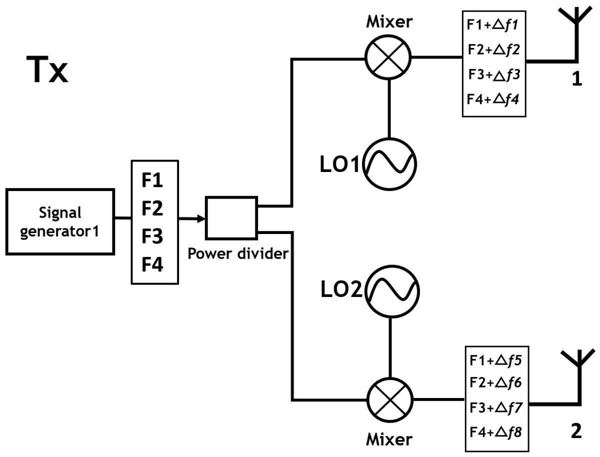


**Figure A.15:** Local oscillator set up

**Measurement Setup 3**

The principle of this setup is to have sixteen continuous and independent frequency tone( Fi + △fi, where i is 1 to 16), and all these sixteen tones will be in the air all the time. At the receiver side each active antenna have access to all sixteen frequency tones at the same time.

1. As shown in the figure A.16, at transmitter side both signal generator generates simultaneously four CW multione(pair of four different tones)

2. Local oscillators transforms pair of four tones (from signal generator) into four sets of four tones as shown in figure A.18, antenna 1 transmit first set, antenna 2 transmit pair second set, antenna 3 transmit third set and antenna 4 transmit fourth sets, all the antennas transmit together.

3. As shown in the figure A.16, at receiver side all the receiving antenna will be active sequentially over the time, at a moment antenna 1 is active and it have access to all sixteen frequency tones which are present over the air.

4. At receiver, raspberry pi is programmed for sixteen carrier frequency and based on that it configured the LO1 and LO1 to generate sixteen carrier frequency which are used in down conversion of received rf signals.

5. Figure A.11 shows receiver set up, `ANT_SEL` is used to select between four pair of antenna(`1_2`, `3_4`, `5_6` and `7_8`, `TX_SEL`) is used to configure the antenna as Rx or Tx between each pair(`1_2`, `3_4`, `5_6` and `7_8`, `TX_SEL`), `PA_ON` is used to enable the power amplifier for Transmitting antenna for each pair(`1_2`, `3_4`, `5_6` and `7_8`, `TX_SEL`).

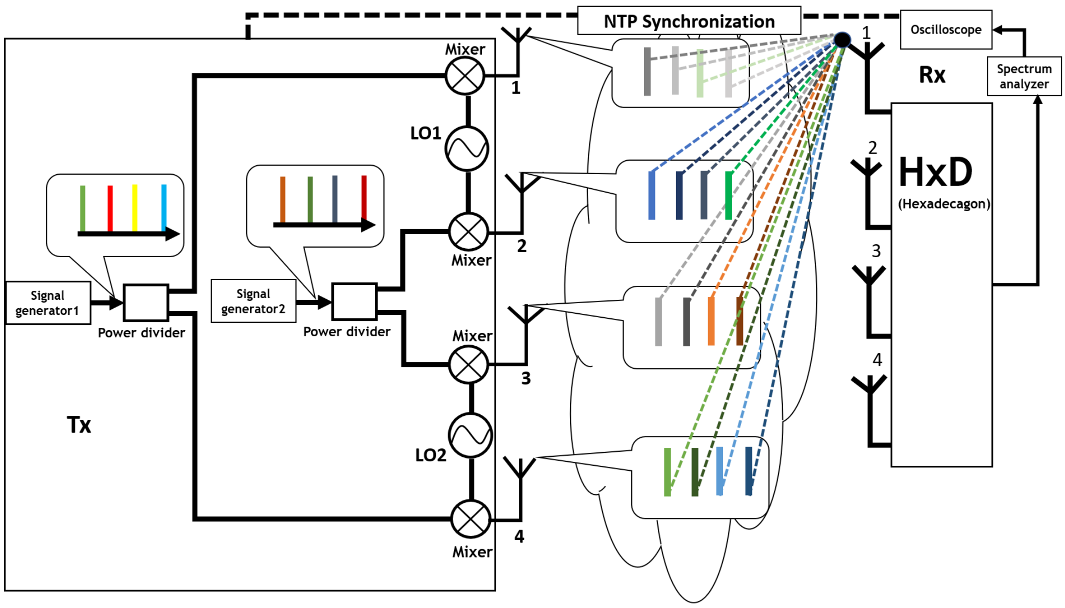


**Figure A.16:** Measurement Setup-3(16 tones, 4Tx and 4Rx)

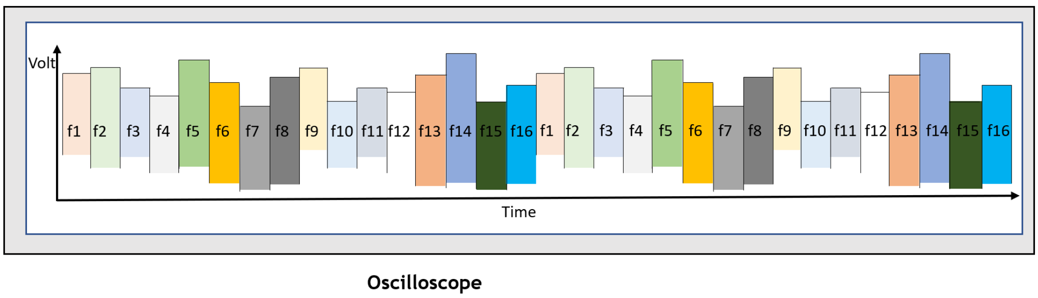


**Figure A.17:** Video signal plot on Oscilloscope (16 tones, 4Tx and 4Rx)

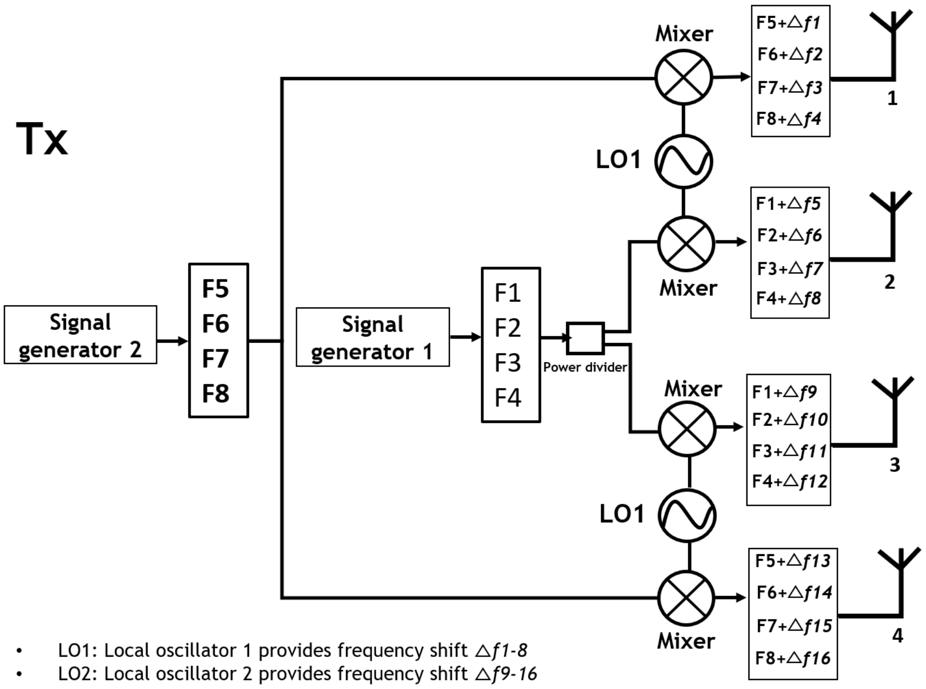


**Figure A.18:** Local oscillator set up

## A.4 Switched Antenna selection and PLL Programming

ADF4371[7]is a fractional or integer N based phase locked loop frequency synthesizers, the voltage controlled VCO oscillator can generate wide range of frequencies from 62.5MHz to 32 GHz. The VCO can have a output in the range 4GHz to 8GHz, there are range of divider(2, 4, 6.., 64) connected to output of VCO and can give output as low as 62.MHz at RF8X. The frequency multiplier at RF16X can give output 8 to 16GHz and frequency multiplier at RF32X can give output of 16 to 32 GHz, figure A.19 shows the functional block diagram of ADF4371 frequency synthesizer.

Figure A.20 shows timing specification and timing diagram for serial port interface(SPI), table on the top of figure A.20 have time specification values: $f_{SCLK}$ is a clock frequency it can attain max value of 50MHz, minimum values of parameter like clock period($t_{SCLK}$), clock pulse width for logic high ($t_{HIGH}$), clock pulse width for low($t_{LOW}$), SDIO setup time($t_{DS}$, hold time for SDIO($t_{DH}$), Falling Edge clock to SDIO bit processing($t_{ACCESS}$), chip select rising time to SDIO data high bit($t_Z$), CS fall time to SCLK rise time($t_S$) and SCLK fall to chip select rise($t_H$).

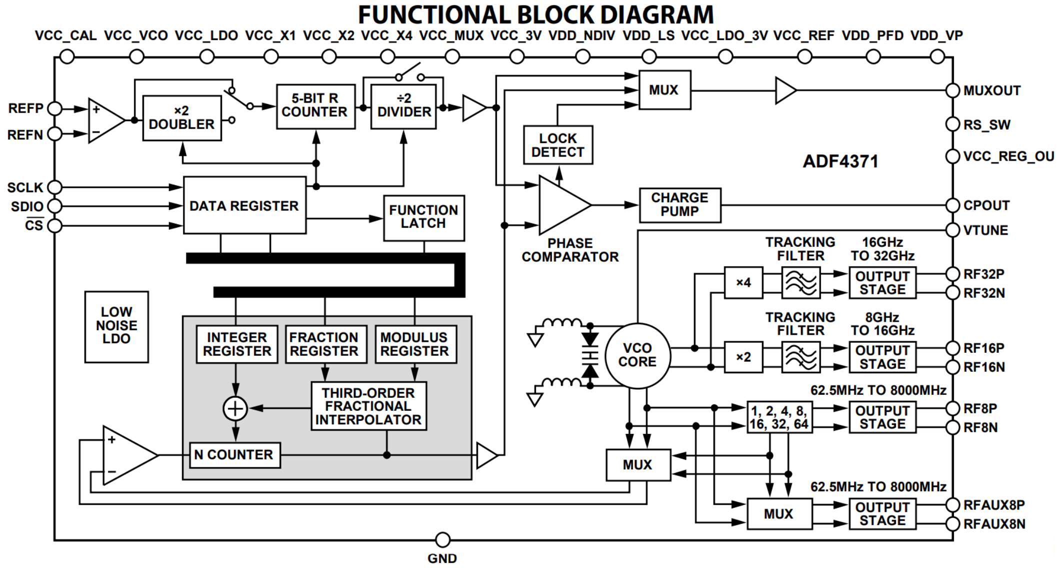


**Figure A.19:** Functional block diagram of frequency synthesizers [7]

### A.4.1 Frequency Synthesizer Theory

$$f_{RFOUT} = \left( INT + \frac{FRAC1 + \frac{FRAC2}{MOD2}}{MOD1} \right) * \frac{f_{PFD}}{RFDivider} \tag{A.1}$$

[7] $f_{RFOUT}$ is the reference input frequency.
INT is integer division factor.
FRAC1 is fractionality.
FRAC2 is auxiliary fractionlity.
MOD1 is the fixed 25-bit modulus.
MOD2 is auxiliary modulus.
RF divider is divider scale that divides the VCO frequency output.

$$f_{PFD} = \frac{REF_{IN} * (1 + D)}{(R(1 + T))} \tag{A.2}$$

[7]

$REF_{IN}$ is the reference input frequency.
D is the $REF_{IN}$ doubler bit.
R is the reference division factor.
T is the reference divide by 2 bit (0 or 1)

### A.4.2 Device Setup Instruction

Serial peripheral interface of ADF3471 is configured by four pin: SCLK(clock), SDIO(data bits), CS(chip select) and MUXOUT(not used in 3 wire SPI), timing

| Parameter | Symbol | Test Conditions/Comments | Min | Typ | Max | Unit |
|---|---|---|---|---|---|---|
| Serial Port Interface (SPI) Timing | | See Figure 2, Figure 3, and Figure 4 | | | | |
| SCLK Frequency | $f_{SCLK}$ | | | | 50 | MHz |
| SCLK Period | $t_{SCLK}$ | | 20 | | | ns |
| SCLK Pulse Width High | $t_{HIGH}$ | | 10 | | | ns |
| SCLK Pulse Width Low | $t_{LOW}$ | | 10 | | | ns |
| SDIO Setup Time | $t_{DS}$ | | 2 | | | ns |
| SDIO Hold Time | $t_{DH}$ | | 2 | | | ns |
| SCLK Falling Edge to SDIO Valid Propagation Delay | $t_{ACCESS}$ | | 10 | | | ns |
| $\overline{CS}$ Rising Edge to SDIO High-Z | $t_Z$ | | 10 | | | ns |
| $\overline{CS}$ Fall to SCLK Rise Setup Time | $t_S$ | | 2 | | | ns |
| SCLK Fall to $\overline{CS}$ Rise Hold Time | $t_H$ | | 2 | | | ns |

***Timing Diagrams***

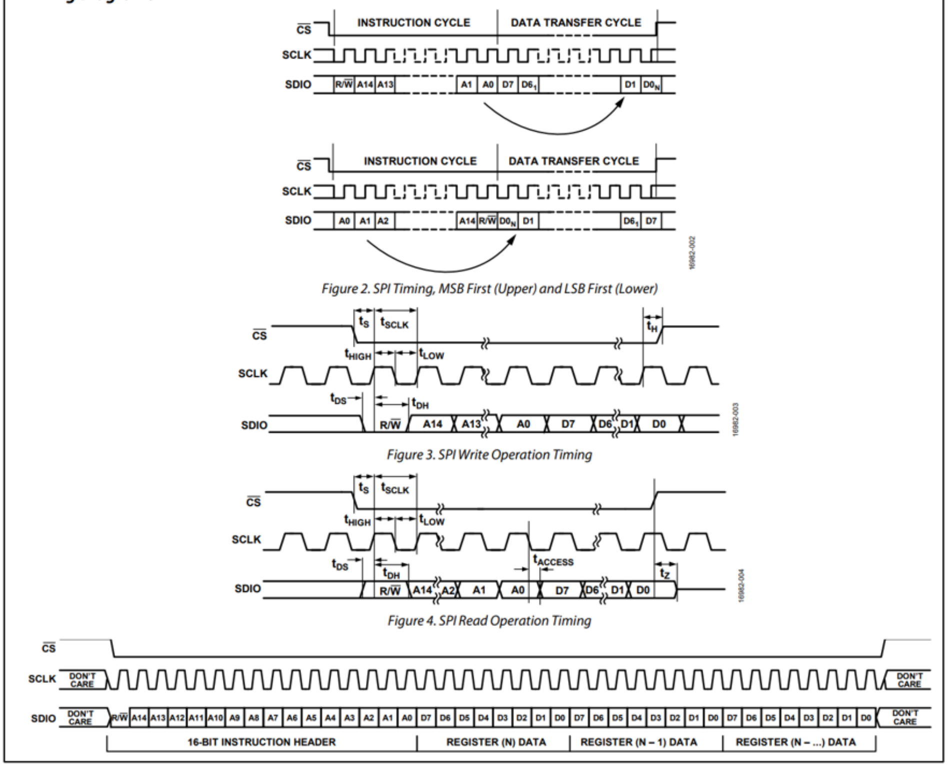


**Figure A.20:** Timing diagram of frequency synthesizers [7] for serial port interface management of SPI interface is configured based on the specification given in figure A.20, SPI instruction consist of 15 bits of register address with 8 data bits.

SPI stream mode is not used in this setup(data bits loaded once). Listed steps for device setup instruction:

1. First step is to initialize the SPI by writing the values to REG0000(address: 0x00, setting: 0x18 for four wire SPI) and REG0001(address: 0x01, setting: 0x00 for master readback control).

2. Next step is to initialization of sequence: Update each register corresponds to the address 0x7C to address 0x10( register summary mentioned on table 10 [7]), values can be updated based on the desired output frequency.

3. Third step is frequency update sequence: values like R, MOD2, FRAC1, FRAC2, and INT, based on specification of ADF4371, autocalibration work fine when $f_{PFD} \leq 125$MHz.

   (a) REG001F (new R_WORD[4:0])
   (b) REG001A (new MOD2WORD[13:8])
   (c) REG0019 (new MOD2WORD[7:0])
   (d) REG0018 (new FRAC2WORD[13:7])
   (e) REG0017 (new FRAC2WORD[6:0])
   (f) REG0016 (new FRAC1WORD[23:16])
   (g) REG0015 (new FRAC1WORD[15:8])
   (h) REG0014 (new FRAC1WORD[7:0])
   (i) REG0011 (new BIT_INTEGER_WORD[15:8])
   (j) REG0010 (new BIT_INTEGER_WORD[7:0])

   Frequency change occur on the register:REG0010 if the $f_{PFD} > 125MHz$; then sequences need to be updated further [7].

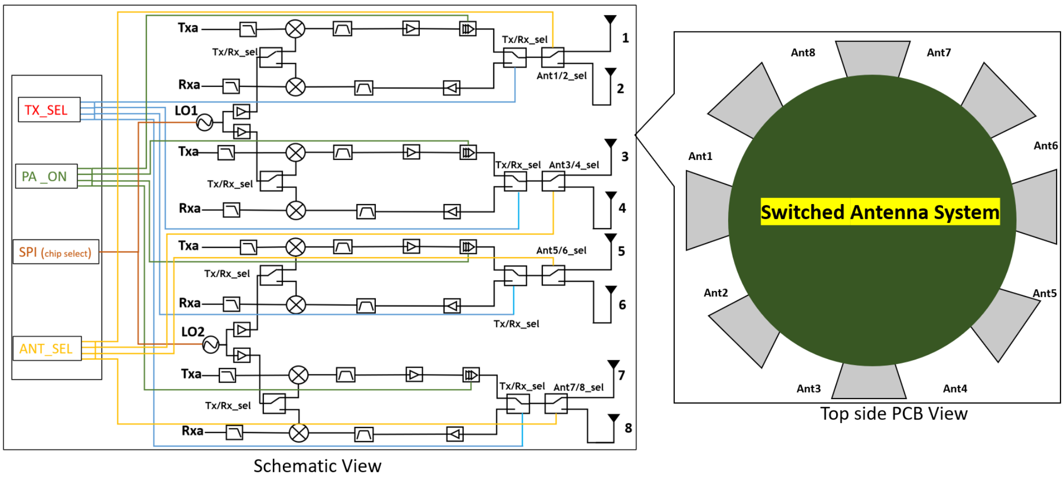


**Figure A.21:** Schematic and PCB view of Hexadecagon

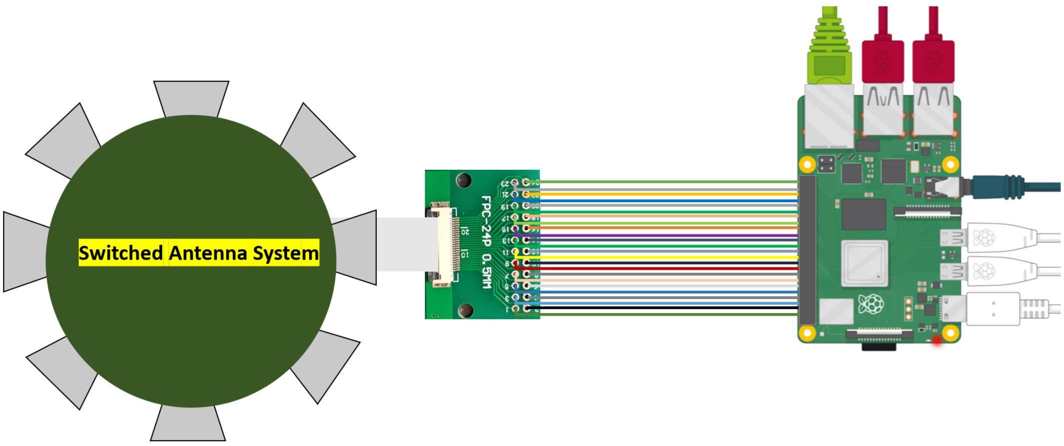


**Figure A.22:** Raspberry Pi[18] with Hexadecagon(HxD) setup

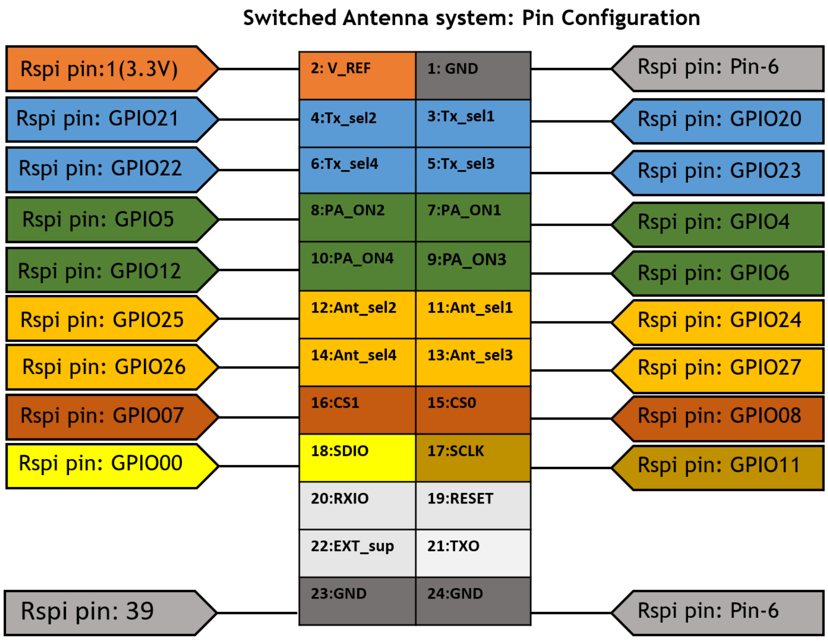


**Figure A.23:** Defined raspberry pins connection with Switched Antenna System

| | Antenna1(Reciever1) | Anttenna3(Reciever2) | Antenna5(Reciever3) | Antenna7(Reciever4) |
|---|---|---|---|---|
| PA1 | 0 | 0 | 0 | 0 |
| PA2 | 0 | 0 | 0 | 0 |
| PA3 | 0 | 0 | 0 | 0 |
| PA4 | 0 | 0 | 0 | 0 |
| TX_sel1 | 0 | 1 | 1 | 1 |
| TX_sel2 | 1 | 0 | 1 | 1 |
| TX_sel3 | 1 | 1 | 0 | 1 |
| TX_sel4 | 1 | 1 | 1 | 0 |
| Ant_sel1 | 1 | 0 | 0 | 0 |
| Ant_sel2 | 0 | 1 | 0 | 0 |
| Ant_sel3 | 0 | 0 | 1 | 0 |
| Ant_sel4 | 0 | 0 | 0 | 1 |
| CS1 | 1 | 1 | 0 | 0 |
| CS2 | 0 | 0 | 1 | 1 |

**Figure A.24:** Bit selection for receiver mode Switched Antenna System

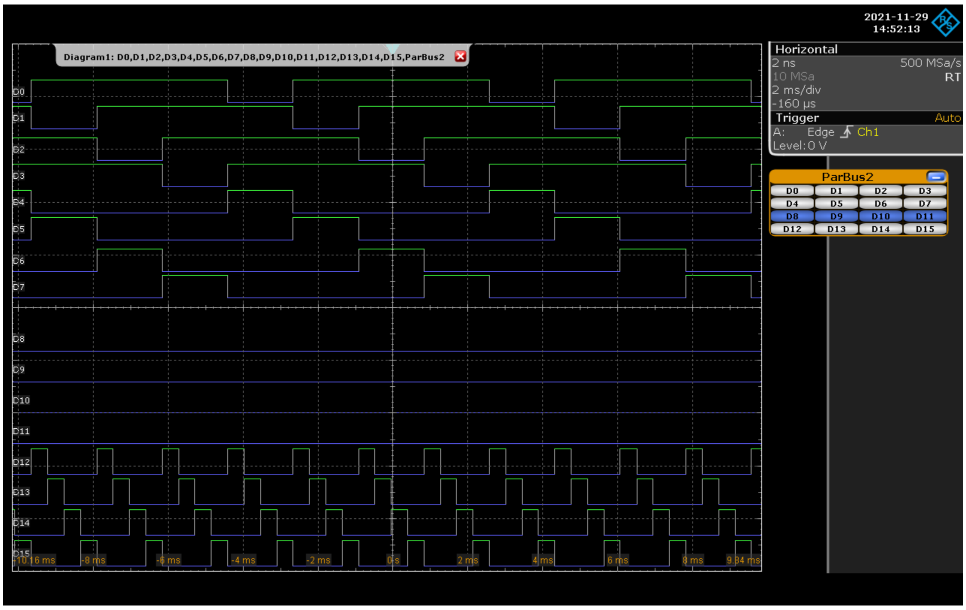

**Figure A.25:** GPIOs bit evaluation on developed program of mutitone(4) generation with oscilloscope

### A.4.3 Four Tone Generation

Figure A.22 shows the connection between raspberry pi and hexadecagon with all GPIOs interface pins, both raspberry pi and hexadecagon connected through 0.5mm 24 pin FPC connector board, figure A.23 shows which pins of raspberry is connected to hexadecagon based on developed program for 4 tone frequency generation. Figure A.21 shows schematic and PCB view of hexadecagon and it contain total 12 switches to control the operation: $TX\_SEL$ pins is used to control the TX/RX switches between all 4 pair of antennas, $PA\_ON$ pins is used to enable the selected power amplifier(for transmitting case), SPI(chip select) is used to enable LO1 and LO2( frequency synthesizer) and $ANT\_SEL$ pins is select antenna between pair of antenna, figure A.24 table is bit level selection for hexadecagon receiving mode: all PAs have low logic, Example: Antenna 1 selected: $TX\_SEL$ bits [0 1 1 1], $ANT\_SEL$ bits [1 0 0 0] and SPI(chip select) bits [1 0].
Developed mutitone(4 tones) program is cross validated with oscilloscope on raspberry pi, all the configured GPIOs are connected to logic inputs([D0 to D3 are $TX\_SEL$ 1 to 3], [D4 to D7 are $ANT\_SEL$ 1,3,5 and 7], [D8-D11 are $PA\_ON$ 1 to 4]), [D12-15 are Frequency tone 1-4]) of oscilloscope as shown in figure A.25, detected logic bits of oscilloscope are correctly matched with table of figure A.24.